Atrial Digital Twins to Assess Arrhythmia Vulnerability and Guide Ablation Therapy

Leverage Patient-Specific Atrial Models to Understand Atrial Fibrillation Mechanisms and Provide Personalized Treatments

Zur Erlangung des akademischen Grades eines

DOKTORS DER INGENIEURWISSENSCHAFTEN (Dr.-Ing.)

von der KIT-Fakultät für

Elektrotechnik und Informationstechnik

des Karlsruher Instituts für Technologie (KIT)

angenommene

DISSERTATION

von

Luca Azzolin, M.Sc.

geb. in Arzignano, Italy

Tag der mündlichen Prüfung: 21.12.2021
Referent: Prof. Dr. rer. nat. Olaf Dössel
Korreferent: Prof. Dr. Javier Sáiz
Korreferent: Dr.-Ing. Axel Loewe

Success is not the key to happiness.
Happiness is the key to success.
If you love what you are doing,
you will be successful.
— Albert Schweitzer

Abstract

Cardiovascular diseases are the leading cause of death worldwide, and atrial fibrillation (AF) is the most prevalent cardiac arrhythmia affecting more than 6 million individuals in Europe, with a cost exceeding 1% of the EU health care system budget (13,5 billion annually). New treatment strategies and the progress achieved in research on AF mechanisms and substrate evaluation methods to date have not been commensurate with an equivalent development of the knowledge and technologies required to individually characterize each patient in search of the most efficient therapy. Catheter ablation is the suggested treatment when anti-arrhythmic drugs are not effective. However, the success rates are still not satisfactory, and a large share of AF patients need to undergo multiple ablation procedures. Computational modelling of the atria bears the potential of better understanding AF patho-mechanisms and tailoring ablation therapy. The content of the thesis is split into two projects involving computer models of human atria anatomy and electrophysiology to build a bridge between medicine and engineering.

The first project leverages computer models to provide deeper insights into AF vulnerability and maintenance mechanisms. This work aimed first at evaluating the impact of the choice of the protocol on AF onset and perpetuation in in-silico experiments. An efficient and automated method to standardize the assessment of AF vulnerability in atrial models was proposed. Then, this thesis sought to quantify the influence of heterogeneous anatomical thickness in AF onset and continuation. AF episodes were induced and analyzed on highly detailed 3D atrial models, including various regional myocardial thicknesses. The results of this work confirmed the findings of previous experimental studies proposing highly heterogeneous anatomical thickness as susceptible areas to maintain AF and probable regions to ablate.

In the second project, I enter the realm of virtual replicas of patients' hearts to tailor arrhythmia characterization and treatment, the so called *cardiac digital twins*. The aim was to develop algorithms delivering atrial models with personalized anatomy augmenting clinical information. This technology was incorporated in a unique pipeline to provide atrial digital twins with patient-specific electrophysiology integrating multiple clinical datasets. The advances described enable the generation of accurate personalized atrial models from medical images and electro-anatomical data. In parallel to advancing the models' personalization, major progress was achieved in translating them into clinical application to support ablation therapy. An automated platform to assess AF vulnerability and identify the optimal ablation targets on anatomical and functional digital twins was realized to provide clinicians

personalized ablation plans to stop AF onset and perpetuation. This work highlighted the importance of digital twins in optimizing existing and exploring new diagnostic and therapeutic approaches, complementing and enriching clinical information with simulated data.

Computational modelling facilitated the multilevel integration of multiple datasets and offered new opportunities for mechanistic understanding, risk prediction and personalized therapy. This thesis changes the paradigm of classification and diagnosis of AF by delivering individualized digital twin models of patients to personalize medicine, unraveling fundamental physiological and pathological mechanisms with implications for clinical treatments.

Zusammenfassung

Herz-Kreislauf-Erkrankungen sind weltweit die häufigste Todesursache, und die Therapien für Patienten, die an Herzinsuffizienz leiden, sind noch nicht optimiert oder abschließend festgelegt. Das Risiko für Herzversagen und Schlaganfall ist bei Patienten mit Vorhofflimmern (AF) erhöht. Vorhofflimmern ist die weltweit am weitesten verbreitete Herzrhythmusstörung, von der mehr als 6 Millionen Menschen in Europa betroffen sind und deren Kosten mehr als 1% des EU-Haushalts im Gesundheitssektor (13,5 Milliarden jährlich) ausmachen. Die neuen Behandlungsstrategien und die Fortschritte in der Erforschung der Vorhofflimmer-Mechanismen standen bisher nicht im Einklang mit einer entsprechenden Entwicklung des Wissens und der Technologien, die erforderlich sind, um jeden Patienten individuell zu behandeln und die effizienteste Therapie zu finden. Die Katheterablation ist die bevorzugte Behandlung, wenn Antiarrhythmika nicht wirksam sind. Die Erfolgsquoten sind jedoch noch immer nicht zufriedenstellend, und ein großer Teil der Vorhofflimmerpatienten muss sich mehreren Katheteruntersuchungen unterziehen. Die computergestützte Modellierung der Vorhöfe birgt das Potenzial, die Pathomechanismen des Vorhofflimmerns besser zu verstehen und die Ablationstherapie anzupassen. Der Inhalt dieser Arbeit ist in zwei Projekte unterteilt, die sich mit Computermodellen menschlicher Vorhöfe befassen, um eine Brücke zwischen Medizin und Technik zu schlagen.

Das erste Projekt nutzt Computermodelle, um tiefere Einblicke in die Anfälligkeit für Vorhofflimmern und deren Aufrechterhaltungsmechanismen zu gewinnen. Es wurden verschiedene Protokolle implementiert und verglichen, um die Auswirkungen der Wahl des Induktionsprotokolls auf die Auslösung und Aufrechterhaltung von Vorhofflimmern in in silico Experimenten zu bewerten. Schließlich wurde eine effiziente und automatisierte Methode zur Standardisierung der Bewertung der Vorhofflimmeranfälligkeit in Vorhofmodellen vorgeschlagen. Anschließend wurde versucht, den Einfluss der heterogenen anatomischen Dicke auf den Beginn und das Fortbestehen von Vorhofflimmern zu quantifizieren. Vorhofflimmer-Episoden wurden in hochdetaillierten volumetrischen Vorhofmodellen mit verschiedenen regionalen Myokarddicken ausgelöst und analysiert. Die Ergebnisse dieser Arbeit bestätigten die Befunde früherer experimenteller Studien, in denen eine sehr heterogene anatomische Dicke als anfälliger Bereich für die Aufrechterhaltung von Vorhofflimmern und als wahrscheinliche gute Region für eine Ablation vorgeschlagen wurde.

Das zweite Projekt befasst sich mit der virtuellen Nachbildungen von Patientenherzen, um die Charakterisierung und Behandlung von Herzrhythmusstörungen maßgeschneidert zu gestalten, die so genannten kardialen digitalen Zwillinge. Unser Ziel war die Entwicklung

von Algorithmen zur Bereitstellung von Vorhofmodellen mit personalisierter Anatomie, die die klinischen Informationen ergänzen. Diese Technologie wurde in eine eigenständige Pipeline integriert, um digitale Vorhofzwillinge mit patientenspezifischer Elektrophysiologie bereitzustellen, die mehrere klinische Datensätze beinhaltet. Die beschriebenen Fortschritte ermöglichen die Erstellung zuverlässiger personalisierter Vorhofmodelle aus medizinischen Bildern und elektrophysiologischen Daten. Parallel zur Weiterentwicklung der Modelle in methodischer Hinsicht wurden große Fortschritte bei der Umsetzung in klinischen Anwendungen erzielt. Eine automatisierte Plattform zur Bewertung der Anfälligkeit für Vorhofflimmern und zur Identifizierung optimaler Ablationsziele auf der Grundlage anatomischer und funktioneller digitaler Zwillinge ermöglichte den Vorschlag personalisierter Ablationspläne, um das Auftreten und Fortbestehen von Vorhofflimmern zu verhindern. Die Ergebnisse sind ein wichtiger Schritt auf dem Weg zu einer patientenspezifischen, modellbasierten Charakterisierung, zum Verständnis und zur Behandlung von Vorhofflimmern.

Die Vorteile im Vergleich zu bestehenden Ansätzen werden in den in dieser Arbeit vorgestellten Studien diskutiert. Unsere Arbeit verändert das Vorgehen bei der Klassifizierung und Diagnose von Vorhofflimmern, indem sie individualisierte digitale Zwillingsmodelle von Patienten zur Verfügung stellt, um die Medizin zu personalisieren und grundlegende physiologische und pathologische mechanismen zu entschlüsseln, die Auswirkungen auf die klinische Versorgung haben.

Sommario

Le malattie cardiovascolari sono la principale causa di morte in tutto il mondo e la fibrillazione atriale (FA) è l'aritmia cardiaca più diffusa, interessando più di 6 milioni di individui in Europa, con un costo che supera l'1% del budget del sistema sanitario dell'UE (13,5 miliardi all'anno). Le nuove strategie di trattamento e i progressi compiuti finora nella ricerca sui meccanismi della FA e sui metodi di valutazione del substrato non sono stati commisurati ad un equivalente sviluppo delle conoscenze e delle tecnologie necessarie per determinare la terapia più efficace per ogni paziente. L'ablazione con catetere è il trattamento suggerito quando i farmaci antiaritmici non sono efficaci. Tuttavia, i tassi di successo non sono ancora soddisfacenti, e una gran parte dei pazienti con FA deve essere sottoposta a multiple procedure di ablazione. La modellazione computazionale degli atri ha il potenziale per comprendere meglio i meccanismi patogenetici della FA e personalizzare la terapia di ablazione. Il contenuto della tesi è diviso in due progetti che coinvolgono modelli computerizzati di anatomia ed elettrofisiologia degli atri umani per costruire un ponte tra medicina e ingegneria.

Il primo progetto sfrutta i modelli computerizzati per fornire approfondimenti sulla vulnerabilità della FA e sui meccanismi di perpetuazione. Questo lavoro mirava innanzitutto a valutare l'impatto della scelta del protocollo d'induzione sull'insorgenza e la perpetuazione della FA in esperimenti in-silico. È stato, infine, proposto un metodo efficiente e automatizzato per standardizzare la valutazione della vulnerabilità della FA nei modelli atriali. Poi, questa tesi ha cercato di quantificare l'influenza dell'etegeneità dello spessore anatomico sull'insorgenza e continuazione della FA. Gli episodi di FA sono stati indotti e analizzati su modelli atriali 3D altamente dettagliati, compresi vari spessori regionali del miocardio. I risultati di questo lavoro hanno confermato i risultati di precedenti studi sperimentali che proponevano spessori anatomici altamente eterogenei come aree suscettibili a mantenere la FA e probabili regioni da ablare.

Nel secondo progetto, mi sono addentrato nel mondo delle repliche virtuali dei cuori dei pazienti per personalizzare la caratterizzazione e il trattamento delle aritmie, i cosiddetti "cardiac digital twins". L'obiettivo era quello di sviluppare algoritmi che fornissero modelli atriali con un'anatomia personalizzata che aumentasse le informazioni cliniche. Questa tecnologia è stata incorporata in un'unica piattaforma per generare digital twins atriali con elettrofisiologia specifica del paziente che integra i dati clinici. I progressi descritti consentono la generazione di accurati modelli atriali personalizzati da immagini mediche e dati elettro-anatomici. Parallelamente all'avanzamento della personalizzazione dei modelli,

sono stati raggiunti importanti progressi nella loro traslazione in applicazioni cliniche per supportare la terapia di ablazione. È stata realizzata una piattaforma automatizzata per valutare la vulnerabilità della FA e identificare i target di ablazione ottimali sui digital twins anatomici e funzionali per fornire ai medici piani di ablazione personalizzati per fermare l'insorgenza e la perpetuazione della FA. Questo lavoro ha evidenziato l'importanza dei digital twins nell'ottimizzazione delle tecniche diagnostiche e terapeutiche esistenti e nell'esplorazione di nuove, completando e arricchendo le informazioni cliniche con dati simulati.

La modellazione computazionale ha facilitato l'integrazione multiscala di più dati e ha offerto nuove opportunità per la comprensione dei meccanismi della FA e la terapia personalizzata. Questa tesi cambia il paradigma della classificazione e della diagnosi della fibrillazione atriale fornendo digital twins individualizzati dei pazienti per personalizzare la medicina, svelando meccanismi fisiologici e patologici fondamentali con implicazioni per i trattamenti clinici.

Resumen

Las enfermedades cardiovasculares son la principal causa de muerte en todo el mundo. La fibrilación auricular (FA) es la arritmia cardíaca más prevalente, afectando a más de 6 millones de individuos en Europa y con un coste superior al 1% del presupuesto del sistema sanitario de la UE (13.500 millones anuales). Hasta la fecha, la investigación de los mecanismos de la FA y evaluación del sustrato no han ido acompañados del desarrollo de las tecnologías necesarias para la personalizacioón de terapias. El tratamiento sugerido cuando los fármacos antiarritmicos no son eficaces es la ablación. Sin embargo, las tasas de éxito aún no son satisfactorias, y una gran parte de los pacientes con FA deben someterse a múltiples procedimientos. La modelización computacional de las aurículas tiene el potencial de brindar un mejor entendimiento de los mecanismos patológicos de la FA y como personalizar el tratamiento de la ablación. El contenido de esta tesis se divide en dos proyectos, que incluyen modelos computacionales de la anatomía y la electrofisiología auricular humana para tender un puente entre la medicina y la ingeniería.

El primer proyecto aprovecha los modelos computacionales para profundizar en el conocimiento de los mecanismos de vulnerabilidad y mantenimiento de la FA. El objetivo de este trabajo es, en primer lugar, evaluar el impacto de la elección del protocolo en la aparición y perpetuación de la FA en experimentos in-silico. Para ello, se propone un método automático que evalúa la vulnerabilidad a FA en modelos de aurícula. A continuación, en esta tesis se cuantifica la influencia del grosor heterogéneo del miocardio en el inicio y la mantenimiento de la FA. Utilizando diferentes grosores regionales del miocardio, se simularon y analizaron episodios de FA en modelos auriculares 3D detallados. Los resultados de este trabajo confirman los hallazgos de estudios experimentales previos en los que se proponía el grosor anatómico altamente heterogéneo como zonas susceptibles de mantener la FA, considerándolas potenciales regiones de ablación.

En el segundo proyecto, me adentré en el ámbito de las réplicas virtuales de corazones de pacientes reales para caracterizar e individualizar el tratamiento de las arritmias, los llamados *cardiac digital twins*. El objetivo principal consiste en desarrollar algoritmos que generen automaticamente modelos computacionales con anatomías auriculares personalizadas que permitan aumentar los datos clínicos. La metodologia anteriormente descrita, se incorpora a un proceso que genera un digital twin auricular con electrofisiología específica para cada paciente, integrando múltiples conjuntos de datos clínicos. Los avances descritos permiten generar modelos auriculares personalizados y precisos a partir de imágenes médicas y datos electroanatómicos. Paralelamente al avance en la personalización de los modelos,

se lograron importantes progresos en su traducción a la aplicación clínica para apoyar la terapia de ablación. Para ello se ha desarrollado una plataforma automatizada para evaluar la vulnerabilidad de la FA e identificar las zonas óptimas en las que realizar la ablación en un digital twin. Esta plataforma tiene el fin de proporcionar a los médicos planes de ablación personalizados para detener la FA. Este trabajo pone de manifiesto la importancia de los digital twins para optimizar los enfoques diagnósticos y terapéuticos existentes y explorar otros nuevos, complementando y enriqueciendo la información clínica con datos simulados.

El modelado computacional facilita la integración multiescala de múltiples conjuntos de datos y ofrece nuevas oportunidades para la comprensión de los mecanismos, la predicción del riesgo de FA y una terapia personalizada. Esta tesis cambia el paradigma de la clasificación y el diagnóstico de la FA al ofrecer modelos individualizados de pacientes para personalizar la medicina, desentrañando mecanismos fisiológicos y patológicos fundamentales con implicaciones para los tratamientos clínicos.

Acknowledgments

This thesis is the result of my scientific work during the last three years and a half at the Karlsruhe Institute of Technology (KIT) at the Institute of Biomedical Engineering (IBT). I would like here to spend few words to sincerely thank all the people who contributed to this success.

First of all, I am expressing my dearest thanks to Prof. Olaf Dössel for giving me the opportunity of being part of this Marie Curie project and of letting me do what I love in a stimulating environment. His contagious enthusiasm and passion for biomedical engineering helped me in being the best version of myself. I would also like to say "gracias!" to Prof. Javier Sáiz for the friendly and inspiring atmosphere I had the pleasure to experience during my secondment in la Universidad Politécnica de Valencia. How can I forget to mention the multiple hours spent discussing in Zoom meetings with Dr. Amir Jadidi and Dr. Martin Eichenlaub. Dear Amir and Martin, it has been a pity not to have collaborated since the beginning, together we managed to obtain excellent scientific results and I learnt the many challenges clinicians encounter when dealing with arrhythmia in the EP lab. I hope I convinced you about the potential of computer models and if that's the case, now it is your time to spread the word.

A special thank goes to Dr. Axel Loewe, from which I learnt to be a better researcher, engineer and I must say, a better person. Your continuous support led me in completing this PhD with numerous accomplishments in such a short time. You were always available when I needed supervision and you motivated me to express my ideas and transform them into novel technology independently. The perfect mix between friendly appreciation and constructive criticism pushed me over my expectations. Your guidance and patience no matter what I was doing has helped develop me into the person I am today, thank you.

During my PhD I had the chance of meeting so many new colleagues and friends around the world, and all of you contributed to this work, even with a simple smile. Thank you all for the fun, the friendship and the shared experiences. There is a piece of each one of you in this thesis. In particular, I would like to spend some words for my team at IBT. Thanks to Dr. Jorge Sánchez for the joint challenges and successes using CARP/openCARP and the special friendship established between us. Your deep multi-scale understandings of atrial fibrillation mechanisms really enlightened me. Thanks to Dr. Ekaterina Kovacheva for the chocolate bars hidden in your drawer and your crazy laughs. I will never forget the fun we had in our office. Another long-term office mate was Andreas Wachter, thank you for your patience in explaining me atrial fiber arrangements and the tricks behind your algorithm. The trip at

Wachter winery will also stay in my memories. Thanks to Laura Unger, our clinical expert. You were always there to answer my questions, from the complex ones to how to describe in a technical way that strange "bump" on the septal wall of electroanatomical maps (transeptal punture). Thanks to Claudia Nagel, without your smiles and your statistical shape model most of this would not have been possible. Thanks to Deborah Nairn for the fun we had when sharing challenges dealing with clinical data. Thanks to Dr. Ady Naber, Dr. Yannick Lutz, Steffen Schuler, Cristian, Carmen and Patty. Our scientific and less scientific discussions, our time spent together, our various experiences helped my integration and my appreciation of different cultures. I would like to conclude the IBT team with Giorgio Luongo, with whom I struggled since the first days with German bureaucracy and I shared most experiences here in Karlsruhe. You are one of my dearest friend and a brilliant colleague. Our collaborations always delivered outstanding works. Let us see what the future will bring us, we should really consider to maintain this teamwork. Thanks to you, Michele and Giulia, I had a second Italian family in Germany.

I would like to thank all members of the Marie Curie project in which I was involved, called MY-ATRIA. The MY-ATRIA consortium gave me the perfect infrastructure to pursue this PhD and the MY-ATRIA team accompanied me in this journey. I would like to thank in particular Rebecca Belletti, you made my stay in Valencia unforgettable and your kind words and smiles comforted me many times. I wish we will stay in contact after my PhD.

Then, I thank all the friends I met during my PhD. I would like to start with my Latino's gang. Thank you Jose for the ridiculous parties and the amazing paellas. Thank you Jon, Diego, Eleonora and Claudia. We had such a great time together in Karlsruhe. Thanks Matteo, Paolo, Luca and Silvia who made my returns in Italy special.

Finally, I would like to thank my strongest team, team Azzolin, my family. Our bond became even more intense with distance. Your unconditional love and determined support led me to this success. Thank you Mamma Paola, your strength and your constant pushing me to do my best contributed to all this. Thank you Papà Sergio, your advice and encouragement have been essential to achieve what I have achieved. Thank you Alberto, the brother everyone would like to have, every time I went back to Italy you made it fun. I'll be always there for you when you'll need it, as you did for me.

Thank you all again, I feel the luckiest person on earth to have you.

Contents

Abbreviations

Ca^{2+}	calcium ion
Cl^{-}	chloride ion
K^{+}	potassium ion
Na^{+}	sodium ion
AF	atrial fibrillation
AP	action potential
AT	atrial tachycardia
AV	atrioventricular
AWT	atrial wall thickness
BB	Bachmann's bundle
BCL	basic cycle lengths
CA	catheter ablation
CDT	cardiac digital twin
CFAE	complex fractionated atrial electrogram
CS	coronary sinus
CT	computed tomography
CT	crista terminalis
CVD	cardiovascular disease
DT	digital twin
EAM	electroanatomical map
IVC	inferior vena cava
LA	left atrium
LAA	left atrial appendage
LGE	late gadolinium enhancement
LSPV	left inferior pulmonary vein
LSPV	left superior pulmonary vein
LVA	low voltage area
MI	mitral isthmus
MRI	magnetic resonance imaging
MV	mitral valve
PM	pectinate muscle
PV	pulmonary vein
PVI	pulmonary vein isolation

RA	right atrium
RAA	right atrial appendage
RD	reentrant driver
RL	roofline
RSPV	right inferior pulmonary vein
RSPV	right superior pulmonary vein
SA	sinoatrial
SR	sinus rhythm
SSM	statistical shape model
SVC	superior vena cava
TMV	transmembrane voltage
TV	tricuspid valve

Chapter 1

Introduction

1.1 Motivation

Cardiovascular diseases (CVDs) are the leading cause of death accounting for 32% of deaths worldwide [1]. Among the 17.9 million people who died in 2019, 85% were caused by heart attack and stroke [1]. Along these diseases, the incidence and prevalence of atrial fibrillation (AF) in particular is today reaching pandemic proportions. AF is the most common sustained disorder of cardiac rhythm that is estimated to affect 1.5%-2% of the general population with a prevalence that increases with age, and reaches nearly 10% in octogenarians. AF is an abnormal heart rhythm characterized by rapid and irregular beating of the atria. Often it starts as brief periods of abnormal beating which become longer and possibly constant over time. The disease is associated with an increased risk of heart failure, dementia, and stroke. The Global Burden of Disease Study estimated in 2010 a prevalence of AF of 373.1/100,000 for women and 596.2/100,000 for men [2]. Despite the higher incidence of AF in men, the prevalence of the disease among women increases among elderly. The costs associated with the care of patients with atrial disease are today reaching monumental proportions: as an example, the total annual costs of AF care in the US are approximately $7 billion and roughly €13.5 billion in the European Union [3–5]. Nearly 75% of the costs of AF represent the direct and indirect costs associated with hospitalization. The societal costs of lost productivity should neither be overlooked. Thus, this is the time actions are needed to improve diagnosis and treatment of atrial disease. Despite the prevalence of AF, the ability to treat AF is not improving, at least as assessed by age-adjusted mortality rate post-diagnosis [6]. Patients suffering of severe atrial dysfunctions are usually eligible for pharmacological, interventional (atrial ablation) or surgical treatment.

In case a patient is not responding to the drug therapy, catheter ablation (CA) is the suggested treatment for AF. CA is a standard-in-practice invasive procedure which aims at isolating the atrial tissue responsible for AF onset and perpetuation, restoring the normal heart rhythm. This is achieved performing small scars around the arrhytmogenic tissue in the heart [7]. However, a clear identification of the optimal target to ablate is still not clear and

different approaches have been proposed (e.g. isolation of selected anatomical structures, ablation of arrhythmic drivers or low voltage areas, etc.) [8–11].

A deeper understanding of the complex functioning of the heart can be achieved by developing computational models [12]. The first mathematical model of cardiac cells was presented over half a century ago. Atrial modeling has raised enthusiasm in the last few decades providing valuable insights into AF patho-physiology. Only lately, the advancement of computational resources as well as cardiac imaging and electrical measurement of the heart moved the focus of interest into using models of the human heart in clinical practice [13, 14]. The integration of computational modelling in the clinics requires a high degree of personalization, representing the patient anatomy and electrophysiology, to guide clinicians in the procedures. However, reliable patient-specific generation of atrial models is challenging due to the complex anatomy and heterogeneous electrophysiological properties of the atrial tissue with respect to the ventricles.

In this thesis, highly detailed computer models were leveraged to uncover the hidden AF mechanisms of initiation and maintenance and tailored virtual hearts were used to foresee the optimal treatment for a specific patient. Novel methods were developed to incorporate experimental and clinical data into models to analyze, characterize and treat AF using in-silico experiments. The full predictive potential of computational modelling was exploited to make a step forward into personalized medicine.

1.2 Objectives of the thesis

The general aim of this thesis is to develop computational models of the human atria with AF to advance the basic understanding of AF onset and perpetuation and guide physicians in AF vulnerability assessment and ablation procedure planning. Personalized computer models can be used to identify the optimal ablation strategy therefore reducing the invasive procedure time and improving the patient's outcome. Two major topics will be integrated in this thesis: the assessment of arrhythmia vulnerability using in-silico experiments and the implementation of personalized atrial models integrating clinical data for tailored ablation strategies. The leading aims of the first project are:

- Develop and propose a method to reproducibly evaluate AF vulnerability in atrial models;
- Evaluate the influence of heterogeneous anatomical thickness in AF onset and perpetuation.

The second topic described in this thesis covers the following aspects:

- Design and implement an automated pipeline to generate patient-specific atrial models augmenting and integrating clinical data;
- Provide a tool helping the cardiologist in tailored ablation planning and predict the patient's outcome.

1.3 Structure of the thesis

The relevant amount of knowledge and publications produced throughout the PhD program has been considered adequate for a cumulative thesis. Having a significant number of published (or at least submitted) studies, the repetition of content already expressed in their best form in the respective articles has been considered dispensable. Nonetheless, this cumulative thesis wants to combine and present all contributions accepted and reviewed by the scientific community as improvements in the technical and clinical field of biomedical engineering.

Chapter 2 and 3 present medical and technical fundamentals necessary for understanding the methods, results, and discussion specified in this thesis:

- **Chapter 2** contains an overview on the medical background relevant for this work. Briefly, human heart anatomy and physiology, patho-physiology of AF, screening modalities and ablation treatment are outlined;
- **Chapter 3** summarizes the multi-scale computational modeling methods used in cardiac electrophysiology. Micro-scale modeling of the cardiac cell and macro-scale models at the tissue and organ level are presented.

Chapter 4 and 5 consist of the main body of the thesis. Here, two major topics are introduced. The link between various manuscripts that are part of the same main topic is explained, followed by the related papers submitted, and published:

- **Chapter 4** contains our contribution on investigating the influence of different inducing protocols on both AF initiation and maintenance (journal paper 1 [15]), along with evaluating the impact of heterogeneous anatomical thickness on AF vulnerability (journal paper 2 [16]);
- **Chapter 5** outlines the studies leveraging patient-specific computational model to guide targeted ablation strategies. A framework to augment missing anatomical structures from geometrical data is implemented (journal paper 3 [17]) and is integrated in a unique pipeline to generate anatomical and functional atrial digital twins of patients with AF (journal paper 4 [18]). Finally, a novel technology to propose personalized ablation strategies and prevent the onset and continuation of AF is developed (journal paper 5 [18]).

Chapter 6 summarizes progress in the field achieved by the portfolio of projects presented here outlining the findings to build cardiac digital twins to personalize ablation. It provides relevant perspectives that could serve as a base for future studies. It draws conclusions on the feasibility of personalized medicine.

Appendix contains the supplementary material of each paper attached in this thesis. A reference is included in the respective manuscript.

During the three and a half years of research leading to this thesis, I published two journal papers and five conference contributions as first author, and additional two journal publications are under review. As a co-author, three journal papers, three conference contributions were published and won an award for patient safety in biomedical engineering in collaboration with Giorgio Luongo [19]. Moreover, I got invited to one international conferences as speaker and I won two travel grants to participate to a Summer School in Oslo and San Diego and to a Gordon Research Conference. To conclude, I supervised seven student theses/projects that partly form the basis of the work presented here (cf. *List of Publications and Supervised Thesis* at the end of this thesis).

Chapter 2

Medical fundamentals

In this chapter, the essential medical fundamentals to understand the studies presented in this thesis are described and put into context. Firstly, the human heart anatomy and physiology are briefly introduced and the atrial anatomy and their fiber architecture is specified. Then, cardiac electrophysiology is summarized with a particular focus on atrial fibrillation. Later, state-of-the-art diagnostic tool as tomographic segmentations and electroanatomical maps are discussed. Finally, ablation therapy as arrhythmia treatment is presented. For a more detailed introduction to the specific topics, the interested reader is referred to the respective references.

2.1 Human heart anatomy and physiology

The human heart is a cone-shaped, muscular hollow organ and its size is comparable to a closed human fist [21]. It is located at the center of the thorax and enclosed in the pericardial sac, which secures the heart during several physiological functions, for example, ensuring smooth movements during contraction or relaxation. The heart is a four-chambered system anatomically and functionally divided by the septum in two halves, each one composed of an atrium and a ventricle. Both chambers are separated by the atrioventricular plane and connected via valves controlling the blood flow (right: tricuspid valve (TV), left: mitral valve (MV)) (Figure 2.1) [22]. The ventricles function as a pump ejecting blood containing oxygen and nutrients from the left ventricle into the aorta and deoxygenated blood with metabolic waste from the right ventricle into the pulmonary arteries. The atria gather the blood flowing from the veins and accessing the heart, consequently preventing circulatory inertia [23]. Specifically, the right atrium collects the deoxygenated blood from the body via the superior (SVC) and inferior vena cava (IVC). The right atrial contraction re-inject the blood into the right ventricle before being pushed into the pulmonary system. Here, the capillary lung bed oxygenates the blood before accessing the left atrium via the pulmonary veins (PVs). Finally, the blood volume flows into the left ventricle through the mitral valve.

The heart supplies blood containing oxygen and nutrients to the organs and other body systems while carrying away carbon dioxide and metabolic waste from the organs in order to

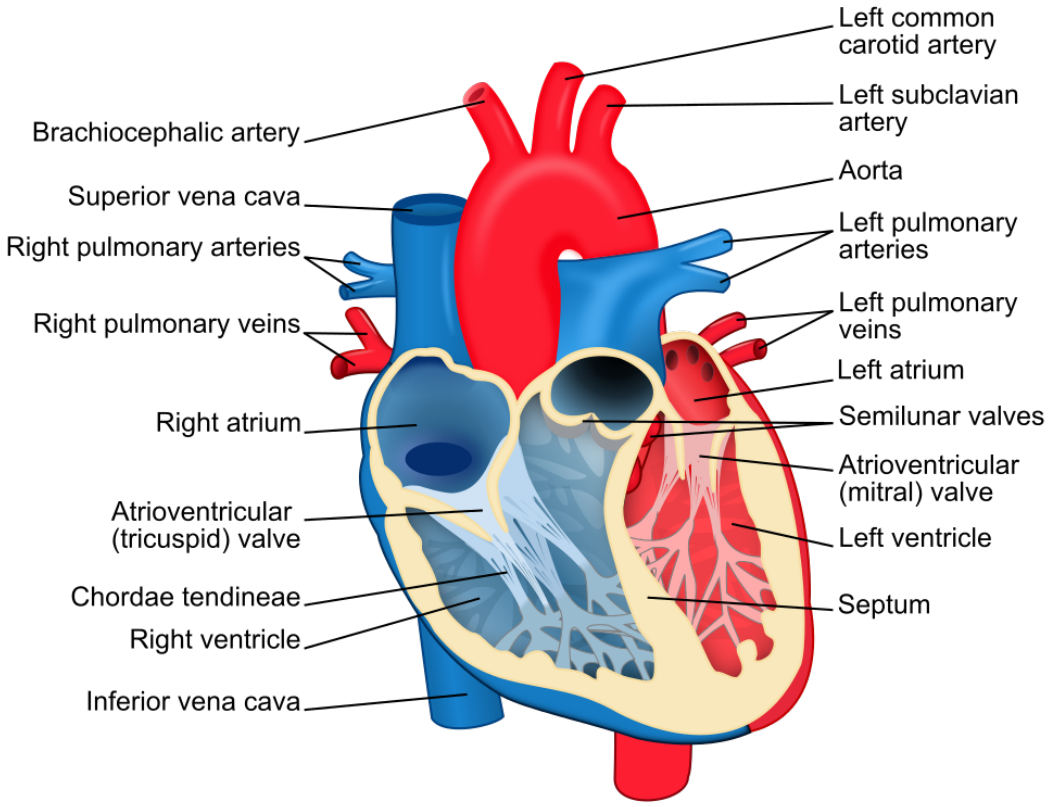

Figure 2.1: Human heart anatomy. Adapted from [20] and licensed under Creative Commons Attribution-Share Alike 3.0 Unported.

excrete them (Figure 2.2). Deoxygenated blood returns from the body to the right atrium via the superior and inferior vena cava. Due to the contraction of the right atrium, the blood is injected into the right ventricle through the tricuspid valve. Subsequently, a ventricular contraction pushes the blood volume into the pulmonary system. After oxygenating the blood in the capillary lung bed, the blood enters the left atrium via four pulmonary veins (PVs), also described as left and right PVs. The blood then flows through the mitral valve into the left ventricle. The contraction of the left ventricle pushes the blood via the aortic valve in the systemic circulation [25].

2.2 Atrial anatomy and fiber architecture

The atria consist of two chambers, left and right, which can be distinguished in various regions with different properties and pronounced muscular bundles (Figure 2.3). The atrial myocardium forms a functional syncytium composed of discrete myocytes electrically coupled to, on average, eleven neighbors via gap junctions [27]. Single myocytes have an elongated shape that roughly resembles a prolate spheroid and has a tendency to be

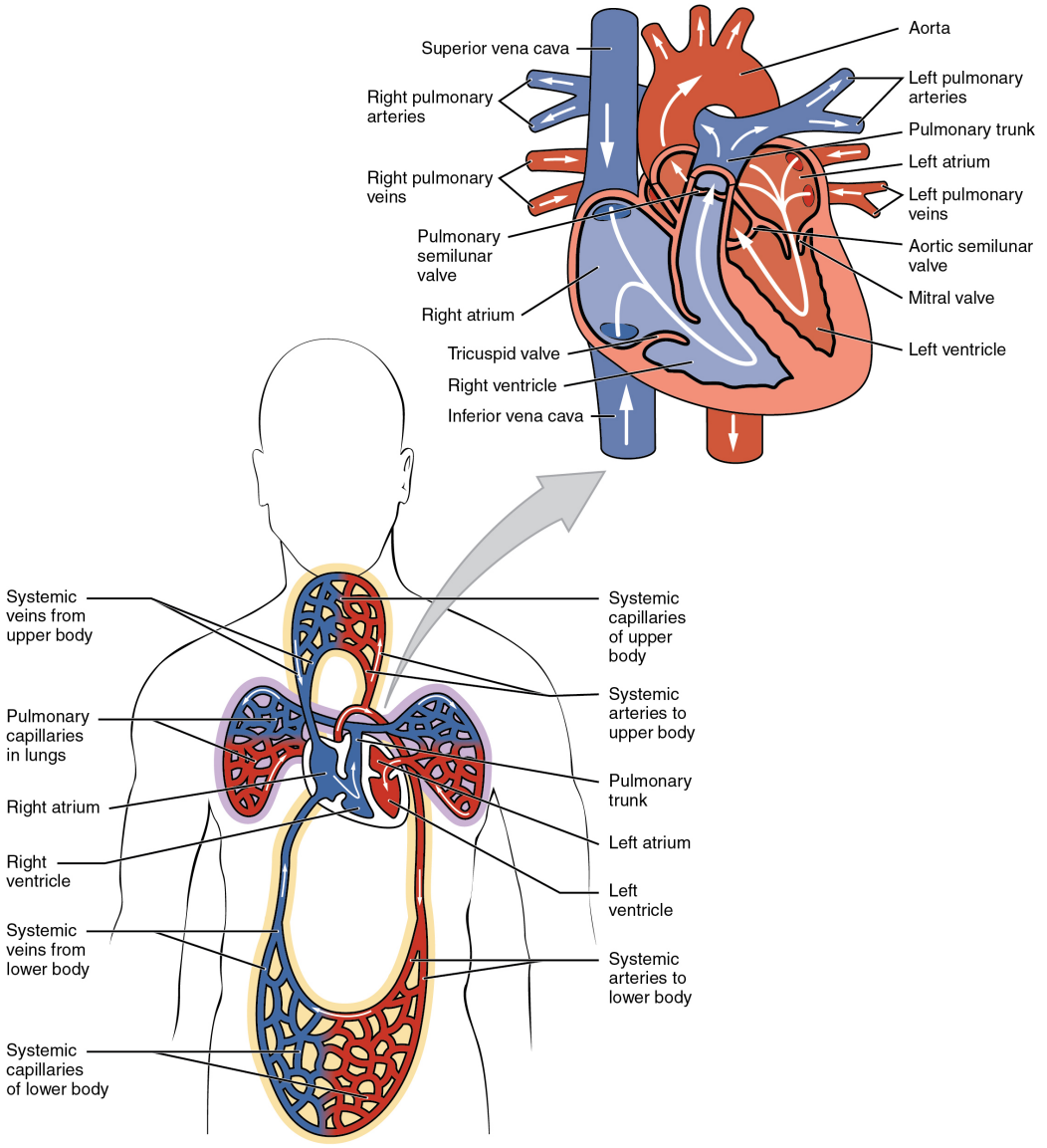

Figure 2.2: Dual system of human circulation. Blue components indicate de-oxygenated blood pathways and red components indicate oxygenated blood pathways. Adapted from [24] and licensed under Creative Commons Attribution-Share Alike 3.0 Unported.

arranged following their longest semi-principal axis. In addition, their conductivity is greater longitudinal to the principal axis than perpendicular to it since the gap junctions are concentrated at the myocytes' extremities and the number of membrane crossing per unit length is lower [27].

The right atrium (RA) is comprised of a collection of independent bundles and can be differentiated into four major components: the right atrial appendage (RAA), the smooth and the rough section of the posterior wall, and the septum [28]. The largest muscle bundles in the RA are the crista terminalis (CT) [28, 29], from 15 to 20 pectinate muscles (PMs) [30, 31]

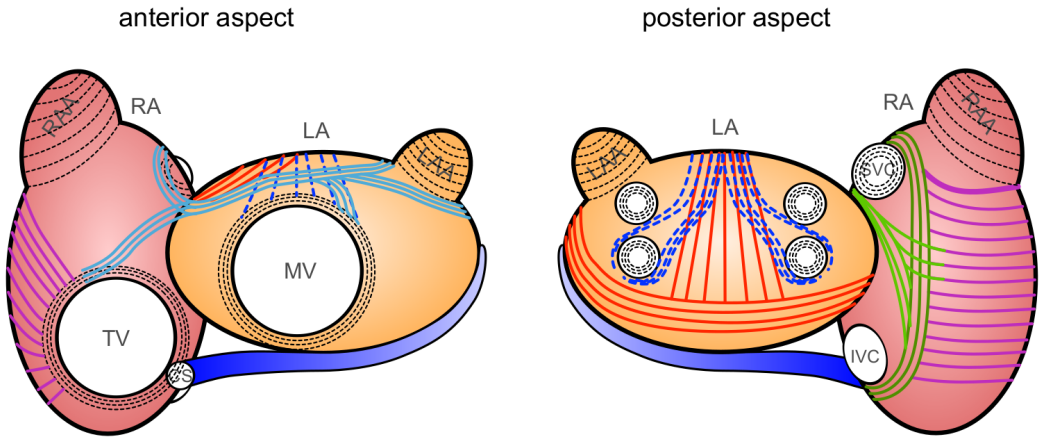

Figure 2.3: Schematic representation of the major atrial fiber bundles and layers. Blue: endocardium, red: epicardium, light blue: Bachmann's bundle, green: crista terminalis and intercaval bundle, pink: pectinate muscles, black: circular fiber orientation around vessel orifices and valves as well in the appendages. Adapted from [26] and licensed under Creative Commons Attribution-Share Alike 3.0.

with complex morphology, Bachmann's bundle (BB), the intercaval bundle, and the tricuspid valve (TV). The smooth and the rough parts of the free wall are separated by the CT ridge [32], the most prominent structure in the RA [28, 29]. The CT runs on the posterior wall emerging from the right side of the SVC orifice, extending on the right side of the IVC orifice towards the coronary sinus (CS) region where it smooths out [22]. The width of the CT reduces from the SVC to the IVC [29]. The posterior wall, in addition, is characterized by the fossa ovalis, the sinoatrial node (SA node) and the atrioventricular node (AV node). Finally, the RA is connected to the ventricle through the atrioventricular opening (TV).

The left atrium (LA) is located with its posterior wall next to the esophagus. It has a smooth endocardial surface [32], with the exception of the left atrial appendage (LAA), located in the supero-anterior region of the left superior pulmonary vein (LSPV), whose endocardium exhibits a rough surface [33]. Two layers of myocardial fibers overlapping each other characterize the LA (Figure 2.3). In contrast to ventricular fiber architecture, in which the myocytes' orientation smoothly varies transmurally, the transmural change in fiber organization between the layers is abrupt. Compared to the right atrium, the fiber orientation is organized in two rather continuous layers (Figure 2.4).

2.2.1 Inter-atrial connections

The atria are electrically decoupled from the ventricles by a valve plane and they are separated from each other by the atrial septum. The septum consists of an isolating layer that separates LA from RA, but both sides of the septum are covered with regular myocardium. Inter-atrial conduction is, therefore, possible only via various inter-atrial bridges [34]. The most prominent inter-atrial bundle is the BB, located on the supero-anterior side. It runs between the appendages surrounding them partially after splitting into two branches [32]. In addition,

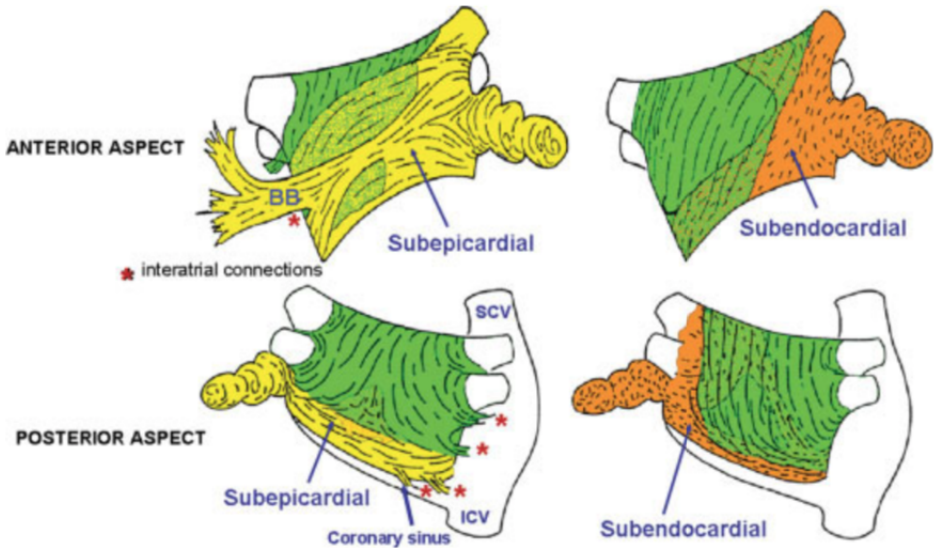

Figure 2.4: Schematic drawing of the left atrium's fiber orientation. Top row: anterior view of epicardium and endocardium. Bottom row: posterior view of epicardium and endocardium. The inter-atrial bundles are marked with red stars. Adapted from [26] and licensed under Creative Commons Attribution-Share Alike 3.0.

the CS consists of functional myocardium also conducting electrical propagation between LA and RA. While the inter-atrial conduction via the BB and the CS is present in most humans, the electrical propagation via additional inter-atrial bundles on the anterior and posterior side is highly variable between individuals [34–36]. Especially the middle and lower inter-atrial bridges, present, respectively, in 67% and 87% of the population [26], are generally non-conductive in old or diseased patients since they are more vulnerable to conduction block due to their thin and fragile structure.

2.2.2 Anatomical wall thickness

Atrial myocardial wall thickness varies non-uniformly between 1 mm and 4 mm [28, 29, 31, 32, 37] (Figure 2.5). Dominant muscular bundles (CT, PMs) characterize the wall thickness in the RA [28, 29]. The CT is the most pronounced structure reaching a thickness of 3.5-4.2 mm [37]. Instead, the LA shows a smoother wall thickness variation, with the posterior and inferior parts thicker than the roof and the pulmonary veins [37, 38].

2.3 Electrophysiology

The variations in transmembrane voltage (TMV) are governed by the excitation of the cardiac cell. Cardiomyocytes contraction is driven by electrical stimulation. The cell membrane is selectively permeable for specific types of ions (mainly Na^+, K^+ , Ca^{2+}) through ionic

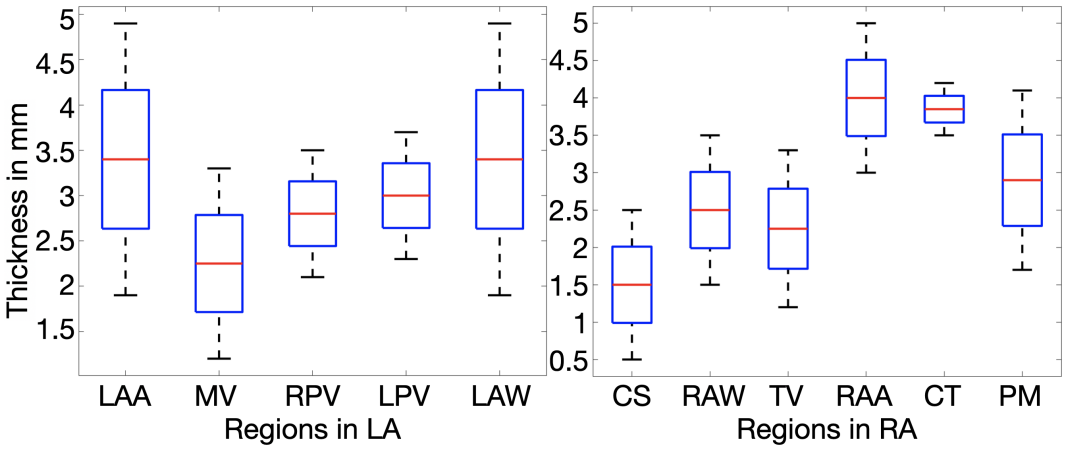

Figure 2.5: Physiological regional anatomical thickness ranges in human atria. Data taken from [28, 29, 31, 32, 37]. LA=left atrium, RA=right atrium, LAA=left atrial appendage, MV=mitral valve, RPV=right pulmonary veins, LPV=left pulmonary veins, LAW=left atrial wall, CS=coronary sinus, RAW=right atrial wall, TV=tricuspid valve, RAA=right atrial appendage, CT=crista terminalis, PM=pectinate muscles.

channels, pumps and exchangers. Each opening is permeable for one or multiple ions. Under physiological conditions and without external stimulation, the distribution of ions in the extracellular and intracellular medium across the cell membrane yields a resting membrane potential of approximately -80 to -90 mV in cardiac cells. The opening and closing of ion channels are controlled by changes in TMV and, consequently, ions move across the membrane. Therefore, the action potential (AP) is defined as the characteristic TMV trace coordinated by the interaction of multiple ion channels. The typical waveform of an AP subdivided into the main four phases is shown in Figure 2.6.

When an external stimulus raises the potential between the extracellular and the intracellular space above a certain threshold, the so-called activation threshold (-50 to -60 mV), the sodium (Na^+) channels open, followed by an abrupt influx of Na^+ ions. This is called depolarization/upstroke phase (Phase 0). The gradual closing of the Na^+ channels leads to the overshoot of +20 mV and a consequent efflux of potassium (K^+) and influx of chloride (Cl^-) ions (Phase 1). Next, the AP settles at about 0 mV leading to the long plateau phase during which calcium (Ca^{2+}) ions flow into the cell balancing the repolarization currents (Phase 2 in Figure 2.6). Dependent on the heart rate and the cell location, the Ca^{2+} inward currents last for 200-400 ms determining also the length of the plateau. With the decay of these Ca^{2+} currents, the cell activation enters the repolarization phase (Phase 3 in Figure 2.6). Mainly slow and rapid K^+ outward currents drive the TMV back to the resting potential of -90 mV. There, the rapid and slow K^+ outward channels close and certain inward K^+ channels open again that are enabled during the resting phase (Phase 4 in Figure 2.6). Here, the cell can be activated again, whereas during the plateau phase, the cell is in the absolute refractory period, i.e., a new activation is not possible. During the repolarization phase, the cell is in the relative refractory period allowing the cell to respond to an activation impulse

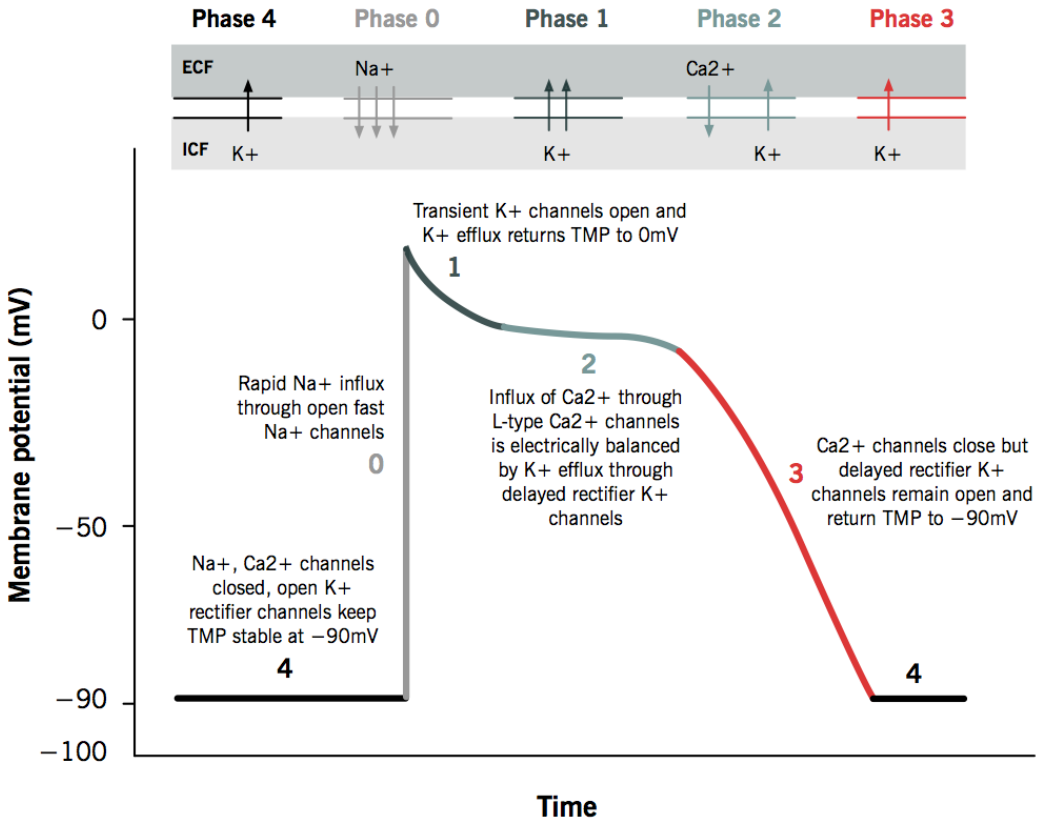

Figure 2.6: Physiological human cardiac action potential. The four characteristic phases of the action potential are presented along with the main ion flux. Phase 0: Upstroke/Depolarization, fast Na^+ influx; Phase 1: Overshoot, Na^+ channels close; Phase 2: Plateau, Ca^{2+} influx; Phase 3: Repolarization, K^+ outflux; Phase 4: Resting membrane potential. Adapted from [39], and licensed under the Creative Commons Attribution-Share 3.0 International License.

but with an attenuated response due to partial repolarization [40]. Gap junctions allow action potentials to spread through the cardiac tissue in a coordinated manner.

At a macroscopical level (Figure 2.7), the electrical activation is started by the sinus node, initiating the process of depolarization. The sinus node (SN) cells are pacemaker cells able to periodically self-excite themselves at a regular rhythm, the so-called sinus rhythm. Typically, the sinus rhythm of an adult human is between 60-80 beats per minute (bpm) in rest. The activation propagates from the SN throughout the right atrium and to the left atrium by means of the Bachmann's bundle. The electrical impulse spreads to the ventricles via the AV node, the second pacemaker in the human heart. A specialized conduction pathway provides a well defined sequence of activation of atria and ventricles. This system consists of a common bundle, the bundle of His (third pacemaker), which separates into two branches when entering the septum. The left and right bundle branches further bifurcate in the Purkinje fibers and propagate along the ventricular myocardium, ensuring a fast stimulation of the whole ventricular wall. The ventricular myocardium is activated from the apex to the base and from the endocardium to the epicardium.

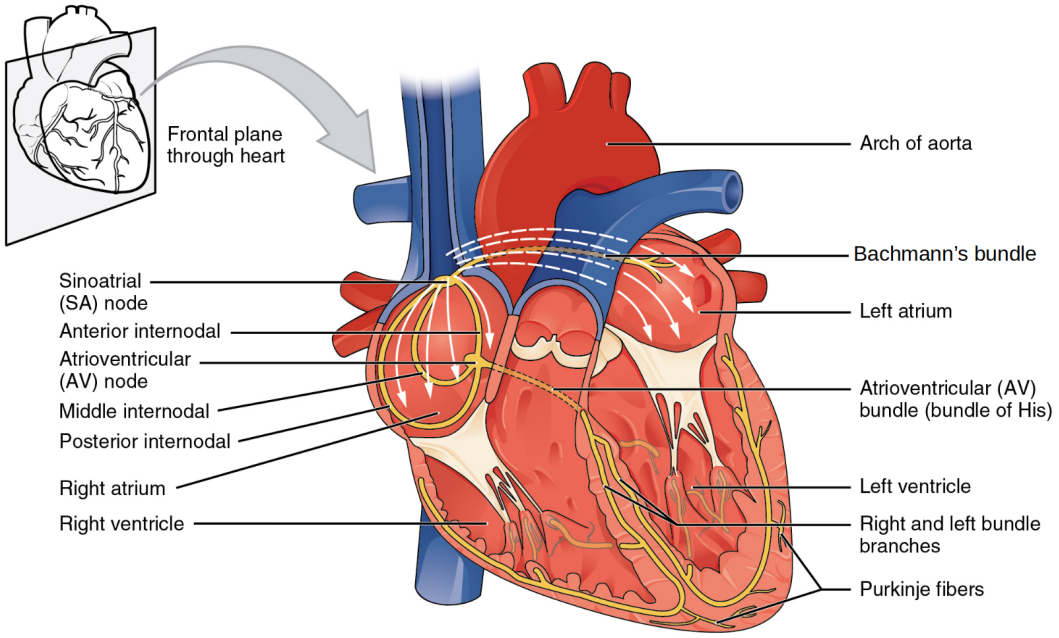

Figure 2.7: Electrical conduction system of the heart. Adapted from [41] and licensed under Creative Commons Attribution-Share Alike 3.0 Unported.

While the physiological rhythm of a healthy heart is driven by the SN, other rhythms are considered as arrhythmias. If the SA node fails to trigger the excitation, the AV node can compensate the primary dysfunction delivering a heart rate of 40-50 bpm. Ultimately, the "Bundle of His" can initiate the heart electrical activity delivering a heart rate of 30-40 bpm [22].

2.4 Atrial fibrillation

Atrial fibrillation (AF) is the most prevalent arrhythmia affecting over 8 million people in the European Union [42]. There is a global prevalence of 43.6 million individuals worldwide suffering from AF or atrial flutter (AFl) [43] with several associated comorbidities leading to significantly higher mortality accounting for 20-30% of all strokes in the general population [43, 44]. AF is characterized as a supraventricular tachyarrhythmia with uncoordinated atrial electrical activation and consequently ineffective atrial contraction [43]. The chaotic and irregular atrial excitation disturbs the sinus rhythm leading to heavy limitations in patients suffering from it [45]. Clinically, AF is categorized as [43]:

- First diagnosed, if no episode was diagnosed before, irrespecitve of its duration or severity;
- Paroxysmal, if episodes are self-terminating within a maximum of 7 days from onset (typically within 48 hours);

- Persistent, if AF episodes are maintained beyond 7 days, including the ones terminated by drugs or electrical cardioversion after 7 days;
- Long-lasting persistent, if AF is sustained for more than one year;
- Permanent, if the arrhythmia is accepted by both patient and physician and no further attempts to restore sinus rhythm are undertaken. In these cases, the rate is controlled [46].

Despite several decades of extensive research, gaps in understanding the mechanisms of AF still exist, making successful treatment particularly challenging. Electrophysiological and structural abnormalities have been shown to underlie AF onset and maintenance [47–49]. However, the contribution of the atrial microstructure to both the development and persistence of AF in the diseased human atria has not been clearly understood. AF can be caused by a variety of pathophysiological mechanisms [50, 51]. These range from structural and electrical abnormalities, tissue remodeling and inflammation [52, 53]. When the atrial myocardium has electrical or structural defects, the atrial contractions become irregular and there is an uncoordinated flow of blood into the ventricles.

Nowadays, AF is thought to be caused by certain triggers, such as a single rapidly firing focus in the atria or rotational re-entrant electrical waves called micro-reentries or rotors [54, 55]. A focal source is a localised trigger depolarizing periodically. Rotors describe a spiral electrical wavefront rotating around a core in clockwise or anticlockwise direction. Both mechanisms can subsequently cause fibrillatory propagation through the heart [54]. Studies have shown that rapid foci firing occurs most frequently in the pulmonary veins or at the base of pulmonary veins [56]. In these locations, the myocardial tissue is prone to instigate repetitive firing or in some cases, episodic re-entrant activation of the veins [57]. The exact mechanisms behind AF initiation due to rapid firing have not been fully elucidated, but it may potentially involve enhanced automaticity, triggered activity or micro-reentry [55, 58]. The focal rapid firing activity in the atria seems to be the main cause of paroxysmal AF and is the rationale behind pulmonary vein isolation as a treatment option. While triggers for persistent AF are commonly also located in the pulmonary veins, exclusive pulmonary vein isolation in persistent AF has a low success rate [14]. Thus other triggers or drivers may be involved in longstanding AF, although they are still not well elucidated [55, 58]. Other mechanisms were also identified as likely AF drivers, i.e., circus movement reentry, leading circle concept, and multiple wavelet hypothesis [59]. Finally, simultaneous sub-epicardial and sub-endocardial optical mapping observations proposed the hypotheses that AF is driven by micro-anatomic intramural reentry. This theory finally suggested that focal sources appearing on the atrial surface are just the manifestation of intramural micro re-entrant waves. Therefore, in this thesis, we only considered rotors as AF driver mechanisms.

Abnormalities to the atrial tissue substrate, causing non-uniform or slowed conduction, can facilitate the maintenance of arrhythmia in persistent AF patients [49]. As a result, multiple excitation wavefronts can propagate through the atrial myocardium and perpetuate the arrhythmia [60]. The high failure rates of pulmonary vein isolation in patients with persistent AF is, therefore, possibly due to the lack of detection and treatment of the abnormal

atrial substrate perpetuating AF [14, 61]. Specific localized areas in the atrium were proposed as "driver domains" acting as unstable reentry circuits [10]. Re-entrant waves within the atrial myocardium are mostly possible due to slow conduction and shorter refractory periods [60].

It is believed that the advancement of paroxysmal to persistent AF is a result of progressive structural and electrical changes in the atria [49]. Fibrosis is a structural change in the atria that has been shown to create abnormal AF substrates that can sustain rotors and further prolong AF. Fibroblasts act by electrically coupling to cardiomyocytes before proliferating and promoting ectopic activity and/or reentry [62]. Along with that, AF inducibility is progressively increased with increasing levels of fibrosis in the heart [49]. This can potentially induce the creation of re-entrant circuits that will further propagate AF [49]. However, even after only 2 weeks of persistent AF, cardiac tissue develops irreversible electrophysiological remodelling [49]. Pathological changes of the cardiac ion channels can lead to ectopic firing by hyperactivating intracellular ion channels [62]. Repeated sympathetic activation of the myocardium can cause remodelling of the cardiac autonomic neural tissue to promote further persistence and recurrence of AF [63]. All these modifications have been shown to occur in the presence of AF, explaining the concept that “AF begets AF” [63, 64]. Therefore, protracted periods of continuous AF episodes heavily affect a patient’s ability to restore and maintain normal sinus rhythm [60]. Along with that, there is also a reduced possibility of spontaneous AF termination [60].

2.5 Multimodality imaging for atrial fibrillation

In this section, an introduction to clinical multimodality imaging to diagnose AF is presented. Imaging techniques for human atria can be separated into non-invasive and invasive methods. Tomographic imaging, for example, computed tomography (CT) and magnetic resonance imaging (MRI), are the standard-in-practice non-invasive imaging techniques, which allow three-dimensional assessment of LA volumes and specific anatomic features. Considered gold standard for assessment of LA volumes [65], is discussed in Sec. 2.5.1. Invasive mapping systems provide real-time electroanatomic information, electrophysiological data and are currently preferred to guide ablation. They are presented in Sec. 2.5.2.

2.5.1 Tomographic imaging

Tomography is imaging by sections or sectioning through the use of any penetrating wave [66]. Nowadays, CT and MRI scans are the most used non-invasive techniques to image the human heart. CT scanners employ a rotating X-ray tube and a series of detectors located in the gantry to quantify X-ray attenuations by different tissues inside the body. Tomographic (cross-sectional) images (virtual "slices") of a body are finally produced, processing the multiple X-ray measurements taken from different angles using reconstruction algorithms. Even though its use is sometimes restricted due to the side effects of the ionizing radiations, CT can be performed on patients with metallic implants or pacemakers where

MRI is contraindicated. Due to its sub-millimeter resolution, CT is preferable for a detailed reconstruction of the heart anatomy and nearby structures.

Instead of X-rays, MRI scanners use strong magnetic fields, magnetic field gradients, and radio waves to generate images of the organs in the body. Cardiac MRI has emerged as a viable tool for interrogating the underlying substrate in AF patients when used in combination with a contrast medium, e.g., gadolinium. Late gadolinium enhancement MRI (LGE-MRI) has the advantage of providing an approximated localisation and quantification of regions with structural remodelling. Late gadolinium enhancement is a result of regional differences in myocardial extracellular volume and different uptake and washout patterns within the extracellular space. It is typically measured around 10-20 min after administration of a gadolinium-based contrast agent. Cardiac MRI of the atrial substrate is not only a tool for management and treatment of arrhythmia but also to individualise the prevention of stroke and major cardiovascular events [67].

The use of image integration during catheter ablation may significantly improve the outcome of the procedure. In patients treated with catheter ablation using image integration, the atrial fibrillation-free survival rate was significantly higher when compared with patients who were treated with conventional electroanatomic mapping alone (atrial fibrillation-free survival rate 88 vs. 69%, $P < 0.05$) [68].

2.5.2 Electroanatomical maps

3D reconstruction of the cardiac anatomy combined with electrophysiological information is the basis for mapping and ablation of complex atrial and ventricular arrhythmias [69]. Precise identification of a catheter tip in 3D space combined with the acquisition of essential information about tissue integrity have largely improved the ability to navigate catheters within the cardiac chambers to areas of interest. Several mapping systems exist. The three most commonly used 3D electroanatomical mapping systems are the Carto system (Biosense Webster, Diamond Bar, California), NavX Ensite (St. Jude Medical, St. Paul, Minnesota) [70] and Rhythmia HDx (Boston Scientific, Marlborough, Massachusetts). All three 3D mapping systems are used to map the cardiac chambers and allow for 3D reconstruction of the mapped chambers. Electroanatomical mapping helps to minimize exposure to ionizing radiation by minimizing fluoroscopy, which is used conventionally to guide catheter manipulation [71].

The recorded signals from a mapping catheter are known as unipolar electrograms. Each electrode measures the extracellular potential with respect to a far away reference ground electrode. Typically, the artifacts produced by the patient, the recording system, and the clinical environment highly affect the unipolar electrograms. The difference between a pair of electrodes constitutes the so-called bipolar electrogram, which is the most common signal used during a typical clinical electrophysiology study. The advantage of computing bipolar signals is that far-field effects cancel out. However, bipolar electrograms are really sensitive to the orientation of the electrode pair in respect to the electric propagation wavefront. Lately, omnipolar electrograms have been proposed as a promising method to overcome the directional dependence of the bipolar electrogram. The omnipolar electrogram calculation

evaluates all possible bipolar electrode orientations using four electrograms and computes the electrode orientation–independent electrograms along the maximal bipolar direction.

An electro-anatomical mapping system is a fundamental tool for guiding ablation procedures. The term electro-anatomical mapping is related to the assignment and displays in real-time encoded information (i.e., voltage, activation time) according to its spatial coordinates.

2.6 Ablation therapy

Catheter ablation is the recommended treatment in patients with AF who are resistant to antiarrhythmic drugs [43, 46]. Currently, this is the therapy with the highest success in terminating AF compared with all other methods [7]. Ablation therapy is a minimal-invasive treatment that consists in destroying the pathological tissue of the heart and restoring sinus rhythm by interrupting abnormal electrical circuits or pacing. Ablation can be performed by heating (radio-frequency ablation) or cooling (cryo ablation) the cardiac tissue. Clinical studies showed comparable effectiveness for both methods in electrically isolating the myocardial tissue [72]. Pulmonary vein isolation (PVI) is since the work of Haïssaguerre et al. [56] in 1998, the standard-of-care in cathether-ablation for AF. The PVs are usually isolated circumferentially from the left atrial myocardium to isolate ectopic triggers and micro-reentries in the PV sleeves. While this technique shows high success in paroxysmal and persistent AF patients, it is still sub-optimal in patients with long-standing persistent AF (<70% [73]). Patients can suffer from frequent recurrence of AF even after successful ablations. In these cases, electrical remodelling and fibrosis are often responsible for the patient's relapse after the initial success. Moreover, the low success rate can be due to the intrinsic progressive degenerative nature of AF, to a still poor understanding of AF triggers and their persistence, and to the limited tools to identify AF drivers. Multiple clinical trials failed to prove the effectiveness of empirical extra-PV ablation techniques (linear ablation[73], complex fractionated atrial electrogram-guided ablation [74], rotor ablation [75], low-voltage-area homogenization [76]) with respect to PVI alone [73]. On the contrary, recent studies that remain to be reproduced reported remarkable success rates of focal sources and rotor ablation [9, 10]. Therefore, tailored ablation strategies guided by computational models [13, 77, 78] could be a valuable tool to improve success-rate of catheter ablation.

Chapter 3

Computational modelling of cardiac electrophysiology

In this chapter, the fundamentals of computational modelling applied to cardiac electrophysiology are presented. Cardiac electrophysiology is intrinsically a complex and multi-scale biophysical and phenomenological problem. Selected approaches ranging from cellular electrical activity to the spread of electrical potential in the heart will be presented. At first, the microscopic level is described with the modeling of cardiac cells in Section 3.1. Then, the computational methods used to simulate electrophysiological phenomena at tissue and organ scale are discussed in Section 3.2. The interested reader is referred to the respective references for a more detailed introduction to the topics.

3.1 Cardiac cell modeling

The ionic membrane currents were firstly described by Hodgkin and Huxley by a mathematical model based on their findings on the giant squid axon [81]. The transmembrane voltage V_m is defined as the difference between the intracellular potential Φ_i and the extracellular potential Φ_e. The cell membrane is represented by an electric circuit with a capacitor and the different ion channels in parallel. The several ion channels are expressed as variable resistors in line with the respective Nernst voltages that are represented by voltage sources. The resulting scheme is a system of nonlinear-coupled ordinary differential equations, which describes the electrical behaviour of a human myocyte by calculating ion concentrations, ionic currents, bindings to intracellular structures, and transmembrane voltage. The change in transmembrane voltage V_m is described by:

$$\frac{dV_m}{dt} = -\frac{I_{ion} + I_{stim}}{C_m}, \tag{3.1}$$

where V_m is the transmembrane voltage (TMV), C_m is the capacity of the cell membrane, I_{stim} is an optional stimulation current and I_{ion} is the ion current through the membrane. Later on, a specific model of human atrial myocytes was delivered by Courtemanche et al.

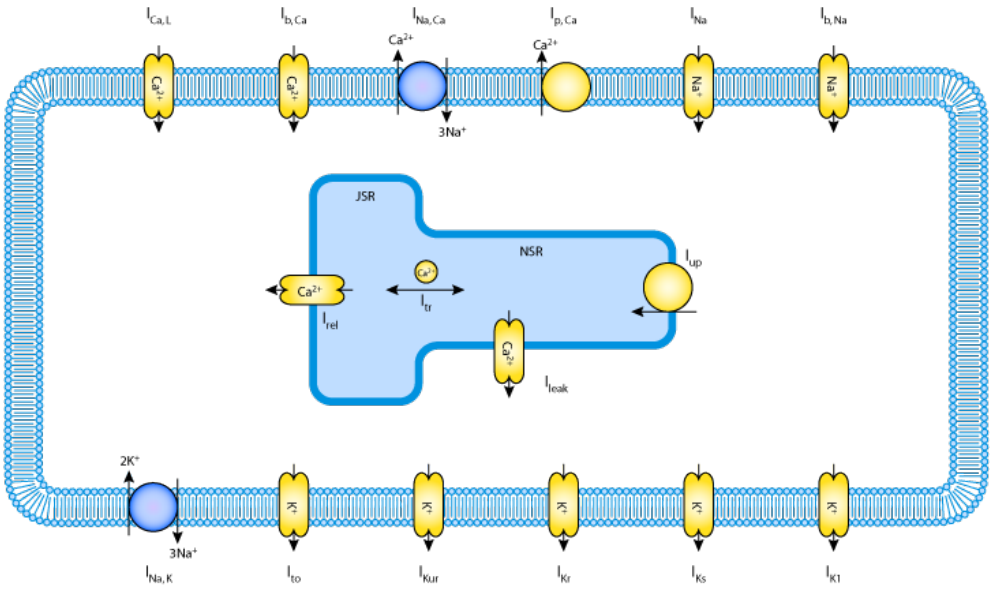

Figure 3.1: A schematic representation of currents, pumps and exchangers included in the Courtemanche-Ramirez-Nattel model. Adapted from [79, 80].

in 1998 [82]. Differently from Hodgkin-Huxley, the Courtemanche model considers more different ionic currents corresponding to ion-channels, exchangers, and pumps (see Figure 3.1). In the Courtemanche model, the net current across the cell membrane I_{ion} is given by the sum of twelve ionic currents, each of them defined following Ohm's law as the product of the specific ion channel conductivity and an ion specific voltage weighted with a product of gating variables. Thus, the results of this model are better suited for the simulation of atrial activity [82].

Moreover, in order to leverage in-silico methods to gain mechanistic insight into AF patho-physiology, and to evaluate therapeutic strategies, it is important to consider in the models the remodeling processes that undergo in the atria exposed to fibrillation for a long time. Maximum conductivities of the ion currents were altered based on a rigorous literature research [59]. For this reason, a modification of the Courtemanche et al. model of human atrial myocytes was used in this thesis (Figure 3.2). The remodeled Courtemanche et al. model provides mechanistic descriptions of how remodeling increases susceptibility to reentry through shortened wavelength facilitating the initiation and maintenance of atrial arrhythmic episodes.

3.2 Tissue and organ modeling

In this section, we present the bidomain equations [84–86], as a model to represent the electrical wave propagation across the myocardium. Then, a simplification of the bidomain

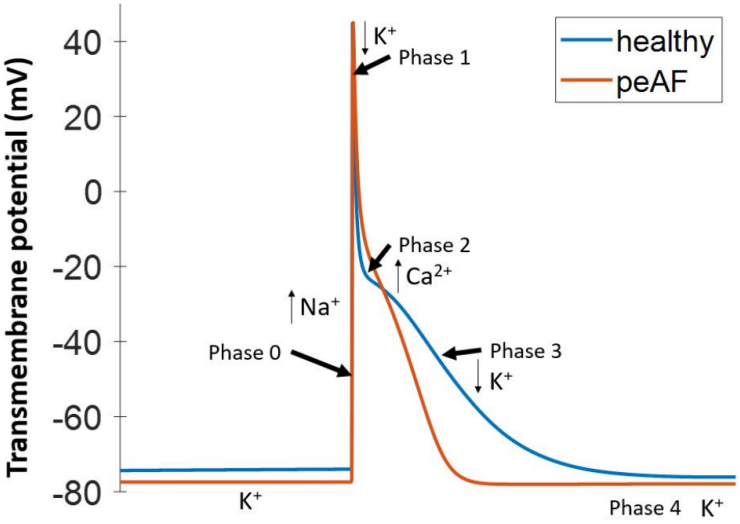

Figure 3.2: AP from an atrial myocyte under AFib remodeling conditions [59]. Adapted from [83].

model, the monodomain equation, is derived. The monodomain equation, due to its easier implementation and computational cost, is used in this work.

3.2.1 Bidomain equations

The bidomain equations [87] can be formulated from Ohm's law and the continuity equation in both intracellular and extracellular domain. The continuity equations are:

$$\nabla \cdot J_i = -I_m, \tag{3.2}$$

$$\nabla \cdot J_e = I_m, \tag{3.3}$$

where J_i and J_e are the current densities (A/m^2) in the intracellular and extracellular domains and I_m is the membrane current per unit volume (A/m^3). The negative sign in equation 3.2 is a sign convention indicating that the current leaving the intracellular domain is positive. Adding equations 3.2 and 3.3 gives

$$\nabla \cdot (J_i + J_e) = 0. \tag{3.4}$$

This implies the conservation of total current.

The membrane current is composed of a capacitive current (I_c) due to the dielectric nature of the cell membrane and an ionic current (I_{ion}) due to currents flowing through different ion channels, pumps and exchangers. Hence

$$I_m = \beta \left(C_m \frac{dV_m}{dt} + I_{ion} \right), \tag{3.5}$$

where V_m is the transmembrane potential (mV), β is the ratio of membrane surface area to tissue volume (surface-to-volume ratio) (1/m), C_m is the membrane capacitance per unit area (F/m^2).

The transmembrane potential can be written in terms of the extracellular (ϕ_e) and intracellular (ϕ_i) potentials as

$$V_m = \phi_i - \phi_e. \tag{3.6}$$

Similarly, the current densities in the intracellular and extracellular domains can be written in terms of intracellular and extracellular potentials as

$$J_i = -\sigma_i \nabla \phi_i, \tag{3.7}$$

$$J_e = -\sigma_e \nabla \phi_e, \tag{3.8}$$

where σ_i and σ_e are the intracellular and extracellular conductivity tensors (S/m).

Using the equations 3.7 and 3.8 in equation 3.4, and eliminating ϕ_i in favor of ϕ_e and V_m, yields

$$\nabla \cdot (\sigma_i + \sigma_e) \nabla \phi_e = -\nabla \cdot (\sigma_i \nabla V_m), \tag{3.9}$$

Equation 3.9 is one of the bidomain equations.

Inserting equation 3.5 to equation 3.3 gives

$$\nabla \cdot (\sigma_e \nabla \phi_e) = -\beta \left(C_m \frac{dV_m}{dt} + I_{ion} \right), \tag{3.10}$$

Equation 3.10 gives the second bidomain equation. Therefore, the final bidomain system is

$$\nabla \cdot (\sigma_i + \sigma_e) \nabla \phi_e = -\nabla \cdot (\sigma_i \nabla V_m), \tag{3.11}$$

$$\nabla \cdot (\sigma_e \nabla \phi_e) = -\beta \left(C_m \frac{dV_m}{dt} + I_{ion} \right), \tag{3.12}$$

Eq. 3.11 is an elliptic partial differential equation (boundary value problem) and Eq. 3.12 is a parabolic equation (reaction-diffusion system).

3.2.2 Monodomain model

The monodomain model describes the current flowing only in the intracellular region of the heart. The bidomain model can be reduced to the monodomain model if we consider the case where the anisotropy ratios of both spaces are equal [88].

Assuming equal anisotropy ratios, i.e $\sigma_e = \lambda \sigma_i$, equation 3.9 becomes

$$\nabla \cdot (\sigma_i) \nabla \phi_e = -\frac{1}{1+\lambda} \nabla \cdot (\sigma_i \nabla V_m). \tag{3.13}$$

Inserting 3.13 into 3.10 gives

$$\frac{\lambda}{1+\lambda} \nabla \cdot (\sigma_i \nabla V_m) = \beta \left(C_m \frac{dV_m}{dt} + I_{ion} \right). \tag{3.14}$$

Equation 3.14 is the monodomain equation. It consists of a single parabolic partial differential equation in terms of V_m only. It is a special case of the bidomain model. It needs less processing time, and is less challenging to solve numerically. Often the monodomain model is sufficient.

Chapter 4

Assessment of arrhythmia vulnerability in-silico

Atrial fibrillation (AF) is a supraventricular arrhythmia characterized by irregular atrial activation. AF is independently associated with a twofold increase in all-cause mortality and increased morbidity, particularly stroke, heart failure, and cognitive impairment [89]. The currently estimated prevalence of AF in adults is between 2% and 4% [90], and a 2.3-fold rise [91] is expected [92, 93], reducing longevity in the general population. AF mostly affects the elderly and people with pre-existing chronic conditions such as cardiac pathologies, thyroid disease, high blood pressure or obesity [94]. During AF, the heart beats with a fast and irregular rhythm, leading to poor and erratic contractions. The distress caused by the symptoms onset can be severe and significantly reduce the quality of life. Even though AF is the most prevalent cardiac arrhythmia worldwide [43], a full comprehension of AF initiation and maintenance mechanisms is still missing.

In clinical practice, AF diagnosis and treatment is guided by electrical stimulation. Currently, various protocols are used to assess AF inducibility before and after ablation procedures and to unveil AF-sustaining areas. However, the underlying atrial substrates responsible for AF onset and perpetuation are still not easily discriminated, which may be one of the causes of the low success rate in the treatment of persistent AF patients. As we discussed in Section 2.4, AF inducibility increases with a higher degree of fibrosis in the heart [49]. However, in order to predict optimal target locations for ablation, a better understanding of the mechanistic influence of fibrosis on AF should be considered in combination with other structural factors, which have been shown to also influence the dynamics of reentrant drivers (RDs) [95]. Theoretical studies have highlighted the role of fiber orientation [96], surface curvature [97], and tissue thickness gradients [98] on the dynamics of RDs. The concept that RDs can drift and stabilize at borders between thin and thick tissue is supported by experimental evidence. Optical recordings in the right atrium (RA) of a sheep have shown that RDs tend to localize in bordering regions between thin and thick pectinate muscles [99]. Moreover, the association of complex fractionated electrograms

with atrial wall thickness (AWT) of the LA has also been reported [100], pointing to the presence of AF promoting substrate in these regions.

These findings show the potential of AWT gradients as a marker for identifying RD locations in the atria. However, neither the influence of AWT gradients on the RD dynamics in realistic atrial geometries nor comparative effects of AWT gradients and fibrotic patches on RDs have been investigated. Reconstruction of the atrial wall from imaging [37] provides a basis for computational modeling of the RD dynamics in patient-specific atrial geometries to understand the role of AWT gradients in influencing RD locations. Elucidating the relationships between AWT gradients, fibrosis, and RD locations can lead to an improved understanding of AF mechanisms and ultimately help identify patient-specific ablation targets, improving treatment efficacy.

In the studies presented in this chapter, we first sought to investigate the influence of different inducing protocols on atrial fibrillation initiation and maintenance [15]. We comprehensively compared state-of-the-art methods and applied our proposed protocol to highly detailed atrial models with and without AF. Our study showed that our method (termed PEERP) provides an effective, standardized and reproducible methodology to assess arrhythmia vulnerability. This study also gave important insights into the statistics of how AF dynamics evolve in time, differentiating regions vulnerable to initiate from the ones prone to sustain AF. Finally, we aimed at leveraging computational modelling to evaluate the influence of structural features as gradient and smoothness of AWT on AF vulnerability [16]. We showed that reentrant-drivers initiated in highly detailed atrial models were drifting towards areas with higher degree of heterogeneity in AWT. Therefore, proposing AWT gradient and curvature as possible measures to identify vulnerable areas to sustain AF.

frontiers in Physiology

ORIGINAL RESEARCH
published: 01 April 2021
doi: 10.3389/fphys.2021.656411

A Reproducible Protocol to Assess Arrhythmia Vulnerability *in silico*: Pacing at the End of the Effective Refractory Period

Luca Azzolin, Steffen Schuler, Olaf Dössel and Axel Loewe*

Institute of Biomedical Engineering, Karlsruhe Institute of Technology (KIT), Karlsruhe, Germany

In both clinical and computational studies, different pacing protocols are used to induce arrhythmia and non-inducibility is often considered as the endpoint of treatment. The need for a standardized methodology is urgent since the choice of the protocol used to induce arrhythmia could lead to contrasting results, e.g., in assessing atrial fibrillation (AF) vulnerabilty. Therefore, we propose a novel method—pacing at the end of the effective refractory period (PEERP)—and compare it to state-of-the-art protocols, such as phase singularity distribution (PSD) and rapid pacing (RP) in a computational study. All methods were tested by pacing from evenly distributed endocardial points at 1 cm inter-point distance in two bi-atrial geometries. Seven different atrial models were implemented: five cases without specific AF-induced remodeling but with decreasing global conduction velocity and two persistent AF cases with an increasing amount of fibrosis resembling different substrate remodeling stages. Compared with PSD and RP, PEERP induced a larger variety of arrhythmia complexity requiring, on average, only 2.7 extra-stimuli and 3 s of simulation time to initiate reentry. Moreover, PEERP and PSD were the protocols which unveiled a larger number of areas vulnerable to sustain stable long living reentries compared to RP. Finally, PEERP can foster standardization and reproducibility, since, in contrast to the other protocols, it is a parameter-free method. Furthermore, we discuss its clinical applicability. We conclude that the choice of the inducing protocol has an influence on both initiation and maintenance of AF and we propose and provide PEERP as a reproducible method to assess arrhythmia vulnerability.

Keywords: arrhythmia, atrial fibrillation, computational modeling, pacing protocol, reproducibility, vulnerability

OPEN ACCESS

Edited by:
David Christini,
SUNY Downstate Medical Center,
United States

Reviewed by:
Caroline Helen Roney,
King's College London,
United Kingdom
Edward Joseph Vigmond,
Université de Bordeaux, France

****Correspondence:***
Luca Azzolin
publications@ibt.kit.edu

Specialty section:
This article was submitted to Cardiac Electrophysiology, a section of the journal Frontiers in Physiology

Received: *20 January 2021*
Accepted: *10 March 2021*
Published: *01 April 2021*

Citation:
Azzolin L, Schuler S, Dössel O and Loewe A (2021) A Reproducible Protocol to Assess Arrhythmia Vulnerability in silico: Pacing at the End of the Effective Refractory Period. Front. Physiol. 12:656411. doi: 10.3389/fphys.2021.656411

1. INTRODUCTION

Atrial fibrillation (AF) is the most frequent cardiac arrhythmia and a progressive pathology associated with high morbidity and mortality (Hindricks et al., 2020). Despite recent advances in both diagnostic and therapeutic techniques, the success rate for the standard-of-care treatment, catheter ablation, is sub-optimal in patients with persistent AF (Verma et al., 2015; Morady and Latchamsetty, 2018). The modest efficacy reflects the complexity of the underlying phenomena and our incomplete understanding of the mechanisms of initiation, maintenance and progression of AF episodes (Andrade et al., 2014; Mann et al., 2018). In clinical practice, electrical stimulation has been widely used to diagnose and guide therapy of arrhythmias. Despite the high prevalence of atrial

rhythm disorders, the sensitivity, specificity and reproducibility of mostly ventricular stimulation has been investigated (DiCarlo et al., 1985; Kudenchuk et al., 1986). An equally critical evaluation of protocols for induction of AF and atrial flutter is currently lacking.

Kumar et al. (2012) highlighted the importance of the choice of the protocol used to induce AF even in patients without AF history and/or structural heart disease. The incidence of initiation and maintenance of AF varied according to gender, method of induction and number of inductions. In addition, the stimulation sites, pacing methods, number of AF inductions, use of pharmacological provocation and the definition of inducibility based on AF duration vary among different studies (Hakan et al., 2004; Essebag et al., 2005; Jaïs et al., 2006; Richter et al., 2006). Currently, various protocols are used to test AF inducibility before and after ablation procedures. For instance, some groups have used burst pacing at a fixed cycle length, while others have paced at the shortest cycle length which resulted in loss of 1:1 capture. Kumar et al. (2012) observed that the incidence of inducible or sustained AF was significantly higher with decremental pacing compared to burst pacing, as was the total duration of induced AF. They concluded that the adoption of AF inducibility as final electrophysiological endpoint is critically dependent on the variations in the definition of inducibility, aggressiveness of AF induction protocol and the number of AF inductions. However, they could not compare burst vs. decremental pacing within the same patient as this is not feasible clinically for ethical reasons. In another clinical study (Krol et al., 1999), a programmed atrial stimulation protocol for induction of sustained arrhythmia was evaluated. They were able to induce and maintain arrhythmic episodes using a train of pulses close to the effective refractory period in 39/44 (89%) patients. The study demonstrated that employing only two atrial sites and three atrial extra-stimuli induced either AF or atrial flutter in 89% of the patients with previous AF history and in 7% of the control group without documented arrhythmias. Moreover, inducibility was proposed as a predictor of long-term AF recurrence (Essebag et al., 2005).

Computational modeling has been proven to be a useful tool for assessing arrhythmia vulnerability (Arevalo et al., 2016; Zahid et al., 2016; Azzolin et al., 2020) and for supporting ablation planning (Lim et al., 2017; Boyle et al., 2019; Loewe et al., 2019; Roney et al., 2020). However, different protocols used to induce arrhythmia in simulations (Krummen et al., 2012; Matene and Jacquemet, 2012; Bayer et al., 2016; Roney et al., 2016, 2018; Zahid et al., 2016; Boyle et al., 2019) are not only making studies difficult to compare, but are also influencing the decision on whether an atrial model is vulnerable to AF and are therefore crucial for identifying the optimal ablation targets. In Boyle et al. (2019), arrhythmic episodes were induced by pacing from 40 evenly distributed sites applying a train of 12 electrical stimuli with decreasing cycle length from 300 to 150 ms. Their choice of protocol was motivated by a previous publication (Roney et al., 2016), in which, however, AF was initiated by delivering five triggering ectopic beats from the right superior pulmonary vein with a fixed coupling interval of 400 ms with the sinus rhythm but variable basic cycle length of 155 or 160 ms, depending on inducibility. In Bayer et al. (2016), each pulmonary vein was individually paced with five beats at a fixed cycle length but different coupling intervals. The values for coupling interval and cycle length were according to Haissaguerre et al. (1998). Roney et al. (2018) tested arrhythmia inducibility via extra stimuli coming from each pulmonary vein. They already highlighted the influence of variable cycle length, pacing intervals and pacing location on arrhythmia initiation. Conversely, Matene and Jacquemet (2012) proposed to induce AF by manually placing 1–6 phase singularities on the atrial surface, reconstructing an activation time map using an interpolation algorithm based on the eikonal equation and using that as initial condition for a monodomain simulation.

Considering the increasing use of catheter ablation and pacing therapies for atrial arrhythmias, which often take the suppression of inducibility as one of the endpoints of treatment, the definition of a commonly acknowledged electrical stimulation protocol is needed. A standardized methodology is critical since the use of different protocols could lead to contrasting conclusions on whether or not a patient or a patient-specific digital twin model is vulnerable to arrhythmia. In this study, we quantitatively evaluate different methods to induce arrhythmia, investigate their impact on both initiation and maintenance of AF episodes and propose an easily reproducible protocol to assess AF vulnerability of a particular atrial model.

2. MATERIALS AND METHODS

2.1. Atrial Models

In this work, two highly detailed volumetric bi-atrial geometry derived from magnetic resonance images were used (Krueger et al., 2013). The tetrahedral mesh had an average edge length of 0.5 mm. Fiber orientation was calculated by a semi-automatic rule-based algorithm (Wachter et al., 2015). We updated the models used in Krueger et al. (2013) by including a pectinate muscle running from the sinus node to the apex of the right atrial appendage to provide a fast activation of the appendage. Different conductivity and anisotropy values were implemented in working myocardium, pectinate muscles, bachmann bundle, inferior isthmus and crista terminalis to consider the heterogeneity in the atria (Loewe et al., 2015, 2016). Conductivities were tuned to reach four different total activation times in sinus rhythm of 130, 151, 179, and 199 ms and respective global average conduction velocities of 0.7, 0.66, 0.55, and 0.49 m/s, respectively. We will refer to these models as H1, H2, H3, and H4. In the second geometry, we applied the same mean global conduction velocity as in model H4. The resulting atrial model had a total activation time of 152 ms and will be referred to as H4B. The total activation times were chosen to be all $\geq$130 ms since patients with a P-wave duration longer than 130 ms were shown to have higher risk for AF (Lemery et al., 2007; Nielsen et al., 2015). Depending on the simulated scenario, the original Courtemanche et al. (1998) model (H1, H2, H3, H4, and H4B) or a variant reflecting AF-induced remodeling (UII and UIV) (Loewe et al., 2014) represented the myocyte membrane dynamics. Fibrotic tissue was included in the regions of both atria most-often exhibiting fibrotic substrate in patients with AF,

which are pulmonary veins antrum, left lateral wall, anterior wall, posterior wall and septum in the left atrium (Akoum et al., 2012; Benito et al., 2018; Higuchi et al., 2018) as well as right atrial appendage and septum in the right atrium (Cao et al., 2010; Akoum et al., 2012).

Two different fibrosis severity stages were implemented: **Figure 1A** shows the Utah stage II case (UII), in which 19% of the left atrial wall (LAW) and 5% of the right atrial wall (RAW) were modeled as fibrotic. In the most severe case (**Figure 1B**), 39% of the LAW and 11% of the RAW was modeled as fibrotic, classifying as Utah stage IV (UIV). To account for structural remodeling and the presence of scar tissue, we set 50% of the elements in the fibrotic regions as almost not conductive (conductivity of 10^{-7} S/m). This approach modeled the macroscopic passive barrier behavior caused by the electrical decoupling of the myocytes in the tissue infiltrated by fibrosis, also referred to as "percolation" (Vigmond et al., 2016). In the other 50%, several ionic conductances were rescaled to consider effects of cytokine-related remodeling (Roney et al., 2016) (−50% g_{K1}, −40% g_{Na}, and −50% g_{CaL}).

2.2. Protocols to Test Inducibility

We tested inducibility of arrhythmic episodes by pacing from stimulus locations placed on the endocardial surface with inter-point distance of 1 cm, resulting in up to 227 evenly distributed points. We systematically evaluated and compared three state-of-the-art methods: phase singularity distribution (PSD), rapid pacing (RP) and pacing at the end of the effective refractory period (PEERP). In all pacing protocols (RP and PEERP), a transmembrane current of 30 μA/cm^2 was injected in an area of 2 × 2 mm. We considered a point to be "inducing" if the application of one protocol at that location, induced and sustained an arrhythmia for at least 1.5 s after the end of the protocol. All the protocols used in this study are available open source in the examples section of openCARP (Vigmond et al., 2003; Sánchez et al., 2020; Augustin et al., 2021) at www.opencarp.org/documentation/examples.

2.2.1. Phase Singularity Distribution

The phase singularity distribution (PSD) method places phase singularities (PSs) in the atria, constructs an activation time map by solving the Eikonal equation and finally uses this as initial state for a monodomain excitation propagation simulation (Jacquemet, 2010; Matene and Jacquemet, 2012). The parameters of this method are the cycle length of the re-entrant wave, the number of PSs to initialize and the rotation direction of each PS. We set a single PS rotating in anti-clockwise direction (looking from the endo- to the epicardium) in one of the 227 points for each of the 227 simulated scenarios. We seeded only one PS for the sake of consistency with the pacing protocols in which we stimulated from one location per simulation. The cycle length was set to 315 and 168 ms, for the original (Courtemanche et al., 1998) model and the chronic AF variant (Loewe et al., 2014), respectively (5% longer than the effective refractory period). However, this method can be applied only in simulations.

2.2.2. Rapid Pacing

The rapid pacing (RP) protocol consists of a train of stimulation pulses with decreasing coupling intervals (CI). We extended the protocol by supporting a variable number of pulses with the same CI before the next decrement. Moreover, we implemented the option to check for successful initiation of an arrhythmia after every stimulation instead of only at the end of the protocol. This extended RP protocol is defined by $\mathrm{RP}_{s,l}^{N,\{B,E\}}$ where N is the number of stimuli with the same CI, $\{B, E\}$ defines if we were checking for the induction of an arrhythmia after every beat (B) or only at the end of the protocol (E), s is the starting CI and l is the last CI, both in ms. The CI was continuously decremented from s to l in steps of 10 ms. s was different for each action potential phenotype: 300 ms for the control case and 200 ms in the AF-induced remodeling setup. l was also distinct between control and AF remodeled and chosen as 200 and 130 ms, respectively. N was incremented from 1 to 4. For example, the RP protocol with $N = 1, s = 200$ ms, $l = 130$ ms and arrhythmia checking only at the end resulted in the following train of pulses:

$$\mathrm{RP}_{200,130}^{1,E} = \{200, 190, \ldots, 140, 130\,\text{check}\}, \tag{1}$$

which is the most common RP protocol (Krummen et al., 2012; Zahid et al., 2016; Boyle et al., 2019). The case $N = 2$ was as follows:

$$\mathrm{RP}_{200,130}^{2,E} = \{200, 200, 190, 190, \ldots, 140, 140, 130, 130\,\text{check}\}. \tag{2}$$

The RP protocol with $N = 1, s = 200$ ms, $l = 130$ ms and arrhythmia checking after every beat yields:

$$\mathrm{RP}_{200,130}^{1,B} = \{200\,\text{check}, 190\,\text{check}, \ldots, 140\,\text{check}, 130\,\text{check}\}. \tag{3}$$

To summarize, the RP protocols were tested with N increasing from 1 to 4 and coupling interval between 300 and 200 ms for the control case and 200 and 130 ms for the AF remodeled case. The parameters of the RP protocols are the maximum number of beats with the same CI, first and last CI, the CI decrement, and the stopping criteria (arrhythmia checking in between or at the end of the protocol). Moreover, the RP is currently used in clinical practice.

2.2.3. Pacing at the End of the Effective Refractory Period

The pacing at the end of the effective refractory period (PEERP) protocol triggers stimuli at the end of the effective refractory period. Therefore, each stimulus was delivered as soon as the underlying tissue had recovered from the previous activation and was able to initiate a new wave propagation. We implemented a run-time binary search method to find the minimum time at which a new depolarization wave could locally spread (effective refractory period) with a temporal resolution of 1 ms. We tested the influence of a temporal ERP uncertainty up to 8 ms in the model UIV. Based on initial experiments, the atrial action potential duration at 94% repolarization computed during sinus rhythm was chosen as first guess of the effective refractory

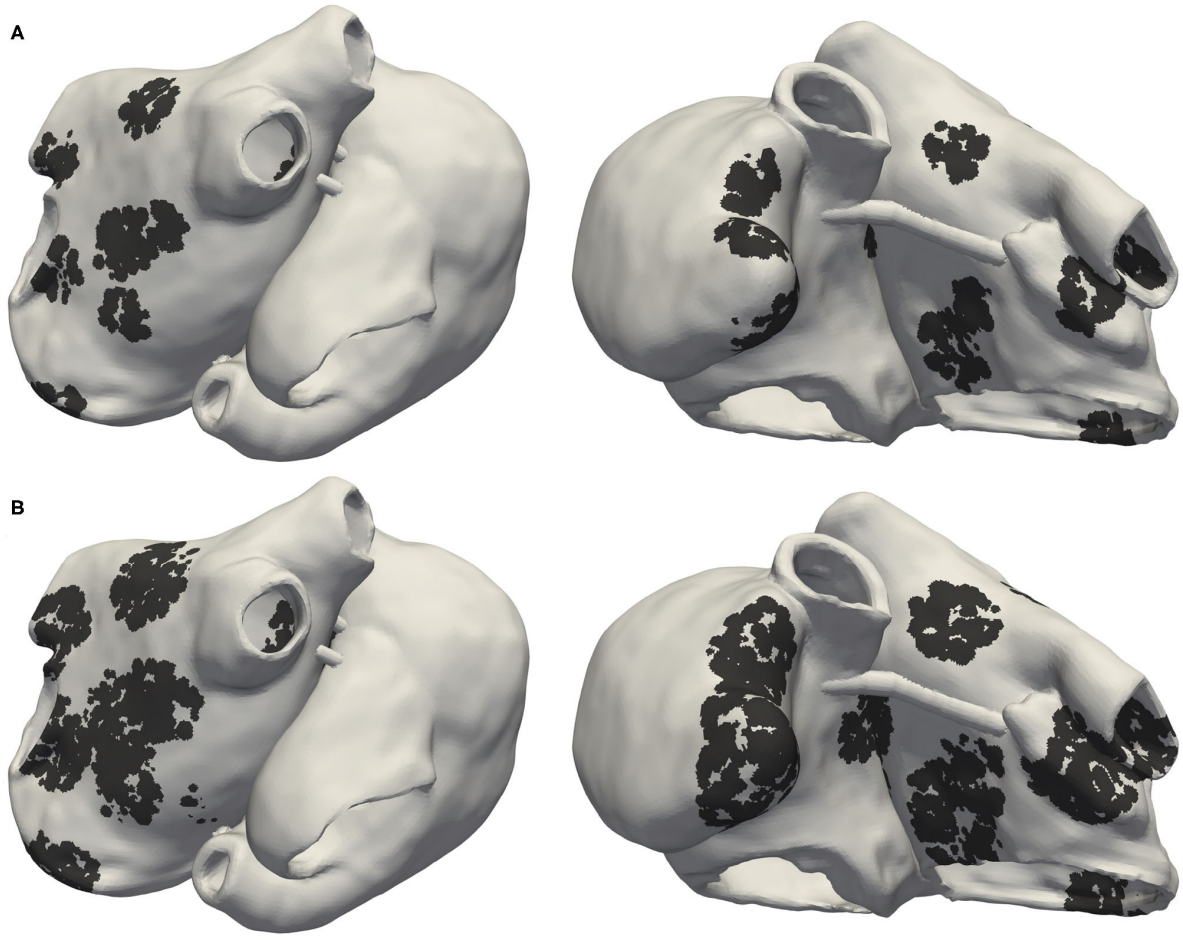

FIGURE 1 | Posterior and anterior view of Utah stage II (UII) model in **(A)** and Utah stage IV (UIV) model in **(B)**. Black regions indicate fibrotic tissue in which 50% of the elements were non-conductive and the remaining 50% electrophysiologically remodeled due to cytokine effects.

period. The criterion for successful wave propagation was a transmembrane potential ≥ -50 mV in at least one node in a ring 4–6 mm around the stimulation site. In this study, the maximum number of beats delivered from one stimulation site was set to 4. Consequently, the stimulation at one pacing location was stopped if the maximum number of beats was reached or if an arrhythmia was initiated. The only parameter for this new PEERP protocol is therefore the maximum number of stimuli to apply at a specific location. We will discuss in section 4.4 how the PEERP could be implemented during *in-vivo* procedures.

2.3. Arrhythmia Classification

Reentrant dynamics can, in many cases, be simplified by considering the behavior of their organizing centers—the PSs. We followed the method presented by Clayton et al. (2006) to detect PSs and track the spatio-temporal behavior of each PS during the whole simulated episode. We defined a PS as long-living PS (llPS) if it was sustained for at least 500 ms. Moreover, we distinguished the llPS which were stable within an area enclosed in a bounding box of 5 cm edge length (stable llPS) for the last simulated 1.5 s, from the ones which were meandering largely (non-stable llPS). The episodes in which no llPS was found were classified in multiple wave fronts (Multi) or flutter (Fl) by visual inspection. We, therefore, classified each arrhythmic episode into four categories: Multi, Fl, non-stable llPS, and stable llPS. The Multi class was defined as a complex and disorganized series of multiple wave fronts merging and colliding with each other without a clearly identifiable llPS. Periodic macro-reentries were interpreted as Fl cases. An example of stable llPSs and multiple wave fronts episodes are shown in **Figure 2**.

2.4. Subdivision of Atria in Spatial Segments

To localize the inducing points and drivers sustaining atrial activity, we partitioned the atria into different regions. The atria were subdivided into 28 segments (**Figure 3**): 19 in the left atrium

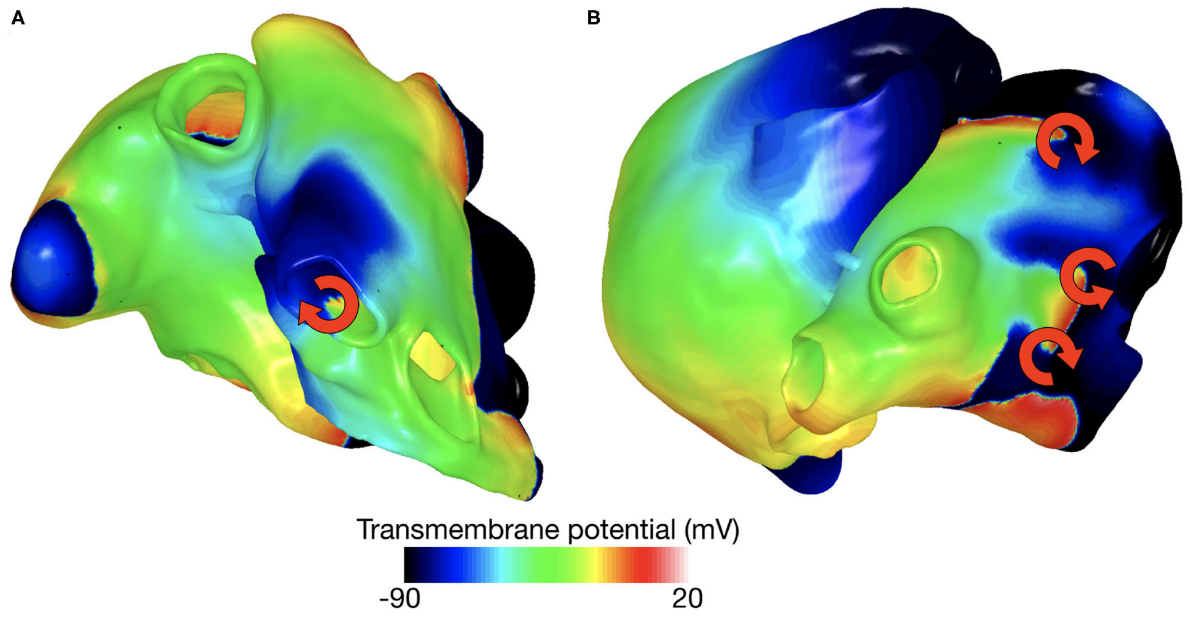

FIGURE 2 | Example of stable llPS **(A)** and multiple wave fronts **(B)**.

[four pulmonary vein segments (LIPV, RIPV, LSPV, and RSPV), four segments at the roof, five segments on the posterior wall, two segments in the septum, four segments on the anterior wall] and nine in the right atrium (inferior and superior vena cava rings, coronary sinus, cavotricuspid isthmus and septum, sinus node, right atrial appendage, anterior wall, four segments on the posterior wall of the RA).

2.5. Computational Tools

The spread of the electrical activation in the atrial myocardium was simulated by solving the monodomain system using openCARP (Vigmond et al., 2003; Sánchez et al., 2020) and a time step of 0.02 ms.

3. RESULTS

3.1. Inducibility

The number of inducing points and the relative frequency of arrhythmic mechanisms induced in each model are shown in **Figure 4**. We would like to recall that $RP^{B}_{300,200}$ and $RP^{E}_{300,200}$ were used for the models H1, H2, H3, H4, H4B, and $RP^{B}_{200,130}$ and $RP^{E}_{200,130}$ for the models UII and UIV. However, in **Figure 4** they are summarized as RP^{B} and RP^{E}. The number of inducing points increased with both a lower average global conduction velocity and higher amount of fibrotic tissue. No arrhythmic episode could be induced and sustained in model H1, which is why this model is not included in the results. PEERP was the only method which induced all the possible arrhythmic mechanisms described in section 2.3 in most of the models (4/5). The application of the RP protocol resulted in inducing a majority of atrial flutter mechanisms in the model UII and no multi-frontal episode in either model with fibrosis. Moreover, the PEERP method initiated arrhythmia from the most segments, averaged over all models, as displayed in **Figure 5**. However, RP^{B} was the only method which could induce and sustain arrhythmia pacing from all the segments in the UIV model. Nonetheless, inducing points belonging to only 4/28 segments were found applying the RP protocol in the model UII. The atrial segments in which inducing points were found to initiate and maintain stable llPSs applying the different protocol can be found in the **Supplementary Material**. In the left atrium, the majority of inducing points were found in segments 4, 5, 7, 9, 18, 19. In the right atrium, the segments 25, 26, 27 were the most inducible.

The CI of RP^{B} at which arrhythmia was initiated was around 130 and 250 ms for the models with and without structural remodeling, respectively (**Figure 6A**). The following tendency was observed: a slight increase of the inducing CI with lower global conduction velocity and higher amount of fibrosis. The inducing number of stimuli with the same CI (N) was in most of the cases $N = 2$ for both RP^{B} and RP^{E}, as presented in **Figure 6B**. However, in the model UIV $N = 1$ was often sufficient to initiate arrhythmic episodes using RP^{B}. The required total number of stimuli to induce arrhythmia by each protocol is displayed in **Figure 6C**. The methods PEERP, RP^{B} and RP^{E} required on average 2.7, 13.6, and 17.6 beats respectively to initiate an arrhythmic episode. The different protocols needed a similar total number of beats when applied to the model H4B, as shown in the **Supplementary Material**.

Furthermore, the application of PEERP resulted in an increasing number of segments in which inducing points

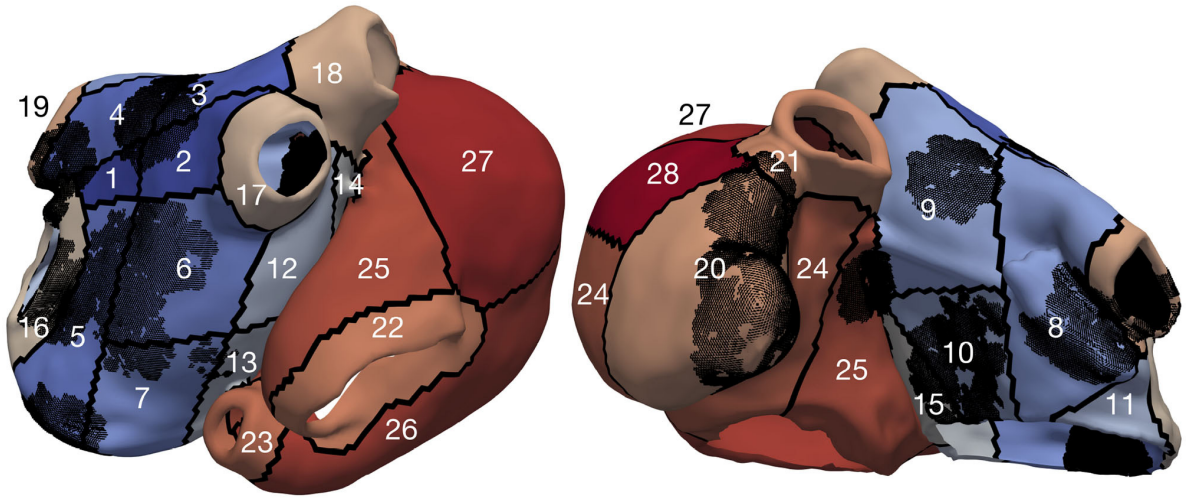

FIGURE 3 | Model UIV partitioned into segments, the black dots represent the fibrotic elements.

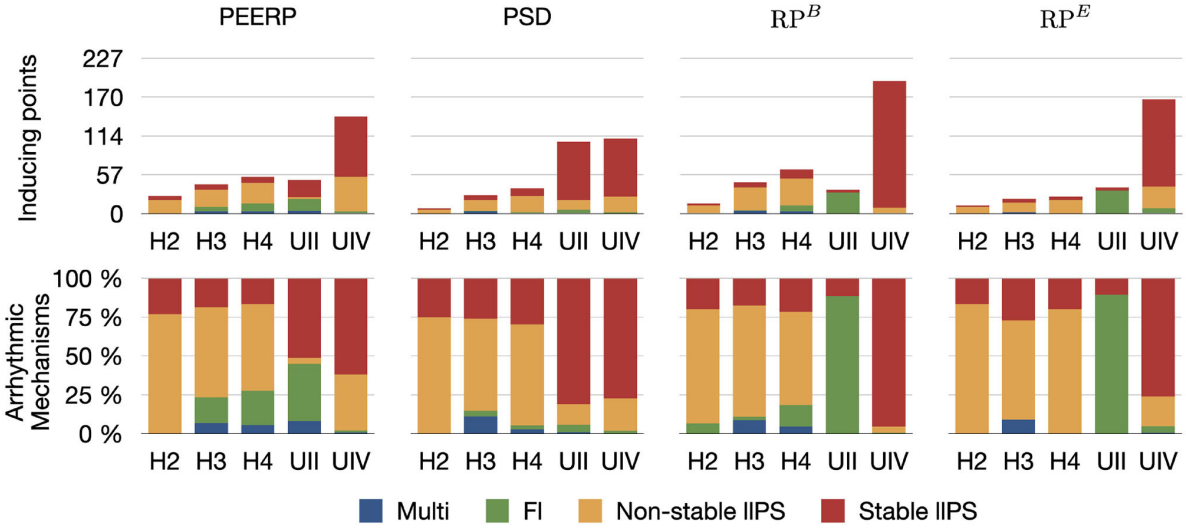

FIGURE 4 | First row: number of inducing points classified per induced arrhythmic mechanism: multiple wave fronts, flutter, non-stable and stable long living phase singularity. Second row: arrhythmic mechanisms induced by each protocol in the different atrial models.

were found with both decreased global CV and greater amount of fibrotic tissue, as shown in **Figure 5**. On one hand, the RP protocols were the only ones to initiate and sustain arrhythmia pacing from almost all the segments in the model UIV. On the other hand, both RP^B and RP^E could induce pacing from only four segments in the model UII.

Moreover, the simulation time required to complete each protocol for one stimulation point was 3.0, 19.5, 8.4 s for PEERP, RP^B, and RP^E, respectively (**Figure 7**).

The number of inducing points found in the model UIV remained stable between 141 and 146 out of 227 stimulation points when increasing the time tolerance for the local effective refractory period computation up to 8 ms as shown in **Figure 8**.

Additionally, subsets of the initial pacing locations were extracted to evaluate the sensitivity of each protocol to a reduction of the number of pacing locations, i.e., an increase of the inter-point distance. The sensitivity was computed as the percentage of stable IIPSs found when pacing from the initial pacing points with 1 cm inter-point distance. We

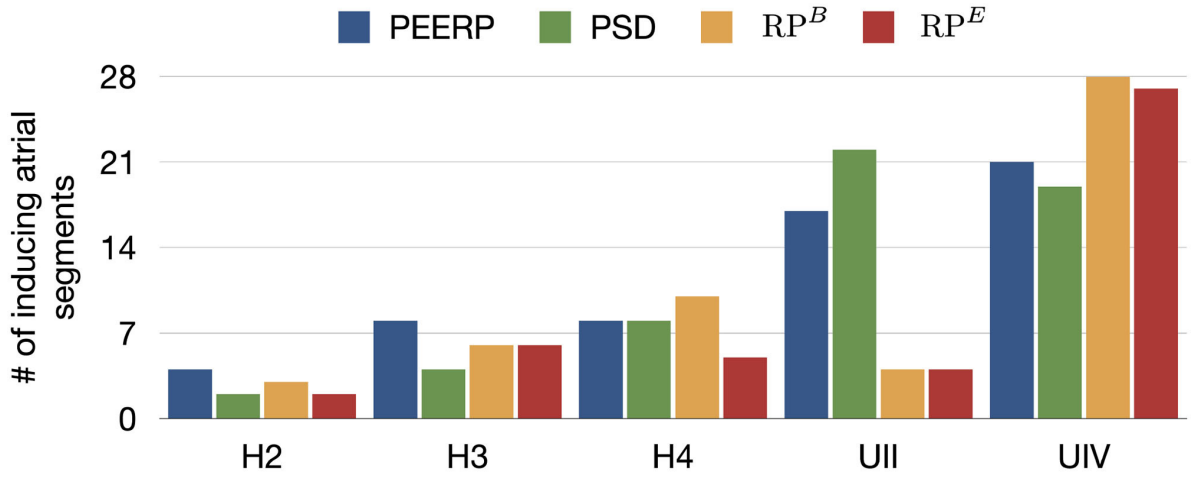

FIGURE 5 | Number of atrial segments in which inducing points were identified applying the various protocols in the different models.

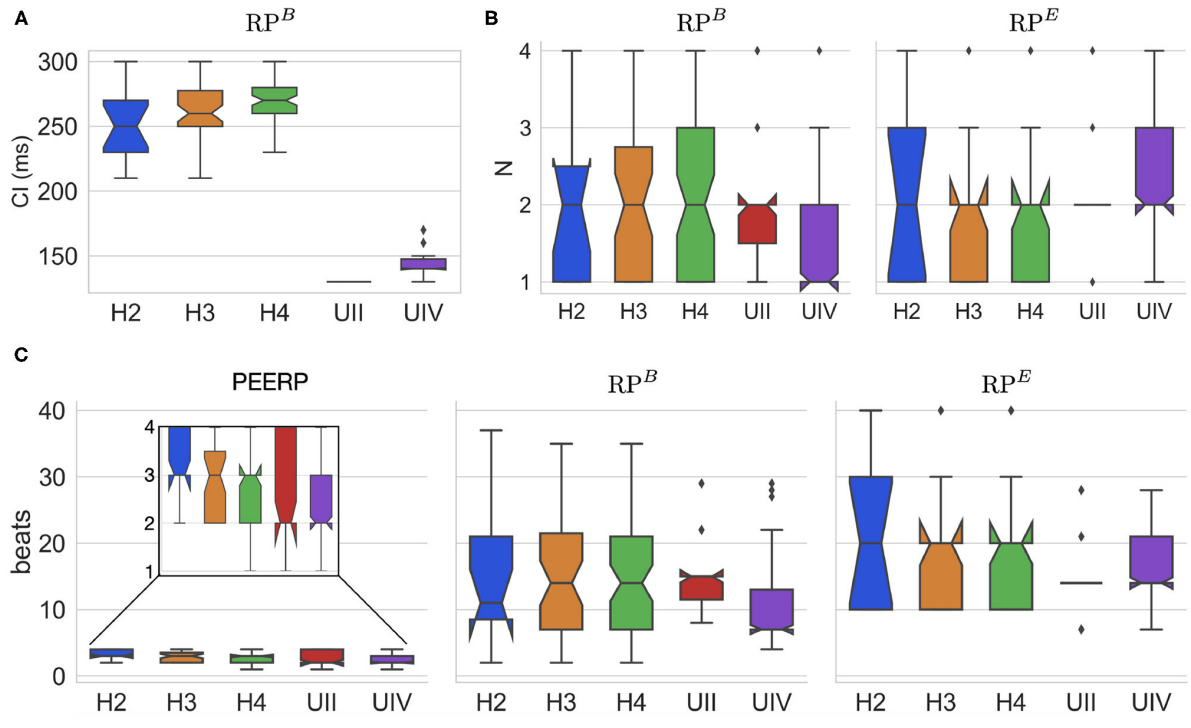

FIGURE 6 | (A) CI at which RP^B induced arrhythmia in each atrial model. **(B)** Number of beats per CI (*N*) needed to initiate arrhythmia in both RP^B and RP^E. **(C)** Total number of beats applied in the protocols PEERP, RP^B, and RP^E inducing arrhythmic episodes.

considered increasing inter-point distances of 1.5, 2, 2.5, and 3 cm. The sensitivity analysis results are presented in **Table 1**. When applying the protocols only at pacing points located 3 cm away from each other, leading to a total of only 11 bi-atrial pacing sites, all the protocols could reproduce more than the 90% of the locations maintaining stable llPSs in the model UIV. The PEERP and the RP^B were the only methods to identify some of the stable llPSs sustaining areas with a greater inter-point distance when applied to all models.

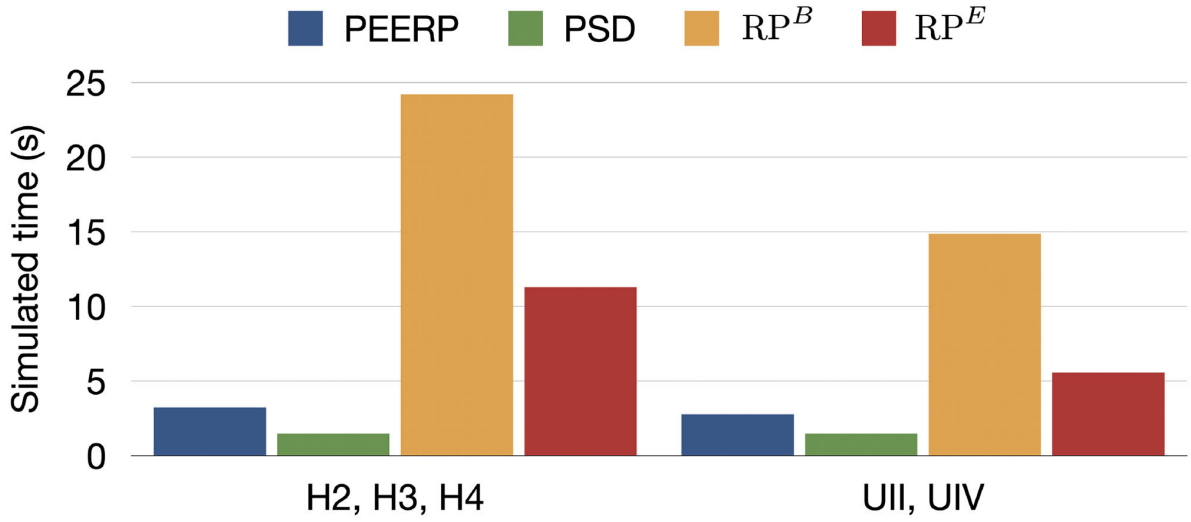

FIGURE 7 | Simulated time required to entirely perform each protocol from one stimulation point in s.

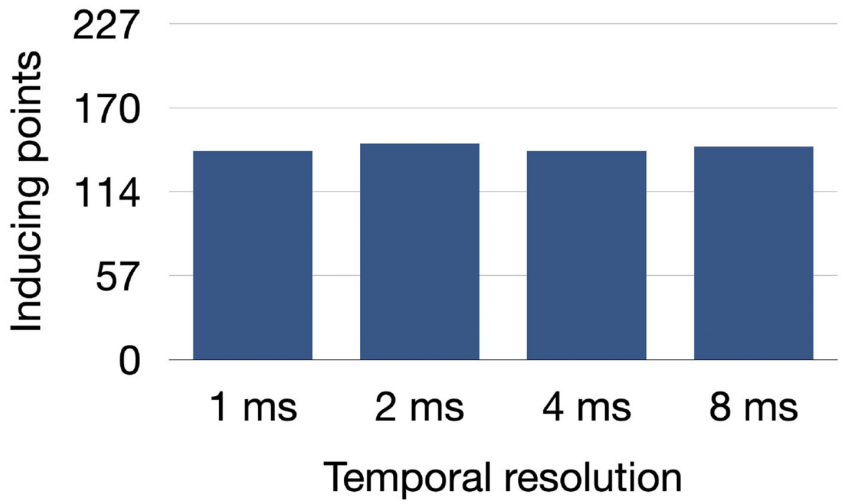

FIGURE 8 | Number of inducing points identified in the model UIV when decreasing the temporal resolution used to find the local effective refractory period in the PEERP method.

3.2. Maintenance

All protocols showed a tendency for increasing number of segments in which stable llPSs were sustained in models with lower global CV or higher percentage of fibrotic remodeling (**Figure 9**). PEERP was the protocol which sustained most stable llPSs in the models without structural remodeling. In the UII and UIV models, the PSD method was the one identifying more segments vulnerable to maintain stable llPSs, followed by PEERP. The RP protocols classified subsets of atrial segments found by the other methods as vulnerable to sustain stable llPSs in most of the cases.

The PEERP method was the only one identifying the left atrial roof (segment 9) as vulnerable for maintenance of stable llPSs in all the models. All the pacing protocols (PEERP and RP) showed most of the stable llPSs in segments located in the left atrium. The inclusion of fibrotic remodeling (models UII and UIV) led to the maintenance of stable llPSs in the segments containing fibrosis. However, PSD classified as vulnerable to maintain many segments located in the right atrium too. Moreover, the PSD method yielded many stable llPSs sustaining in segments without fibrosis in the models UII and UIV. Independent of the choice of the inducibility protocol, most of the stable llPSs were maintained

TABLE 1 | Sensitivity of each protocol in the different atrial models to increased inter-point distance.

Atrial model	Protocol			
	PEERP	**PSD**	RP^B	RP^E
H2	1.5 cm (83.3%) 2 cm (83.3%) 2.5 cm (83.3%) 3 cm (33.3%)		1.5 cm (100.0%)	1.5 cm (100.0%)
H3	1.5 cm (50.0%) 2 cm (37.5%)	1.5 cm (42.9%)	1.5 cm (62.5%) 2 cm (25.0%)	1.5 cm (16.7%)
H4	1.5 cm (22.2%)	1.5 cm (81.8%) 2 cm (36.4%) 2.5 cm (36.4%)	1.5 cm (57.1%) 2 cm (7.1%) 2.5 cm (7.1%)	
UII	1.5 cm (92.0%) 2 cm (24.0%) 2.5 cm (24.0%)	1.5 cm (92.9%) 2 cm (84.7%) 2.5 cm (71.8%) 3 cm (69.4%)	1.5 cm (50.0%)	1.5 cm (50.0%)
UIV	1.5 cm (97.7%) 2 cm (97.7%) 2.5 cm (94.3%) 3 cm (94.3%)	1.5 cm (97.6%) 2 cm (96.5%) 2.5 cm (96.5%) 3 cm (96.5%)	1.5 cm (98.9%) 2 cm (97.3%) 2.5 cm (97.3%) 3 cm (97.3%)	1.5 cm (96.9%) 2 cm (96.9%) 2.5 cm (96.9%) 3 cm (96.9%)

in the left posterior wall, roof, and septum (segments 5, 6, 9, 14, 16, 25, 27). The atrial segments in which stable llPSs were sustained after applying the different protocols can be found in the **Supplementary Material**.

The distance between the centers of the path traveled by stable llPSs and their corresponding inducing points was around 5–7 cm in most models using PEERP and RP^B (**Figure 10**). Applying PSD and RP^E the distance was between 2.5 and 5 cm in the models without AF specific remodeling and between 5 and 7 cm in the others.

All induction protocols sustained on average one stable llPSs per simulation, as shown in **Figure 11**.

4. DISCUSSION

4.1. Inducibility

Each of the four protocols was applied at 227 locations for each of the seven atrial models, resulting in 6,356 3D bi-atrial electrophysiological simulations. This is, to the best of our knowledge, one of the most extensive computational studies on the influence of pacing protocols on AF inducibility and maintenance. Regarding the vulnerability to induce arrhythmia, we demonstrated that the PEERP method provokes a bigger variety of different mechanisms compared to the other protocols. PEERP was able to induce diverse degrees of arrhythmia complexity, ranging from a flutter mechanism to chaotic multiple wave fronts. PEERP unveiled these complex mechanisms in most of the models which could potentially sustain them, even in the cases in which it was not the protocol with the highest number of inducing points. Furthermore, we showed that PEERP yields, overall, the highest number of segments from which arrhythmia could be induced (**Figure 5**), meaning that this protocol is less dependent on the pacing location.

The results of the sensitivity analysis (**Table 1**), confirmed the ability of the methods PEERP to identify a good percentage of the total stable llPSs in all the models even with pacing locations placed at a greater inter-point distance between each other. These results are in line with Krol et al. (1999), who could induce arrhythmia in 89% of patients with AF history with a train of stimuli close to the effective refractory period from a couple of pacing locations.

Moreover, we tested the influence of a temporal uncertainty up to 8 ms for the effective refractory period on the final number of inducing points (**Figure 8**). Since the number of inducing points remained relatively constant when increasing the temporal tolerance, the PEERP method can be used to assess atrial model vulnerability to AF with a temporal resolution up to 8 ms without affecting the results markedly.

The application of the PEERP method showed that a similar number of beats (2–3) was needed to initiate arrhythmia in all the models used in this study. This result matches with the findings by Krol et al. (1999), where three extra-stimuli were enough to initiate either AF or atrial flutter in patients both with and without history of AF. When fixing the maximum number of beats to 3, PEERP becomes a parameter-free method suitable to test inducibility in various electrophysiological models. Moreover, the smaller simulation time needed to perform the entire PEERP method from one stimulation point could give the possibility to test inducibility from more pacing locations to ensure the identification of all possible arrhythmic episodes which can arise in a given atrial model.

Moreover, we showed a strong dependence of the induced episodes on the CI of the RP protocol (**Figure 6**). Moreover, this

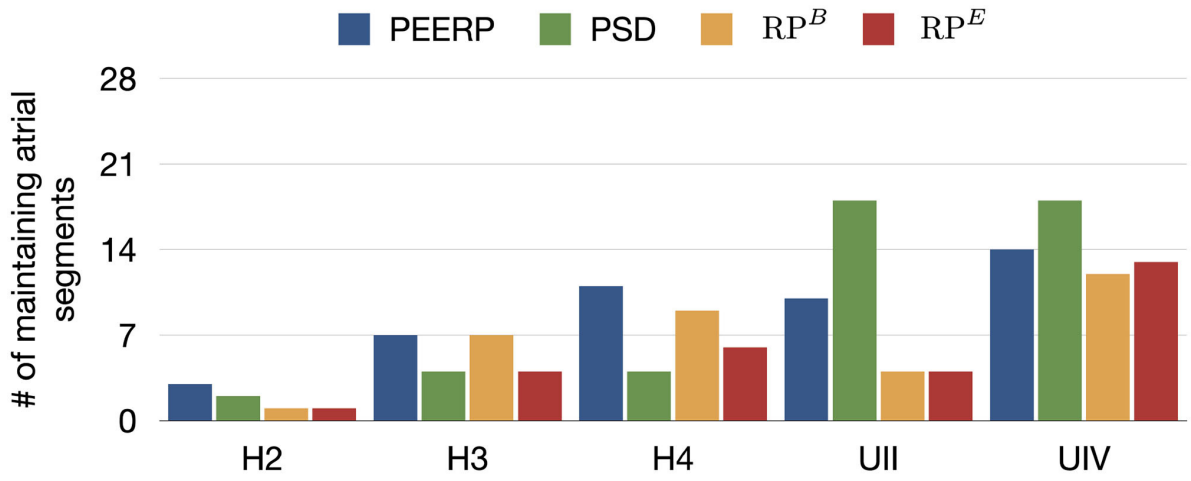

FIGURE 9 | Number of maintaining atrial segments after applying each protocol in all the 227 stimulus locations. We simulated 1.5 s after the end of each protocol to observe the evolution of the arrhythmia.

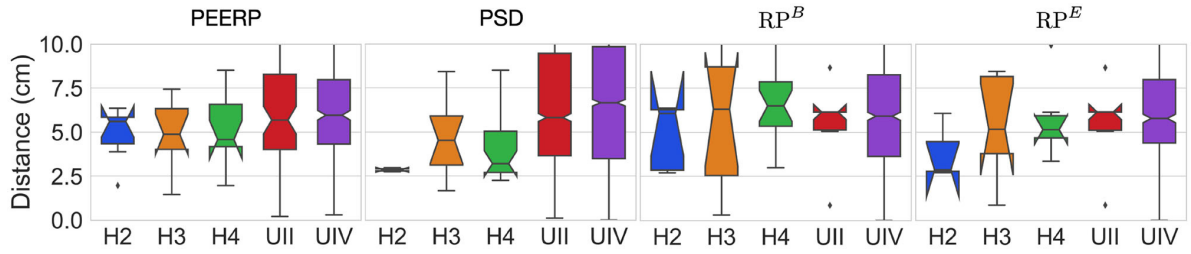

FIGURE 10 | Geodesic distance between inducing points and centers of the path covered by stable IIPSs.

parameter had to be tuned for each ionic model. We noticed that a smaller CI was needed to induce arrhythmia in models less vulnerable to initiate AF (higher CV or limited fibrosis). This is in agreement with the need of being more aggressive to induce AF in patients belonging to less severe AF subgroups. The small number of IIPSs initiated by the RP in the model UII clearly showed the limitation of user defined CI window. Furthermore, we noticed that a single beat per CI is usually not enough to induce arrhythmia and then a second beat with the same CI is needed. More than two beats with the same CI rarely induced arrhythmia. This could confirm the clinical finding of Kumar et al. (2012), who found a protocol with decreasing CI (decremental pacing) to be more effective in inducing AF than a fast train of pulses with fixed CI (burst pacing).

Our study highlighted the importance of checking for arrhythmia initiation after every beat. Without this as a stopping criterion for the protocol, many arrhythmic episodes induced by previous stimuli were terminated by subsequent stimuli. Indeed, RP^B initiated arrhythmia before reaching the lowest CI and with a lower number of beats per CI than the predefined maximum $N = 4$ (**Figure 6**). Finally, arrhythmic episodes were always more easily initiated by applying RP^B compared with RP^E, however

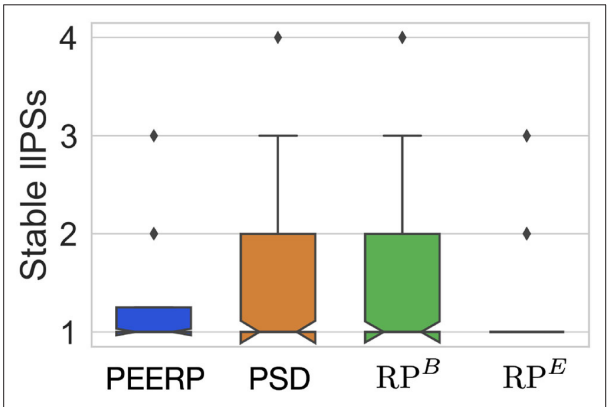

FIGURE 11 | Number of stable IIPSs per simulation with the different induction protocols.

at a much higher computational cost. Our results are in line with clinical findings by Kumar et al. (2012), where inducibility differed depending on the method of induction, the number of

induction attempts and the patient (in our case represented by different atrial models).

The segments in which most of the inducing points were found were also the ones including most anatomical and/or electrophysiological heterogeneity (e.g., pulmonary veins, mitral valve and posterior wall in the left atrium, crista terminalis and pectinate muscles in the right atrium).

4.2. Maintenance

The areas identified as vulnerable to sustain reentries were different between the various protocols, confirming the importance of the choice of the induction protocol not only in initiation but also in maintenance of AF.

Krol et al. (1999) were able to induce AF by applying stimuli close to the effective refractory period even in patients without previous AF history. In line with these findings, PEERP-induced stable llPSs were maintained in the models without fibrotic remodeling but slower global conduction velocity.

There was a strong correlation between maintenance of stable llPSs and presence of fibrotic tissue, mostly when applying pacing protocols (PEERP and RP). As shown in Azzolin et al. (2020), the regions of the crista terminalis and pectinate muscles (located in segments 25 and 27) were prone to sustain AF in the right atrium due to their high degree of heterogeneity in fiber architecture and conduction velocity.

The PSD method labeled areas in the right atrium (segments 24 and 27) as highly vulnerable to sustain llPSs, which almost no other protocol found. This was because PSD is by definition setting PSs as initial conditions and could lead to PSs maintained close to the point in which they were initiated, mostly if not attracted by fibrotic tissue patches.

The arrhythmia check as stopping criteria played an important role not only in the initiation but also in the maintenance of stable llPSs, since it led to the identification of different segments as vulnerable to sustain reentry when comparing RP^B and RP^E.

The average geodesic distance of 5–7 cm between rotor cores and corresponding inducing points showed that, in most cases, stable llPSs sustain in areas not in the pacing location's neighborhood. Consequently, we needed to check arrhythmia initiation in the whole atria, not only in the proximity of the stimulation point.

The PEERP recognized the areas which we expected to be more vulnerable to sustain rotors, highly heterogeneous regions or containing fibrotic tissue. Moreover, the PEERP identified most of the segments classified as vulnerable to maintain stable llPSs by the other protocols too. This showed a high sensitivity and specificity of the PEERP method in discriminating between areas which are prone to sustain stable rotors.

4.3. Clinically Important Observations

We noticed stable llPSs dominating in atrial models including fibrotic tissue and perpetuating mostly in segments containing fibrosis. This confirmed the link between re-entrant drivers dynamics and the fibrotic tissue distribution (McDowell et al., 2015; Zahid et al., 2016). On the contrary, non-stable llPSs prevailed in atria without structural remodeling.

Moreover, we showed that not only fibrotic tissue distribution and conduction velocity, but also the induction protocol are influencing both initiation and progression of AF episodes, confirming what was clinically displayed by Kumar et al. (2012).

Different arrhythmic mechanisms were induced in our atrial models, with various degree of complexity. This could support that the rivaling theories of rotors (Krummen et al., 2015) and multiple wavelet (Moe, 1962) were both right and can co-exist. Sometimes one mechanism dominates and sometimes the other.

4.4. Clinical Applicability of the PEERP Protocol

Rapid decremental pacing and burst pacing are considered as state-of-the-art protocols to induce arrhythmia in the atria (Essebag et al., 2005; Kumar et al., 2012). Moreover, suppression of inducibility with these protocol has been used as endpoint of ablation treatment by various groups (Hakan et al., 2004; Essebag et al., 2005; Jaïs et al., 2006). However, the strong influence of the chosen protocol to initiate and maintain AF has been previously shown (Kumar et al., 2012) and was confirmed mechanistically in our work. Furthermore, the lack of a consensus regarding which method to use to test inducibility makes studies hard or impossible to reproduce and to compare. Patient hearts are electrophysiologically diverse and human atrial myocardium is intrinsically heterogeneous, calling for a pacing protocol which is as much as possible independent from human-defined parameters (e.g., basic cycle length, coupling interval, and decreasing step). A programmed atrial stimulation protocol (Krol et al., 1999) pacing close to the effective refractory period has shown positive predictive accuracy in inducing AF of 95% using only a few pacing locations and three atrial stimuli. We showed that an automatically adjustable pacing protocol stimulating at the end of the effective refractory period is able to initiate arrhythmia episodes with on average only 2–3 stimulations, in accordance with what was observed in Krol et al. (1999). However, effective refractory period is clinically normally determined by a pacing protocol, like S1–S2 or rampdown. Therefore, it is dependent on the exact pacing protocol and location. Moreover, the determination of local effective refractory period with pacing protocols will take some time and is only feasible with limited spatial resolution. In contrast, RP protocols require no setup, and in fact, may be clinically faster than local estimation of effective refractory period. However, Verrier et al. (2016) presented a method to assess atrial repolarization without provocative electrical stimuli using standard clinical catheters. This opens the possibility of applying our proposed PEERP method in clinical practice under the assumption that repolarization time can be measured accurately enough to obtain unidirectional block using, e.g., the approach suggested by Verrier et al. (2016). We showed that a temporal resolution up to 8 ms should be sufficient to assess AF inducibility.

To the best of our knowledge, the PSD method is not clinically applicable. In contrast, pacing protocols are common in clinical practice during invasive electrophysiological procedures using a pacing catheter. However, other techniques could be used

to deliver electrical stimuli on demand. Crocini et al. (2016) and Scardigli et al. (2018) presented optogenetics as a feasible way to manipulate cardiac wave propagation and to discharge customized stimulation patterns across the whole heart with reaction time within 2 ms.

4.5. Limitations

Our atrial geometry did not include heterogeneous atrial wall thickness, which has been shown to influence the dynamics and stability of reentrant drivers (Azzolin et al., 2020). However, we are confident that our results hold in presence of heterogeneity in atrial wall thickness, since the shown consistency of results with the PEERP on the variety of cases we investigated also translates to new variations. In our study, only two different atrial anatomies were used. A deeper analysis on the influence of geometrical variability on AF vulnerabilty could be addressed by the use of atrial shape models (Nagel et al., 2021). We carried out monodomain simulations which could have affected the dynamics of AF, even if the bidomain equations did not show significant difference in reproducing the wave propagation in thin-walled atrial tissue (Potse et al., 2006). Due to the computational cost of this extensive study, we decided to limit the simulation time to 1.5 s after initiation of an arrhythmia. A meandering PS observed in our study could potentially stabilize later and affect the areas of maintenance. Clinically, testing of inducibility is mostly performed after ablation. The inclusion of ablation lines could potentially change the results of both inducibility and maintenance of AF episodes. They will, on one hand, limit the available space for AF to be sustained. On the other hand, different ablation patterns could provide additional substrate for reentries to be initiated and maintained. The scope of this work is to show how the choice of the induction protocol affects AF vulnerability in different atrial models. The next step could be to provide patient-specific ablation strategies to terminate the sustained AF episodes.

5. CONCLUSION

Our study highlights the influence of different arrhythmia induction protocols for the assessment of both AF initiation and maintenance of AF. Our newly proposed PEERP protocol offers a reproducible, comprehensive and computationally fast method to assess vulnerability. PEERP was able to provoke different degrees of arrhythmia complexity and unveil areas prone to maintain AF with a low number of stimuli, thus computationally inexpensive. The open source availability will facilitate adoption of the parameter-free PEERP method as a community standard. Therefore, we suggest the PEERP protocol (with $N = 4$) as a default protocol for future studies. This work is a basis to increase comparability and reproducibility of *in silico* arrhythmia vulnerability studies and could prove feasible to be applied clinically as well.

DATA AVAILABILITY STATEMENT

The datasets presented in this study can be found in online repositories. The names of the repository/repositories and accession number(s) can be found at: www.opencarp.org/documentation/examples.

AUTHOR CONTRIBUTIONS

LA and AL conceived and designed the study. LA constructed the atrial models, implemented the protocols, ran the simulations, analyzed the data, and drafted the manuscript. SS developed the method to subdivide the atria into segments and to compute the geodesic distance. All authors edited and approved the manuscript.

FUNDING

The research was supported by the European Union's Horizon 2020 research and innovation programme under the Marie Skłodowska-Curie grant agreement No. 766082 (MY-ATRIA project). We gratefully acknowledge support by Deutsche Forschungsgemeinschaft (DFG) (project ID LO 2093/1-1). We acknowledge support by the KIT-Publication Fund of the Karlsruhe Institute of Technology.

ACKNOWLEDGMENTS

The authors thank Jorge Patricio Arciniegas Sánchez and Laura Unger for their valuable suggestions and discussions. The authors thank Claudia Nagel for her precious feedback on the manuscript. This work was performed on the supercomputer ForHLR II funded by the Ministry of Science, Research and Arts of Baden-Württemberg and by the German Federal Ministry of Education and Research.

SUPPLEMENTARY MATERIAL

The Supplementary Material for this article can be found online at: https://www.frontiersin.org/articles/10.3389/fphys.2021.656411/full#supplementary-material

REFERENCES

Akoum, N., McGann, C., Vergara, G., Badger, T., Ranjan, R., Mahnkopf, C., et al. (2012). Atrial fibrosis quantified using late gadolinium enhancement MRI is associated with sinus node dysfunction requiring pacemaker implant. *J. Cardiovasc. Electrophysiol.* 23, 44–50. doi: 10.1111/j.1540-8167.2011.02140.x

Andrade, J., Khairy, P., Dobrev, D., and Nattel, S. (2014). The clinical profile and pathophysiology of atrial fibrillation: relationships among clinical features, epidemiology, and mechanisms. *Circ. Res.* 114, 1453–1468. doi: 10.1161/CIRCRESAHA.114.303211

Arevalo, H. J., Vadakkumpadan, F., Guallar, E., Jebb, A., Malamas, P., Wu, K. C., et al. (2016). Arrhythmia risk stratification of patients after myocardial infarction using personalized heart models. *Nat. Commun.* 7:11437. doi: 10.1038/ncomms11437

Augustin, C., Bayer, J., Bishop, M., Caforio, F., Campos, F., Costa, C. M., et al. (2021). *openCARP (v5.0)*. Karlsruhe: RADAR4KIT. doi: 10.35097/389

Azzolin, L., Luongo, G., Rocher, S., Saiz, J., Doessel, O., and Loewe, A. (2020). "Influence of gradient and smoothness of atrial wall thickness on initiation and maintenance of atrial fibrillation," in *Computing in Cardiology Conference (CinC)*, (Rimini). doi: 10.22489/CinC.2020.261

Bayer, J. D., Roney, C. H., Pashaei, A., Jaïs, P., and Vigmond, E. J. (2016). Novel radiofrequency ablation strategies for terminating atrial fibrillation in the left atrium: a simulation study. *Front. Physiol.* 7:108. doi: 10.3389/fphys.2016.00108

Benito, E. M., Cabanelas, N., Nuñez-Garcia, M., Alarcón, F., Figueras I Ventura, R. M., Soto-Iglesias, D., et al. (2018). Preferential regional distribution of atrial fibrosis in posterior wall around left inferior pulmonary vein as identified by late gadolinium enhancement cardiac magnetic resonance in patients with atrial fibrillation. *Europace* 20, 1959–1965. doi: 10.1093/europace/euy095

Boyle, P. M., Zghaib, T., Zahid, S., Ali, R. L., Deng, D., Franceschi, W. H., et al. (2019). Computationally guided personalized targeted ablation of persistent atrial fibrillation. *Nat. Biomed. Eng.* 3, 870–879. doi: 10.1038/s41551-019-0437-9

Cao, H., Xue, L., Wu, Y., Ma, H., Chen, L., Wang, X., et al. (2010). Natriuretic peptides and right atrial fibrosis in patients with paroxysmal versus persistent atrial fibrillation. *Peptides* 31, 1531–9. doi: 10.1016/j.peptides.2010.04.019

Clayton, R., Zhuvhkova, E., and Panfilov, A. V. (2006). Phase singularities and filaments: simplifying complexity in computational models of ventricular fibrillation. *Prog. Biophys. Mol. Biol.* 90, 378–398. doi: 10.1016/j.pbiomolbio.2005.06.011

Courtemanche, M., Ramirez, R. J., and Nattel, S. (1998). Ionic mechanisms underlying human atrial action potential properties: insights from a mathematical model. *Am. J. Physiol.* 225, 301–321. doi: 10.1152/ajpheart.1998.275.1.H301

Crocini, C., Ferrantini, C., Coppini, R., Scardigli, M., Yan, P., Loew, L. M., et al. (2016). Optogenetics design of mechanistically-based stimulation patterns for cardiac defibrillation. *Sci. Rep.* 6:35628. doi: 10.1038/srep35628

DiCarlo, L. A., Morady, F., Schwartz, A. B., Shen, E. N., Baerman, J. M., Krol, R. B., et al. (1985). Clinical significance of ventricular fibrillation-flutter induced by ventricular programmed stimulation. *Am. Heart J.* 109, 959–963. doi: 10.1016/0002-8703(85)90235-2

Essebag, V., Baldessin, F., Reynolds, M. R., McClennen, S., Shah, J., Kwaku, K. F., et al. (2005). Non-inducibility post-pulmonary vein isolation achieving exit block predicts freedom from atrial fibrillation. *Eur. Heart J.* 26, 2550–2555. doi: 10.1093/eurheartj/ehi507

Haissaguerre, M., Jaïs, P., Shah, D. C., Takahashi, A., Hocini, M., Quiniou, G., et al. (1998). Spontaneous initiation of atrial fibrillation by ectopic beats originating in the pulmonary veins. *N. Engl. J. Med.* 339, 659–666. doi: 10.1056/NEJM199809033391003

Hakan, O., Aman, C., Lemola, K., Cheung, P., Hall, B., Good, E., et al. (2004). Noninducibility of atrial fibrillation as an end point of left atrial circumferential ablation for paroxysmal atrial fibrillation. *Circulation* 110, 2797–2801. doi: 10.1161/01.CIR.0000146786.87037.26

Higuchi, K., Cates, J., Gardner, G., Morris, A., Burgon, N. S., Akoum, N., et al. (2018). The spatial distribution of late gadolinium enhancement of left atrial magnetic resonance imaging in patients with atrial fibrillation. *JACC Clin. Electrophysiol.* 4, 49–58. doi: 10.1016/j.jacep.2017.07.016

Hindricks, G., Potpara, T., Dagres, N., Arbelo, E., Bax, J. J., Blomström-Lundqvist, C., et al. (2020). 2020 ESC guidelines for the diagnosis and management of atrial fibrillation developed in collaboration with the european association of cardio-thoracic surgery (EACTS). *Eur. Heart J.* 42, 373–498. doi: 10.1093/eurheartj/ehaa612

Jacquemet, V. (2010). An eikonal approach for the initiation of reentrant cardiac propagation in reaction-diffusion models. *IEEE Trans. Biomed. Eng.* 57, 2090–2098. doi: 10.1109/TBME.2010.2051156

Jaïs, P., Hocini, M., Sanders, P., Hsu, L., Takahashi, Y., Rotter, M., et al. (2006). Long-term evaluation of atrial fibrillation ablation guided by noninducibility. *Heart Rhythm* 3, 140–145. doi: 10.1016/j.hrthm.2005.11.012

Krol, R., Saksena, S., Prakash, A., Giorgberidze, I., and Mathew, P. (1999). Prospective clinical evaluation of a programmed atrial stimulation protocol for induction of sustained atrial fibrillation and flutter. *J. Interv. Cardiac Electrophysiol.* 3, 19–25. doi: 10.1023/A:1009863220699

Krueger, M. W., Seemann, G., Rhode, K., Keller, D. U. J., Schilling, C., Arujuna, A., et al. (2013). Personalization of atrial anatomy and electrophysiology as a basis for clinical modeling of radio-frequency ablation of atrial fibrillation. *IEEE Trans. Med. Imaging* 32, 73–84. doi: 10.1109/TMI.2012.2201948

Krummen, D. E., Bayer, J. D., Ho, J., Ho, G., Smetak, M. R., Clopton, P., et al. (2012). Mechanisms of human atrial fibrillation initiation: clinical and computational studies of repolarization restitution and activation latency. *Circ. Arrhythm. Electrophysiol.* 5, 1149–59. doi: 10.1161/CIRCEP.111.969022

Krummen, D. E., Swarup, V., and Narayan, S. M. (2015). The role of rotors in atrial fibrillation. *J. Thorac. Dis.* 7, 142–151. doi: 10.3978/j.issn.2072-1439.2014.11.15

Kudenchuk, P. J., Kron, J., Walance, C. G., Murphy, E. S., Morris, C. D., Griffith, K. K., et al. (1986). Reproducibility of arrhythmia induction with intracardiac electrophysiologic testing: patients with clinical sustained ventricular tachyarrhythmias. *J. Am. Coll. Cardiol.* 7, 819–828. doi: 10.1016/S0735-1097(86)80342-4

Kumar, S., Kalman, J. M., Sutherland, F., Spence, S. J., Finch, S., and Sparks, P. B. (2012). Atrial fibrillation inducibility in the absence of structural heart disease or clinical atrial fibrillation. *Circ. Arrhythm. Electrophysiol.* 5, 531–536. doi: 10.1161/CIRCEP.111.968859

Lemery, R., Birnie, D., Tang, A. S. L., Green, M., Gollob, M., Hendry, M., et al. (2007). Normal atrial activation and voltage during sinus rhythm in the human heart: an endocardial and epicardial mapping study in patients with a history of atrial fibrillation. *J. Cardiovasc. Electrophysiol.* 18, 402–408. doi: 10.1111/j.1540-8167.2007.00762.x

Lim, B., Hwang, M., Song, J.-S., Ryu, A.-J., Joung, B., Shim, E. B., et al. (2017). Effectiveness of atrial fibrillation rotor ablation is dependent on conduction velocity: an *in-silico* 3-dimensional modeling study. *PLoS ONE* 12:e0190398. doi: 10.1371/journal.pone.0190398

Loewe, A., Krueger, M. W., Holmqvist, F., Dossel, O., Seemann, G., and Platonov, P. G. (2016). Influence of the earliest right atrial activation site and its proximity to interatrial connections on p-wave morphology. *Europace* 18, iv35–iv43. doi: 10.1093/europace/euw349

Loewe, A., Krueger, M. W., Platonov, P. G., Holmqvist, F., Dŏssel, O., and Seemann, G. (2015). Left and right atrial contribution to the P-wave in realistic computational models. *Lect. Notes Comput. Sci.* 9126, 439–447. doi: 10.1007/978-3-319-20309-6_50

Loewe, A., Poremba, E., Oesterlein, T., Luik, A., Schmitt, C., Seemann, G., et al. (2019). Patient-specific identification of atrial flutter vulnerability–a computational approach to reveal latent reentry pathways. *Front. Physiol.* 9:1910. doi: 10.3389/fphys.2018.01910

Loewe, A., Wilhelms, M., Dŏssel, O., and Seemann, G. (2014). Influence of chronic atrial fibrillation induced remodeling in a computational electrophysiological model. *Biomed. Eng.* 59, S929–S932. doi: 10.1515/bmt-2014-5012

Mann, I., Sandler, B., Linton, N., and Kanagaratnam, P. (2018). Drivers of atrial fibrillation: theoretical considerations and practical concerns. *Arrhythm. Electrophysiol. Rev.* 7, 49–54. doi: 10.15420/aer.2017.40.3

Matene, E., and Jacquemet, V. (2012). Fully automated initiation of simulated episodes of atrial arrhythmias. *Europace* 14, v17–v24. doi: 10.1093/europace/eus271

McDowell, K. S., Zahid, S., Vadakkumpadan, F., Blauer, J., MacLeod, R. S., and Trayanova, N. A. (2015). Virtual electrophysiological study of atrial fibrillation in fibrotic remodeling. *PLoS ONE* 10:e0117110. doi: 10.1371/journal.pone.0117110

Moe, G. K. (1962). On the multiple wavelet hypothesis of atrial fibrillation. *Archiv. Int. Pharmacodyn. Thér.* 140, 183–188.

Morady, F., and Latchamsetty, R. (2018). Source determination in atrial fibrillation. *Arrhythm. Electrophysiol. Rev.* 7:165. doi: 10.15420/aer:2018:25:2

Nagel, C., Schuler, S., Dössel, O., and Loewe, A. (2021). A bi-atrial statistical shape model for large-scale *in silico* studies of human atria: model development and application to ECG simulations. *arXiv* 2102.10838. Available online at: https://arxiv.org/abs/2102.10838

Nielsen, J. B., Kuhl, J. T., Pietersen, A., Graff, C., Lind, B., Struijk, J. J., et al. (2015). P-wave duration and the risk of atrial fibrillation: results from the copenhagen ECG study. *Heart Rhythm* 12, 1887–1895. doi: 10.1016/j.hrthm.2015.04.026

Potse, M., Dubé, B., Richter, J., Vinet, A., and Gulrajani, R. M. (2006). A comparison of monodomain and bidomain reaction-diffusion models for action potential propagation in the human heart. *IEEE Trans. Biomed. Eng.* 53, 2425–2435. doi: 10.1109/TBME.2006.880875

Richter, B., Gwechenberger, M., Filzmoser, P., Marx, M., Lercher, P., and Gössinger, H. D. (2006). Is inducibility of atrial fibrillation after radio frequency

ablation really a relevant prognostic factor? *Eur. Heart J.* 27, 2553–2559. doi: 10.1093/eurheartj/ehl307

Roney, C. H., Bayer, J. D., Cochet, H., Meo, M., Dubois, R., Jaïs, P., et al. (2018). Variability in pulmonary vein electrophysiology and fibrosis determines arrhythmia susceptibility and dynamics. *PLoS Comput. Biol.* 14:e1006166. doi: 10.1371/journal.pcbi.1006166

Roney, C. H., Bayer, J. D., Zahid, S., Meo, M., Boyle, P. M. J., Trayanova, N. A., et al. (2016). Modelling methodology of atrial fibrosis affects rotor dynamics and electrograms. *Europace* 18, iv146–iv155. doi: 10.1093/europace/euw365

Roney, C. H., Beach, M. L., Mehta, A. M., Sim, I., Corrado, C., Bendikas, R., et al. (2020). *In silico* comparison of left atrial ablation techniques that target the anatomical, structural, and electrical substrates of atrial fibrillation. *Front. Physiol.* 11:572874. doi: 10.3389/fphys.2020.572874

Sánchez, J., Nothstein, M., Neic, A., Huang, Y. L., Prassl, A. J., Klar, J., et al. (2020). "openCARP: an open sustainable framework for *in-silico* cardiac electrophysiology research," in *Computing in Cardiology Conference (CinC)*, Vol. 47, (Rimini). doi: 10.22489/CinC.2020.111

Scardigli, M., Müllenbroich, C., Margoni, E., Cannazzaro, S., Crocini, C., Ferrantini, C., et al. (2018). Real-time optical manipulation of cardiac conduction in intact hearts. *J. Physiol.* 596, 3841–3858. doi: 10.1113/JP276283

Verma, A., Jiang, C., Betts, T. R., Chen, J., Deisenhofer, I., Mantovan, R., et al. (2015). Approaches to catheter ablation for persistent atrial fibrillation. *N. Engl. J. Med.* 372, 1812–1822. doi: 10.1056/NEJMoa1408288

Verrier, R. L., Fuller, H., Justo, F., Nearing, B. D., Rajamani, S., and Belardinelli, L. (2016). Unmasking atrial repolarization to assess alternans, spatiotemporal heterogeneity, and susceptibility to atrial fibrillation. *Heart Rhythm* 13, 953–961. doi: 10.1016/j.hrthm.2015.11.019

Vigmond, E., Pashaei, A., Amraoui, S., Cochet, H., and Hassaguerre, M. (2016). Percolation as a mechanism to explain atrial fractionated electrograms and reentry in a fibrosis model based on imaging data. *Heart Rhythm* 13, 1536–1543. doi: 10.1016/j.hrthm.2016.03.019

Vigmond, E. J., Hughes, M., Plank, G., and Leon, L. J. (2003). Computational tools for modeling electrical activity in cardiac tissue. *J. Electrocardiol.* 36, 69–74. doi: 10.1016/j.jelectrocard.2003.09.017

Wachter, A., Loewe, L., Krueger, M. W., Dössel, O., and Seemann, G. (2015). Mesh structure-independent modeling of patient-specific atrial fiber orientation. *Curr. Direct. Biomed. Eng.* 1, 409–412. doi: 10.1515/cdbme-2015-0099

Zahid, S., Cochet, H., Boyle, P. M., Schwarz, E. L., Whyte, K. N., Vigmond, E. J., et al. (2016). Patient-derived models link re-entrant driver localization in atrial fibrillation to fibrosis spatial pattern. *Cardiovasc. Res.* 110, 443–454. doi: 10.1093/cvr/cvw073

Conflict of Interest: The authors declare that the research was conducted in the absence of any commercial or financial relationships that could be construed as a potential conflict of interest.

Influence of Gradient and Smoothness of Atrial Wall Thickness on Initiation and Maintenance of Atrial Fibrillation

Luca Azzolin[1], Giorgio Luongo[1], Sara Rocher Ventura[2], Javier Saiz[2], Olaf Dössel[1], Axel Loewe[1]

[1] Institute of Biomedical Engineering, Karlsruhe Institute of Technology, Karlsruhe, Germany
[2] Ci2B, Universitat Politècnica de València, Valencia, Spain

Abstract

This work uses a highly detailed computational model of human atria to investigate the effect of spatial gradient and smoothing of atrial wall thickness on inducibility and maintenance of atrial fibrillation (AF) episodes. An atrial model with homogeneous thickness (HO) was used as baseline for the generation of different atrial models including either a low (LG) or high thickness gradient between left/right atrial free wall and the other regions. Since the model with high spatial gradient presented non-natural sharp edges between regions, either 1 (HG1) or 2 (HG2) Laplacian smoothing iterations were applied. Arrhythmic episodes were initiated using a rapid pacing protocol and long-living rotors were detected and tracked over time. Thresholds optimised with receiver operating characteristic analysis were used to define high gradient/curvature regions. Greater spatial gradients increased the atrial model inducibility and unveiled additional regions vulnerable to maintain AF drivers. In the models with heterogeneous wall thickness (LG, HG2 and HG1), $73.5 \pm 8.7\%$ *of the long living rotors were found in areas within 1.5 mm from nodes with high thickness gradient, and* $85.0 \pm 3.4\%$ *in areas around high endocardial curvature. These findings promote wall thickness gradient and endocardial curvature as measures of AF vulnerability.*

1. Introduction

Atrial fibrillation (AF) is a frequent and progressive heart condition correlated with high morbidity and mortality. The lack of basic understanding of underlying atrial dysfunctional and structural substrates may be the cause of the low success rate in treatment of persistent AF patients. Computational heart modelling could aid the development of quantitative tools to evaluate the influence of structural features on AF vulnerability.

Recent theoretical studies have highlighted the effect of surface curvature [1] and tissue gradient [2] on the dynamics of re-entrant drivers (RDs). The anchoring of scroll waves to regions with heterogeneous atrial wall thickness have been proven both experimentally and computationally [3]. However, simplified models were used and no detailed atrial model have been exploited to assess correlation between these structural features and regions vulnerable to initiate and maintain AF.

We used a detailed 3-dimensional computational model of human atria including anatomical wall thickness. We varied the spatial gradient between adjacent regions and the degree of smoothing at transitions.

We hypothesized that heterogeneous thickness influences both initiation and maintenance of AF episodes. Moreover, we sought to investigate the drift of meandering scroll waves along regions of large spatial gradients in wall thickness.

2. Methods

2.1. Atrial models generation

In this work, a highly detailed volumetric bi-atrial geometry derived from magnetic resonance images was used [4]. The volumetric mesh had an average edge length of 0.4 mm and a homogeneous wall thickness (HO) of 3 mm. This model was used as baseline for the generation of 3 model variants varying the regional myocardial thickness and the smoothness between the different regions of the atria. The heterogeneous myocardial thickness was introduced following the method proposed in [5] consisting in moving the endocardial nodes in the normal direction until the desired Euclidean distance between the endocardial node and the closest node on the epicardium is reached. The regional thickness ranges were taken from [6–8] and are shown in Fig. 1. The blue stars mark the final regional thickness value for the model with low gradient (LG) between the left/right atrial wall (LAW)/(RAW) and the other regions. The thickness values in the model with a high gradient between LAW/RAW and the other regions are indicated by red stars. Moreover, since the later model entailed unrealistically sharp edges at the transition between regions with highly different thickness, we ap-

plied 1 iteration (HG1) or 2 iterations (HG2) of Laplacian smoothing to the endocardial surface.

Fiber orientation was calculated by a semi-automatic rule-based algorithm [9]. A variant of the Courtemanche et al. model reflecting atrial fibrillation-induced remodeling was used as ionic model [10]. Nine regions with different anisotropy ratio were implemented to consider the heterogeneity in the atria [11]. Conductivities of all models were tuned to reach a last sinus rhythm activation time of 160 ms and a global longitudinal conduction velocity of 0.7 m/s. The spreading of the electrical wave along the myocardium was simulated by solving the monodomain system using openCARP/CARP [12].

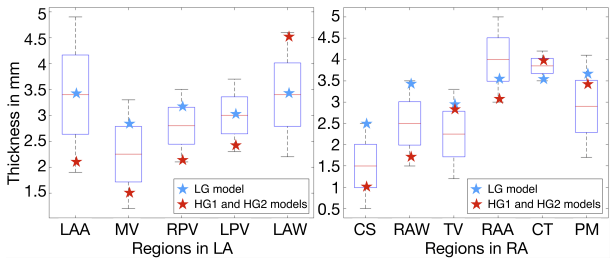

Figure 1. Regional thickness for the models LG, HG1 and HG2 (left atrial appendage=LAA, mitral valve=MV, right pulmonary veins=RPV, left pulmonary veins=LPV, coronary sinus=CS, tricuspid valve=TV, right atrial appendage=RAA, crista terminalis=CT, pectinate muscles=PM).

2.2. Thickness gradient and endocardial curvature

To better identify the cause of scroll wave drifting, we computed two thickness features: thickness gradient and endocardial curvature. The curvature of the endocardial surface at each node was calculated as $1/R$, where R is the radius of the fitted osculating sphere.

2.3. Protocol to test inducibility

We tested inducibility of arrhythmic episodes by pacing from 48 evenly distributed points on the endocardial surface with an inter-point distance of 2 cm. The rapid pacing protocol consisted in a train of pulses with decreasing coupling interval from 160 ms to 110 ms. We considered a point to be 'inducing' if by pacing from that location, an arrhythmia was induced and sustained for at least 1.5 s after the last beat of the pacing protocol.

2.4. Detection and tracking of AF dynamics

Reentrant waves have an organising center in many cases. In 3D this is known as filament, which represents the center-line of a scroll wave. We followed the method presented in [13] to detect filaments and we tracked the spatio-temporal behavior of each filament along the whole episode duration. We defined long-living rotors as filaments sustained for at least 500 ms.

2.5. Optimal threshold for high thickness gradient and endocardial curvature

An iterative binary classification (filaments present vs. not present) was computed to create receiver operating characteristic (ROC) curves. Thickness gradient and endocardial curvature were used as discriminators for the ROC curves. The optimum operating point on the ROC curve was defined as the point on the curve with the shortest distance to the top left corner of the graph and it was selected as threshold.

3. Results and Discussion

3.1. Inducibility

In model HO, 12 points were 'inducing' (10 lead to macro reentries, 2 to micro reentries). We observed 13 'inducing' points in model LG (10 macro reentries, 3 rotors) and 16 points in model HG1 (6 macro, 10 micro). Furthermore, we identified 16 'inducing' points in model HG2 (11 macro, 5 rotors). Number and location of the 'inducing' points for each model are summarized in Tab.1. The models with higher gradient between LAW/RAW and the other regions (HG1 and HG2) were more vulnerable regarding initiation of reentrant episodes compared with models with more homogeneous thickness (HO and LG). We observed the development of microreentries when pacing precisely in the areas with high thickness gradient. Moreover, the combination of high gradient and sharper edges (model HG1) had the highest number of points inducing rotors.

3.2. Maintenance

In total, 4 long-living rotors were sustained in average for 978.8 ms in the model HO regions CT, PMs and RAA. Fig. 2 shows the filaments of these reentries with most of them drifting along the CT or moving in confined areas of the RAA. No micro reentries were maintained in the CS or MV with similar behavior in the model LG. In the model LG, we identified a total of 7 long-living rotors with an average lifespan of 921.7 ms and most of them were moving

Model	Macroreentries	Microreentries			
		PMs	CT	MV	CS
HO	10	2			
LG	10	3			
HG1	6	5	1	3	1
HG2	11	2	2	1	

Table 1. Number of point inducing reentrant arrhythmic episodes in each model classified in macro reentry and micro reentry. The points inducing micro reentries are further divided per location.

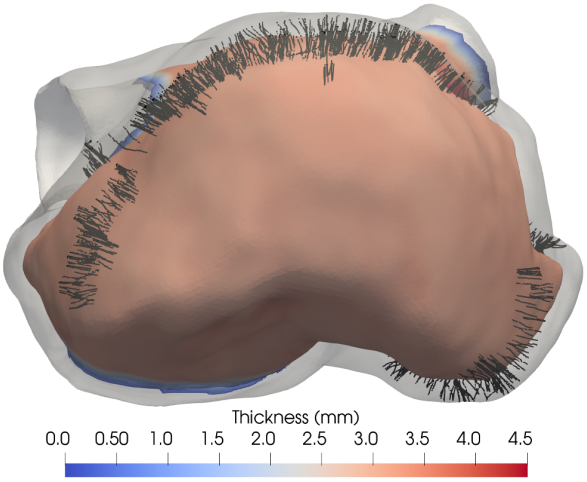

Figure 2. Filaments of long-living rotors in the right atrium of model HO (black lines). The endocardial surface is colored according by wall thickness. Pectinate muscles view.

along the PMs. In the models HG1 and HG2, we identified more reentrant wave meandering following the PMs or the MV and, finally, being maintained close to the steps between RAW and CS, CT or RAA, as shown in Fig. 3. We found a total of 11 and 16 long-living rotors maintaining in average for 1021.5 ms and 982.5 ms in the models HG2 and HG1, respectively. Nodes in which a long-living rotor was found (see Fig. 4), mostly corresponded to locations with high gradient magnitude and surface curvature (see Fig. 4). We detected 70.5%/78.7%/71.3% of filaments in areas within 1.5 mm from the regions with high thickness gradient and 81.1%/87.1%/86.9% of filaments in areas within 1.5 mm from the regions with high endocardial curvature, in the models LG, HG2 and HG1 respectively. The optimal thresholds extracted from the ROC curves were 0.1/0.2/0.46 mm/mm for the gradient magnitude and 0.7/0.8/0.96 mm^{-1} for the curvature, for the models LO, HG2 and HG1, respectively. In our simulations, no fibrotic tissue was included to clearly analyse the effect of anatomical thickness features on reentry dynamics.

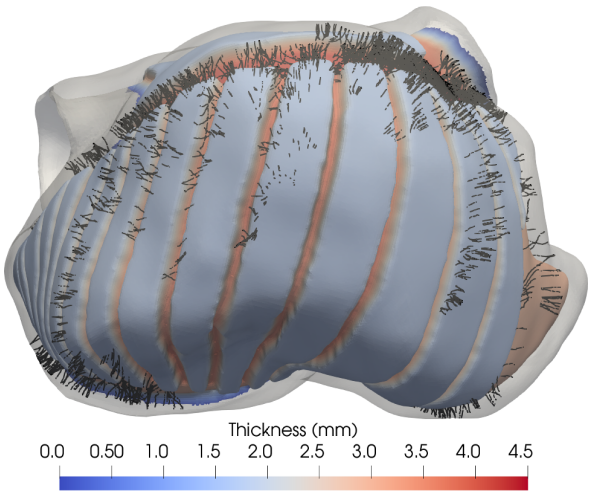

Figure 3. Filaments of long-living rotors in the right atrium of model HG2 (black lines). The endocardial surface is colored according by wall thickness. Pectinate muscles view.

4. Conclusion

In this work, we showed that the gradient and the degree of smoothing of anatomical thickness influence both the vulnerability to initiate and to maintain atrial fibrillation episodes. We presented how thickness heterogeneity increased not only the number of pacing location from which it was possible to induce an arrhythmia but also the complexity of the arrhythmia, developing more micro reentries. The inclusion of higher gradient highlighted pathways followed by meandering rotors (PMs), as shown experimentally [14] and unveiled new areas vulnerable to sustain drivers (CS and MV). Furthermore, we showed how rotors are attracted by steep edges and are drifting to the border between regions with different thickness, as theoretically predicted in [2]. Furthermore, we noticed that the degree of smoothing affected inducibility, increasing the number of points initiating rotors, and sustainability, leading to a higher number of long-living drivers. We conclude that wall thickness gradient and curvature could be valuable a priori measures to assess AF vulnerability and predict maintenance areas to ablate.

Acknowledgments

Research supported by the European Union's Horizon 2020 research and innovation programme under the Marie Skłodowska-Curie grant agreement No.766082 (MY-ATRIA project).

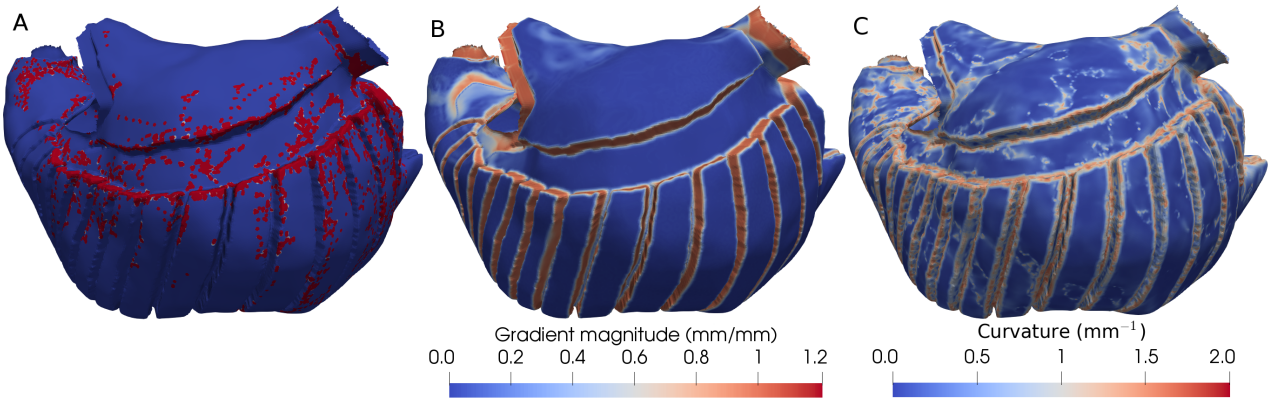

Figure 4. Model HG1: A) endocardial nodes in which a long-living rotor was encountered are shown in red; B) thickness gradient magnitude; C) endocardial curvature showed as inverse of the osculating sphere radius. Crista terminalis and pectinate muscles view.

References

[1] Dierckx H, Brisard E, Verschelde H, Panfilov AV. Drift laws for spiral waves on curved anisotropic surfaces. Phys Rev E 2013;88:012908.

[2] Biktasheva IV, Dierckx H, Biktashev VN. Drift of scroll waves in thin layers caused by thickness features: Asymptotic theory and numerical simulations. Phys Rev Lett 2015; 114:068302.

[3] Yamazaki M, Mironov S, Taravant C, Brec J, Vaquero LM, Bandaru K, Avula UM, Honjo H, Kodama I, Berenfeld O, Kalifa J. Heterogeneous atrial wall thickness and stretch promote scroll waves anchoring during atrial fibrillation. Cardiovasc res 2012;94(1):48–57.

[4] Krueger MW, Seemann G, Rhode K, Keller DUJ, Schilling C, Arujuna A, Gill J, O'Neill MD, Razavi R, Dössel O. Personalization of atrial anatomy and electrophysiology as a basis for clinical modeling of radio-frequency ablation of atrial fibrillation. IEEE Trans Med Imaging 2013;32(1):73–84.

[5] Rocher-Ventura S, Martínez-Mateu L, López-Pérez AD, Ferrer Albero A, Sáncez-Quintana D, Saiz Rodríguez FJ. A three-dimensional model of the human atria with heterogeneous wall thickness and fibre transmurallity - a realistic platform for the study of atrial fibrillation. CinC 2019;1–4.

[6] Suenari K, Nakano Y, Hirai Y, Hiroshi O, Noboru O, Yuko M, Shigeyuk U, Kenta K, Takehito T, Chikaaki M, Mai F, Kazuaki C, Yasuki K. Left atrial thickness under the catheter ablation lines in patients with paroxysmal atrial fibrillation: insights from 64-slice multidetector computed tomography. Heart and Vessels 2013;28:360–368.

[7] Varela M, Morgan R, Theron A, Dillon-Murphy D, Chubb H, Whitaker J, Henningsson M, Aljabar P, Schaeffter T, Kolbitsch C, Aslanidi OV. Novel mri technique enables non-invasive measurement of atrial wall thickness. IEEE Trans Med Imaging 2017;36(8):1607–1614.

[8] Wi J, Lee H, Uhm J, Kim J, Pak H, Lee M, Kim YJ, Joung B. Complex fractionated atrial electrograms related to left atrial wall thickness. J Cardiovasc Electrophysiol 2014; 25(11):1141–1149.

[9] Wachter A, Loewe L, Krueger MW, Dössel O, Seemann G. Mesh structure-independent modeling of patient-specific atrial fiber orientation. Curr Dir in Biomed Eng 2015; 1:409–412.

[10] Loewe A, Wilhelms M, Dössel O, Seemann G. Influence of chronic atrial fibrillation induced remodeling in a computational electrophysiological model. Biomed Eng 2014; 59(S1):S929–S932.

[11] Loewe A, Krueger MW, Platonov PG, Holmqvist F, Dössel O, Seemann G. Left and right atrial contribution to the P-wave in realistic computational models. Lect Notes Comput Sci 2015;9126:439–447.

[12] Vigmond EJ, Hughes M, Plank G, Leon LJ. Computational tools for modeling electrical activity in cardiac tissue. J Electrocard 2003;36:69–74.

[13] Clayton R, Zhuvhkova E, Panfilov AV. Phase singularities and filaments: Simplifying complexity in computational models of ventricular fibrillation. Prog Biophys Mol Biol 2006;90:378–398.

[14] Hansen BJ, Zhao J, Csepe TA, Moore BT, Li N, Jayne LA, Kalyanasundaram A, Lim P, Bratasz A, Powell KA, Simonetti OP, Higgins RS, Kilic A, Mohler PJ, Janssen PM, Weiss R, Hummel JD, Fedorov VV. Atrial fibrillation driven by micro-anatomic intramural re-entry revealed by simultaneous sub-epicardial and sub-endocardial optical mapping in explanted human hearts. Eur Heart J 2015;36(35):2390–2401.

Address for correspondence:

Luca Azzolin
Fritz-Haber-Weg 1, 76131 Karlsruhe, Germany
publications@ibt.kit.edu

Chapter 5

Personalized and integrated atrial models for tailored ablation strategies

Catheter ablation (CA) is a well-established strategy for restoring sinus rhythm in AF patients who do not respond well to anti-arrhythmic drugs, with success rates of up to 70% in patients with episodes of AF lasting less than 1 week (paroxysmal AF). CA typically relies on the insertion of a catheter into the atria, where it delivers high amounts of localized energy for the destruction and isolation of arrhythmogenic substrates without affecting the surrounding areas [101]). The widely accepted CA strategy to restore sinus rhythm is the electrical isolation of pulmonary vein (PV) sleeves in the left atrium (LA), which are believed to be the primary substrate for the generation of the ectopic beats and/or anchoring of re-entrant drivers (RDs) responsible for triggering and sustaining AF in the LA [61, 102, 103].

Approximately 30% of AF patients are asymptomatic, which leads to delayed diagnosis and the development of persistent AF. In these patients, the success rate with CA drops to 42% [104], often requiring additional ablation procedures. A potential factor for the failure of CA in these patients is the presence of high degrees of electrophysiological and structural remodeling, which alters the AF substrate, making it harder to predict the locations of AF drivers. Therefore, by changing the focus of ablation strategies from anatomic to patient-specific functional targets, the efficiency of CA could be greatly improved.

Recent advances in catheter and electro-anatomic mapping technologies have enabled the development of more patient-specific ablation strategies that complement the existing standard approaches (PV isolation (PVI)), in persistent AF. These can directly target: (i) AF sources (ectopic triggers or RDs) identified invasively using basket catheters (Narayan et al., 2014) or non-invasively using body surface electrodes (Haissaguerre et al., 2014) and (ii) regions where the atrial substrate is expected to be arrhythmogenic, such as fibrotic tissue [48, 105] and low voltage areas [106, 107]. The role of RDs as drivers for AF has been long recognized [102, 103]. However, RD-guided ablation is limited by the challenges of mapping and visualizing electrical activity on the endocardial surface with sufficiently

high resolution. This can explain contradictory outcomes of multi-centre trials, in which some show favorable outcomes of RD-guided ablation [108], while others have failed to find advantages in this approach compared to PVI [109].

Computational models applied to the medical field are boosting the capacity to draw diagnoses and prognoses. Future treatments will be tailored not only to current health status and data but also to an accurate projection of the pathways to restore health by model predictions. Providing therapies tailored to each patient is the vision of precision medicine, enabled by the increasing ability to capture data about individual patients and build the 'digital twin' (DT) of a patient.

Virtual replicas of patient hearts built by integrating information from clinical data and representing available clinical observations are defined as cardiac DTs [110]. They provide a framework to integrate and augment experimental and clinical data, enabling the identification of mechanisms and predicting outcomes, even under unseen scenarios. Cardiac DTs were shown to be a valid methodology to help clinicians in the decision making process in diagnosis [111], therapy stratification [112] and planning [13, 78] due to their inherent predictive potential. Cardiac DTs are also considered a powerful new approach and valid cost-effective alternative in the safe and ethical testing of novel electrophysiological device therapies. In general, cardiac DT workflows consist of two stages, an anatomical and a functional twinning stage, that give rise to various challenges that must be addressed. However, workflows to generate high fidelity virtual patient cohorts of cardiac models that are both anatomically and electrophysiologically personalized were only lately discussed and are still not sufficiently efficient, robust and accurate for advanced clinical applications [113, 114].

In the studies presented in this chapter, we firstly aimed to propose a highly automated pipeline to augment missing anatomical structures and provide ready-to-use patient-specific atrial models from clinical data [17]. A bi-atrial statistical shape model [115] was used to cover atrial shape variability and to generalize to unseen geometries augmenting clinical data. The implemented framework was shown to accurately represent the original geometry derived from either an electroanatomical map (EAM) or a magnetic resonance imaging (MRI) segmentation. It was able to infer the anatomy of the right atrium even using information only from the left atrium. Therefore, we identified a comprehensive methodology to build anatomical DT augmenting the geometries derived from clinical data. Secondly, we sought to test our previously developed framework on a cohort of 29 patients, including both left atrium MRI segmentations and EAMs. This included pre-processing of the clinical data and a functional twinning step to deliver fully personalized models representing the patient electrophysiology [18]. The pipeline delivered atrial DTs with a surface-to-surface distance to the original maps within the voxel resolutions integrating fiber arrangement and anatomical structures annotation in a fast and reproducible way. In addition, our novel methodology to personalize the simulated spread of depolarization better represented the clinical measurements compared with state-of-the-art methods. The easy multilevel integration of multiple datasets and automated model generation made possible from our platform is a step forward towards standardized assessment of arrhythmia vulnerability and

testing of ablation strategies. Finally, we investigated the success of performing tailored ablation lines compared to previously proposed ablation strategies [116]. Our proposed personalized ablation plan was applied to the atrial models cohort previously generated and outperformed all other ablation strategies. According to this study, the best ablation strategy would be: a) identification of AF-perpetuating areas e.g. by searching for areas with high dominant frequency; b) ablate these areas and add connecting lines to the nearest orifice or former ablation site; c) test the ablation success with the PEERP [15] and in case AF is not terminated go back to a). In this way, the patient-specific models post-ablation resulted in being non-inducible for AF. The last two algorithms are currently under review for being patented.

Automated Framework for the Augmentation of Missing Anatomical Structures and Generation of Personalized Atrial Models from Clinical Data

Luca Azzolin[1], Claudia Nagel[1], Deborah Nairn[1], Jorge Sánchez[1], Tianbao Zheng[1], Martin Eichenlaub[2], Amir Jadidi[2], Olaf Dössel[1], Axel Loewe[1]

[1] Institute of Biomedical Engineering, Karlsruhe Institute of Technology, Karlsruhe, Germany
[2] University Heart Center Freiburg-Bad Krozingen, Bad Krozingen, Germany

Abstract

Personalized computational models are often generated from electroanatomical maps, which might lack important anatomical structures like the appendages, or from imaging data which are potentially affected by segmentation uncertainty. A bi-atrial statistical shape model (SSM) was shown to cover atrial shape variability. We hypothesized that it could, therefore, also be used to infer the shape of missing structures and deliver ready-to-use models to assess atrial fibrillation vulnerability in silico. We implemented a highly automatized pipeline to generate a personalized computational model by fitting the SSM to the clinically acquired geometries. We applied our framework to a geometry coming from an electroanatomical map and one derived from magnetic resonance images (MRI). Only landmarks belonging to the left atrium and no information from the right atrium were used in the fitting process. The left atrium surface-to-surface distance between electroanatomical map and a fitted instance of the SSM was 2.26±1.95 mm. The distance between MRI segmentation and SSM was 2.07±1.56 mm and 3.59±2.84 mm in the left and right atrium, respectively. Our semi-automatic pipeline provides personalized computational models representing the original anatomy well by fitting a SSM. We were able to infer the shape of the right atrium even in the case of using information only from the left atrium.

1. Introduction

Atrial fibrillation (AF) is the most common sustained cardiac arrhythmia and is associated with high morbidity and mortality [1].

Computational models of the human heart built from clinical data have been used in in silico experiments to study arrhythmias and propose personalized treatments. However, the process of building a digital twin of a patient's heart directly from clinical geometrical data can be challenging since imaging data can be influenced by segmentation uncertainty and electroanatomical maps can be missing relevant anatomical structures (right atrium, appendage, veins).

Recently, a bi-atrial statistical shape model (SSM) covering the relevant anatomical variability required for in-silico electrophysiological experiments was presented and generalized well to unseen geometries [2].

Moreover, due to the complex myocardial structure, it is hard to reconstruct the atrial fiber direction and annotate the anatomical regions in an automated way.

In this work, we implemented an automated framework to augment missing anatomical structures and output a ready-to-use personalized computational model by fitting an SSM to the initial surface coming from clinical data, automatically label the different regions in the atria and compute the fiber orientation [3].

The pipeline was applied on a clinical dataset including both a geometry derived from MRI and an electroanatomical map.

2. Methods

2.1. Dataset

A high density electroanatomical bi-atrial map was taken in sinus rhythm prior to pulmonary vein isolation using a 20-pole mapping catheter and the CARTO 3 system (Biosense Webster Inc., Diamond Bar, CA, USA). Another bi-atrial geometry was derived by the segmentation of magnetic resonance images [4].

2.2. Rigid alignment and landmark generation

The atrial orifices (e.g. pulmonary veins, mitral valve in the left atrium) were automatically identified and labelled using a clustering algorithm presented in [3]. The only landmarks required were the apex point of the atrial appendages. The surface mesh coming from clinical data was

then pre-aligned to a bi-atrial SSM [2] using a rigid transformation matrix derived by minimizing the weighted sum of squared deviations between the atrial orifices centroids of the two surfaces. We decided to rigidly align in space before proceeding with the fitting to avoid a representation of translation and rotation parameters in the eigenmodes of the fitted SSM. The geometries used in this work were not included in the process of building the SSM. 35 characteristic points were automatically identified using geodesic paths connecting the previously marked orifices in the left atrium (10 in the pulmonary veins, 4 around the mitral valve ring, 4 in the roof, 2 in the septum, 1 in the left lateral wall, 9 in the anterior wall, 5 in the posterior wall) and used for the subsequent fitting procedure. If the left atrial appendage was present in the target geometry, a further landmark was added at the apex of the appendage.

2.3. Non-rigid shape model fit using Iterative Closest Points and Gaussian Process regression

We aimed to non-rigidly fit our SSM to a target surface using Iterative Closest Points (ICP) and Gaussian Process (GP) regression in order to establish correspondence between the two surfaces. This is different from the typical rigid ICP, which consists of finding the best rigid transformation between two meshes. Briefly, the main steps of the rigid ICP are the following: i) find candidate correspondences between the mesh to be aligned and the target by attributing the closest point on the target mesh as a candidate; ii) solve for the best rigid transform between the moving mesh and the target mesh using Procrustes analysis; iii) transform the moving mesh using this transformation; iv) repeat until we reach the limit number of iterations. The non-rigid ICP algorithm, which we used here for model fitting, performs the same steps. However, instead of finding a rigid transformation, it finds a non-rigid one using GP regression. The non-rigid transformation consists of the deformation that is encoded in the SSM eigenmodes. Given a set of points (in this case belonging to an instance of the SSM), we attribute the closest point on the target as a candidate correspondence to each of the points in the set. The returned sequence of points contains the candidate correspondences to the input points. The first main idea behind ICP is to use the candidate correspondences in a GP regression to find the best model instance explaining the observed deformations even though the correspondences are not perfect. We then defined a function that, when given a sequence of identifiers of model points and their candidate correspondence positions, computes a GP regression based on the resulting deformation field and returns the eigenmodes of the model instance fitting the candidate deformations best. These coefficients were then used as input to produce a bi-atrial geometry that fits our target LA. The non-rigid fitting of our SSM was implemented using ScalismoLab (`https://scalismo.org`).

2.4. Automated region annotation and fiber generation algorithm

Anatomical region annotation and fiber orientation calculations were performed using a highly automated pipeline based on a Laplace-Dirichlet-rule-based-method [3, 5]. The user interaction was further reduced by decreasing the number of required manually selected seed points from four to two (tip of left and right atrial appendage). The two additional landmarks needed previously on the left atrial appendage basis are now automatically identified by solving an additional Laplace equation using openCARP [6]. The algorithm was further improved by including the option of generating a bilayer model [7] in the case that only an endocardial surface mesh is given.

2.5. SSM fitting quality measures

The quality of the SSM fitting to the target clinical map was evaluated by computing the surface-to-surface distances using the *vtkDistancePolyDataFilter* (Kitware, Clifton Park, NY, USA).

3. Results and Discussion

The volume of the LA MRI segmentation was 80 mL and the corresponding best fitting instance had a blood pool volume of 75 mL. The original RA volume was 126 mL and the augmented RA that was obtained from fitting only the LA was 133 mL. We would like to recall that no information coming from the RA image was used to infer the RA mesh. Fig. 1 shows the result of the fitting procedure. We can notice how the fitted SSM instance represented the original MRI geometry very well, even using only few landmarks in the LA. The LA and RA computed surface-to-surface distances were 2.07 ± 1.56 mm and 3.59 ± 2.84 mm, respectively (Fig. 3). The average distance of 3.59 mm between the original segmentation and the inferred RA is remarkable if we think that we are in the range of less than 2 voxel diameters [8] omitting segmentation uncertainty. Regions with distances higher than 5 mm were located close to the inferior vena cava. This could be due to the incomplete segmentation of the vein's opening in the original manual segmentation.

The original electroanatomical map left atrium volume was 109 mL and the best fitted SSM instance resulted in a volume of 97 mL. The SSM fitted the left atrial wall very well (Fig. 2) even if the input anatomy had a lower quality compared to an MRI/CT segmentation. The surface-to-surface distance was 2.26 ± 1.95 mm as shown in Fig. 3.

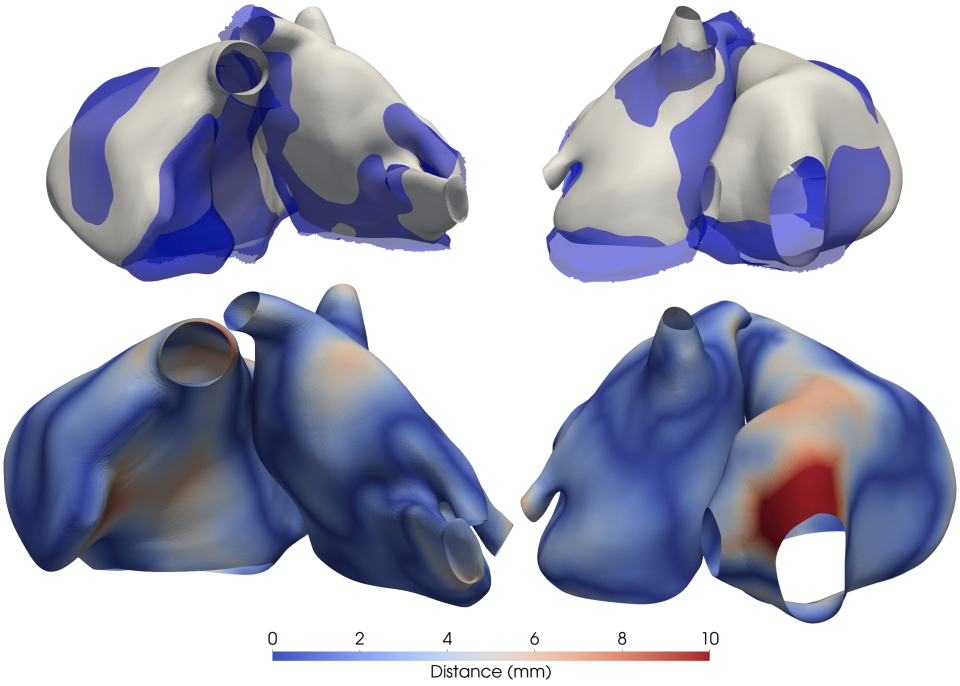

Figure 1. Top row: anterior (left) and posterior view (right) of the best fitting SSM instance (grey) to the target MRI segmentation (semi-tansparent blue). Bottom row: anterior and posterior view of the surface-to-surface distance between fitted SSM instance and target mesh shown on the fitted SSM instance.

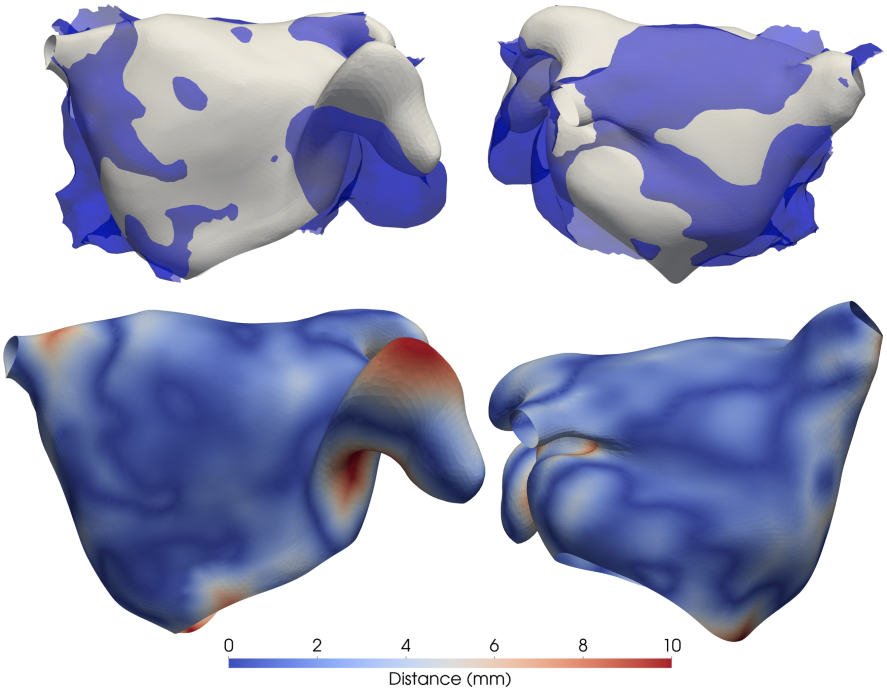

Figure 2. Top: anterior and posterior view of the SSM instance (grey) best fitting to the target CARTO electroanatomical map (semi-transparent blue). Bottom: anterior and posterior view of the surface-to-surface distance between the fitted SSM instance and the target mesh shown on the fitted SSM instance.

Electroanatomical maps only partly cover the full volume of the left atrial appendage and therefore necessarily cause high surface-to-surface distances in that region.

The SSM was able to generalize well to unseen geometries and accurately represent important anatomical features including the left atrial volume. This work demonstrates a proof of concept on two example meshes. Performance on a bigger virtual population remains to be shown. Moreover, updating the SSM with more clinical data could further improve the patient-specific generalization in regions with high inter-individual variability such as as the appendages.

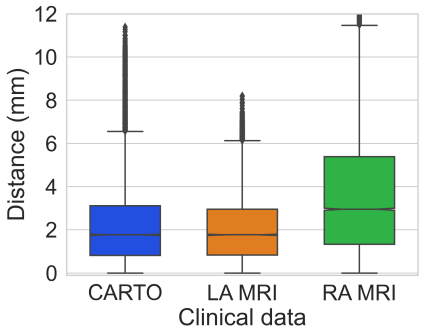

Figure 3. Surface-to-surface distances between the target mesh derived from clinical data (MRI or CARTO) and the corresponding fitted SSM. The RA mesh was purely inferred from the LA MRI landmarks and the SSM, no RA imaging data was used to inform the bi-atrial instance of the SSM.

4. Conclusion

We presented a semi-automatic pipeline that provides a ready-to-use personalized computational model by fitting a statistical shape model to a surface geometry obtained from clinical maps. The resulting augmented atrial model derived by the fitting algorithm represented the original anatomy very well and carefully reproduced the atrial volume even in the case of using only landmarks located in the left atrium to infer the right atrium.

Acknowledgments

This work was supported by European Union's Horizon 2020 research and innovation programme under the Marie Skłodowska-Curie grant agreement No.766082 (MY-ATRIA project), the EMPIR programme co-financed by the participating states and from the European Union's Horizon 2020 research and innovation programme under grant MedalCare 18HLT07, and by Deutsche Forschungsgemeinschaft (DFG) (project ID 391128822, SuLMaSS).

References

[1] Hindricks G, Potpara T, Dagres N, Arbelo E, Bax JJ, Blomström-Lundqvist C, Boriani G, Castella M, Dan GA, Dilaveris PE, Fauchier L, Filippatos G, Kalman JM, La Meir M, Lane DA, Lebeau JP, Lettino M, Lip GYH, Pinto FJ, Thomas GN, Valgimigli M, Van Gelder IC, Van Putte BP, Watkins CL. 2020 ESC guidelines for the diagnosis and management of atrial fibrillation developed in collaboration with the european association of cardio-thoracic surgery (EACTS). European Heart Journal 8 2020;.

[2] Nagel C, Schuler S, Dössel O, Loewe A. A bi-atrial statistical shape model for large-scale in silico studies of human atria: model development and application to ecg simulations. Medical Image Analysis 2021;102210.

[3] Zheng T, Azzolin L, Sanchez J, Dössel O, Loewe A. An automated pipeline for generating fiber orientation and region annotation of patient-specific atrial model. Current Directions in Biomedical Engineering 1 2021;1(1):409–412.

[4] Krueger MW, Seemann G, Rhode K, Keller DUJ, Schilling C, Arujuna A, Gill J, O'Neill MD, Razavi R, Dössel O. Personalization of atrial anatomy and electrophysiology as a basis for clinical modeling of radio-frequency ablation of atrial fibrillation. IEEE Trans Med Imaging 2013;32(1):73–84.

[5] Piersanti R, Africa PC, Fedele M, Vergara C, Dedè L, Corno AF, Quarteroni A. Modeling cardiac muscle fibers in ventricular and atrial electrophysiology simulations. Computer Methods in Applied Mechanics and Engineering 1 2021; 373:113468.

[6] Plank G, Loewe A, Neic A, Augustin C, Huang YL, Gsell MA, Elias Karabelas Mark Nothstein JS, Prassl AJ, Seemann G, Vigmond EJ. The openCARP simulation environment for cardiac electrophysiology. Computer Methods and Programs in Biomedicine 2021;208:106223.

[7] Labarthe S, Bayer J, Coudiere Y, Henry J, Cochet H, Jais P, Vigmond E. A bilayer model of human atria: mathematical background, construction, and assessment. Europace European Pacing Arrhythmias and Cardiac Electrophysiology Journal of the Working Groups on Cardiac Pacing Arrhythmias and Cardiac Cellular Electrophysiology of the European Society of Cardiology 1 2014;16 Suppl 4:iv21–iv29.

[8] Karim R, Blake LE, Inoue J, Tao Q, Jia S, Housden RJ, Bhagirath P, Duval JL, Varela M, Behar J, Cadour L, Van der Geest RJ, Cochet H, Drangova M, Sermesant M, Razavi R, Aslanidi O, Rajani R, Rhode K. Algorithms for left atrial wall segmentation and thickness - evaluation on an open-source CT and MRI image database. Medical image analysis 12 2018;50:36–53.

Address for correspondence:

Luca Azzolin
Fritz-Haber-Weg 1, 76131 Karlsruhe, Germany
publications@ibt.kit.edu

AugmentA: Patient-specific Augmented Atrial model Generation Tool

Luca Azzolin, Martin Eichenlaub, Claudia Nagel, Deborah Nairn, Jorge Sánchez, Laura Unger, Olaf Dössel, Amir Jadidi, and Axel Loewe

***Abstract*— Digital twins of patients' hearts are a promising tool to assess arrhythmia vulnerability and to personalize therapy. However, the process of building personalized computational models can be challenging and requires a high level of human interaction. A pipeline to standardize the generation of a patient's atrial digital twin from clinical data is therefore desirable. We propose a patient-specific Augmented Atria generation pipeline (AugmentA) as a highly automated framework which, starting from clinical geometrical data, provides ready-to-use atrial personalized computational models. AugmentA consists firstly of a preprocessing step applied to the input geometry. Secondly, the atrial orifices are identified and labelled using only one reference point per atrium. If the user chooses to fit a statistical shape model (SSM) to the input geometry, it is first rigidly aligned with the given mean shape before a non-rigid fitting procedure is applied. AugmentA automatically generates the fiber orientation and finds local conduction velocities by minimizing the error between the simulated and clinical local activation time (LAT) map. The pipeline was tested on a cohort of 29 patients on both segmented magnetic resonance images (MRI) and electroanatomical maps of the left atrium. Moreover, the pipeline was applied to a bi-atrial volumetric mesh derived from MRI. The pipeline robustly integrated fiber orientation and anatomical region annotations in 38.4±5.7 s. The error between in-silico and clinical LAT maps was on average 12.7 ms. In conclusion, AugmentA offers an automated and comprehensive pipeline delivering atrial digital twins from clinical data in procedural time.**

I. Introduction

Atrial fibrillation (AF) is a cardiac arrhythmia characterized by uncoordinated and chaotic atrial activation affecting more than 40 million people worldwide [1]. AF is the most prevalent arrhythmia and is associated with an increased long-term risk of other cardiovascular diseases. Computational modeling provides a novel framework to assess initiation, maintenance, and progression of AF in a personalized manner [2]–[7]. Cardiac digital twins (CDT) are digital replicas of patient hearts systematically integrating clinical data that match like-for-like all available clinical observations [8], [9]. Due to their intrinsic predictive ability, CDTs are a promising tool for precision medicine and personalised treatment aiding clinical decision making and providing an efficient and cost-effective platform for testing ethically and safely innovative therapies. However, current frameworks to deliver CDT integrating both the anatomical and functional twinning phases, referring to the inference of model anatomy and electrophysiology from clinical data, are not sufficiently efficient, robust, and accurate for advanced clinical and industrial applications. Several techniques to generate different sorts of atrial models have been presented covering a range of complexity and level of detail. Personalized computational models have been developed from either imaging data, e.g. derived from computed tomography (CT) or magnetic resonance images (MRI) [4], [10]–[12], or electroanatomical maps [13]. However, a standardized pipeline for generating personalised atrial computer models from geometries derived from either of the described recording modalities remains unavailable. Lately, Razeghi et al. presented the CemrgApp open source platform for image processing to provide MRI segmentation including fibrotic tissue distribution derived from late gadolinium enhancement (LGE) intensity in a semi-automatic and user-friendly way [14]. In addition, Williams et al. published an open source platform to import, preprocess and analyze electroanatomical mapping data [15]. What is missing today is a pipeline that ingests the segmentations as provided for example by CemrgApp and the functional information as provided for example by openEP and builds a simulation-ready digital twin model. Building such model directly from clinical geometrical data remains a challenging process since imaging data can be influenced by various degrees of segmentation uncertainty [16] and electroanatomical maps can miss relevant anatomical structures (right atrium, appendage, veins). Recently, Nagel et al. presented a bi-atrial statistical shape model (SSM) covering the relevant anatomical variability required for in-silico electrophysiological experiments and well generalizing to unseen geometries [17]. Moreover, SSM were shown to be a valuable tool to generate large cohorts of ready-to-use atrial models to run electrophysiological simulations [18].

Even more complicated is the functional twinning phase, where the spatio-temporal myocardial depolarisation is retrieved by clinical data possibly affected by noise and uncertainty. In particular, late gadolinium enhancement distribution and/or electroanatomical maps can be used to infer cardiac tissue characteristics and estimate conduction velocity [13], [19]–[22].

We aimed to develop and provide a highly automated pipeline to generate personalized computational models of human atria augmented with population-level a-priori knowledge (fiber orientations and region annotation) suitable for in-silico experiments. We designed the platform to enhance usability and reproducibility requiring minimal user interaction.

II. Materials and Methods

The automated modeling pipeline for generating detailed personalized computational models of human atria is illustrated in Fig. 1. The input can be an atrial surface obtained from an electroanatomical mapping system or derived from tomographic imaging segmentation (e.g. MRI or CT). In the case of a surface with closed orifices, the pipeline proceeds with the opening of atrial orifices as described in Sec. II-B and in Sec. II-C. Next, the user can decide to proceed to fit a SSM to the target anatomy in case the user would like to augment possible missing anatomical structures or to resolve segmentation uncertainties. Provided that the quality of the original geometry is ensured, the user can directly proceed to the resampling step presented in Sec. II-H. If the desired workflow includes fitting an SSM to the target geometry, the pipeline will first label the atrial orifices as presented in Sec. II-D, automatically prealign the target mesh to the average geometry of the SSM and generate the landmarks needed for the fitting procedure as explained in Sec. II-E. Consequently, the SSM is fitted as detailed in II-F. Then, the resulting model is resampled as specified in Sec. II-H. Finally, the atrial anatomical regions are annotated and fiber orientation is computed as described in Sec. II-I. We quantitatively evaluated and compared four different methodologies to estimate conduction velocity from clinical data in Sec. II-J. The proposed highly automated atrial modeling pipeline was tested on both electroanatomical maps and MRI segmentations in a cohort of 29 patients further detailed in Sec. II-A.

A. Dataset

A cohort of 29 persistent AF patients (65±9 years, 86% male) for which both electroanatomical maps and MRI segmentations of the left atrium (LA) were available were included in this study. High density electroanatomical left atrial maps (2170±478 sites) were acquired in sinus rhythm prior to pulmonary vein isolation using a 20-polar mapping catheter (Lasso-Nav or PentaRay-catheter, Biosense Webster Inc., CA, USA) and the CARTO 3 system (Biosense Webster Inc., CA, USA). The post-processing of the LA LGE-MRI (3 Tesla, Somatom Skyra, Siemens Healthcare, Erlangen, Germany)) was performed by an independent expert laboratory (ADAS3D Medical, Barcelona, Spain) blinded to any clinical data. The study was approved by the institutional review board, registered in the German WHO primary registry DRKS (unique identifier: DRKS00014687), and all patients provided written informed consent prior to enrollment. Moreover, a bi-atrial geometry was derived by Subject 3 presented in Krueger et al. [4]. No electroanatomical map was available in this case.

B. Mitral valve opening annotation

For the case of a closed surface with no valve openings provided as input to the pipeline, we implemented an automated algorithm to estimate the location of the mitral valve (MV) opening. The method differs depending on whether an electroanatomical map or an MRI segmentation is supplied.

- If the input closed surface comes from an electroanatomical map, the peak-to-peak bipolar voltage was calculated from all EGM signals of the electroanatomical map in the window of the QRS complex. The QRS complex was found using the ECGdeli toolbox on the ECG lead V3 [23], [24]. Areas of high voltage (values above the 75 % voltage percentile) were considered as the MV due to the ventricular far field causing high voltages in this area. To ensure only the MV was identified and not atrial wall areas, points were only considered if they had high voltage during QRS and a low bipolar voltage ($<$0.5 mV) outside of the QRS complex.
- Since for the closed atrial surface derived from MRI, no electrogram signals are available which can be used to identify the MV, the existing mean shape of the LA where the MV was marked was used [25]. The mean shape was rigidly aligned and correspondence was established to each new patient geometry [25]. Afterwards, the area marked as MV in the mean shape could then be identified in the new geometry.

C. Mesh pre-processing and removing valves and veins

Geometries directly derived from clinical data usually do not have a sufficient mesh quality for electrophysiological monodomain simulations [26]. Therefore, regardless of the input, AugmentA proceeds with a mesh pre-processing step, which consists in removing self-intersections and degenerate elements, while regions of the surface without defects are left unmodified. The pymeshfix Python module [27] is used in this mesh pre-processing step. Then, the veins are identified as the regions with highest surface curvature, due to their anatomical cylindrical configuration. Briefly, the surface curvature at each node is calculated as $1/R$, where R is the radius of the fitted osculating sphere, as in [28]. The parameter R is set to 3 cm in both LA and right atrium (RA). Areas with a surface curvature higher than 1.1 times the surface curvature median value are labeled as high curvature. Then, the pipeline proceeds with opening the MV. The algorithm is different depending on whether the input geometry comes from tomographic imaging or electroanatomical mapping:

- In the case of a mesh derived from imaging data, the center of mass of the region marked as MV is computed after the co-registration presented in Sec. II-B and all the elements with a distance less than 2 cm [29] from the center of mass are removed to create the opening. Afterwards, the user has to manually select the atrial appendage apex. The pipeline continues with the clipping of the pulmonary veins by removing the elements that belong to high curvature regions and are not including the manually marked left atrial appendage apex.
- In the case of an electroanatomical map, all the elements enclosed in a sphere around the center of mass of the region marked as MV and with a diameter computed as the largest distance between all the points labelled as MV are removed. A maximum diameter of 4 cm [29] is set as upper bound to be consistent with the dimension of

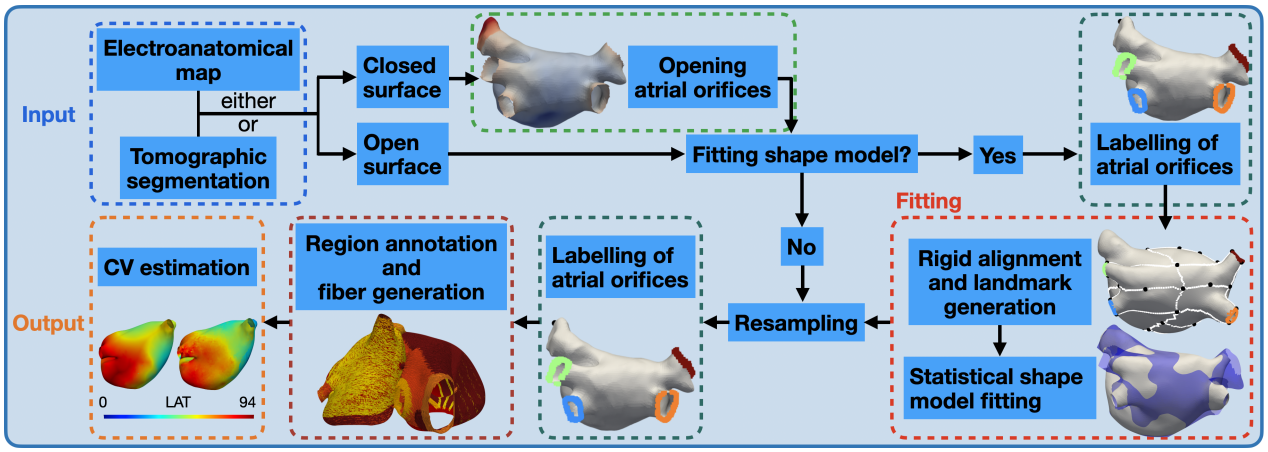

Fig. 1. Overview of the proposed pipeline for the generation of personalised computational atrial models from different clinical anatomical data.

the MV opening from the imaging data. Occasionally, a geometrical artifact caused by the transseptal puncture is present in the electroanatomical maps. In those cases, the reference point is chosen at the tip of the transseptal puncture instead of the left atrial appendage apex. Later, the veins are identified as the areas with both high curvature and low bipolar voltage (lower than 0.5 mV), since the left atrial appendage mostly presents high voltage and veins mostly present low voltage. Each vein's ring is generated by clipping all the elements intersecting a sphere centered at the point with maximum curvature and with variable radius chosen as the distance between the highest curvature point and the closest one with bipolar voltage higher than 0.5 mV, as shown in Fig. 3. The high curvature region manually marked as geometrical artifact due to the transseptal puncture is left out in the clipping procedure. The remaining high curvature and high voltage regions are annotated as possible left atrial appendage and the vertex with highest curvature as the apex. Following the the clipping step, the resulting processed geometry with the final openings and the automatically identified apex of the appendage is visualized using PyVista [30]. At this point, the user can decide to manually select a different vertex which is going to be used as reference point in the following labelling step.

D. Automatic labelling of atrial orifices

The atrial orifices (pulmonary veins, MV in the LA and inferior & superior vena cava, tricuspid valve, coronary sinus in the RA) are automatically identified and labelled using a clustering algorithm presented in [31]. The only landmarks required are the apex points of the left and right atrial appendages. Briefly, the atrial orifices can be detected as the boundary edges. For the LA, the MV is determined as the largest connected boundary and the rest of the rings are clustered twice to distinguish between left and right as well as inferior and superior pulmonary veins using k-means clustering. At first, the pulmonary veins belonging to the cluster closer to the left atrial appendage (LAA) are labelled as left pulmonary veins (LPV). The remaining cluster is marked as right pulmonary veins (RPV). Secondly, the LPV are further separated into superior and inferior. The left inferior pulmonary vein is detected as the cluster closest to the LAA. The right inferior pulmonary vein is set as the one belonging to the same side as the left inferior pulmonary vein of the plane passing through the LPV, RPV and the MV centers of mass. For the orifices of the RA, the tricuspid valve (TV) is identified as the largest one. The cluster closest to the apex point of the right atrial appendage (RAA) is labelled as superior vena cava (SVC). The smallest of the remaining two rings is marked as coronary sinus (CS) and the other as inferior vena cava (IVC). Subsequently, a plane passing through the centers of the SVC, IVC and TV is used to identify a band between the IVC and the SVC and to divide the TV into a septal (TV_S) and a lateral wall part (TV_L). These are used as boundary conditions in the region labelling and fiber generation algorithm presented in Sec. II-I.

E. Rigid alignment and landmark generation

After the labelling of the atrial orifices, the user can choose whether to proceed with fitting a SSM to the target geometry or directly jump to the resampling step followed by region annotation and fiber generation. In case the user wants to fit a SSM to the target geometry, a rigid alignment in space is required before the fitting procedure since translation and rotation are not represented by eigenmodes of the SSM. The transformation matrix was derived by minimizing the weighted sum of squared deviations [32] between the atrial orifices centroids of the two surfaces. 36 characteristic points were then automatically identified in the LA using geodesic paths connecting the previously marked orifices. 10 landmarks in the pulmonary veins, 4 around the MV ring, 4 in the roof, 2 in the septum, 1 in the left lateral wall, 9 in the anterior wall, 5 in the posterior wall, 1 at the LAA apex) were used for the subsequent fitting procedure. The location of the

landmarks on the relative paths can be found in Sec. S.II. of the Supplementary Material.

F. Non-rigid shape model fit using Iterative Closest Points and Gaussian Process regression

We aimed at establishing correspondence between a bi-atrial SSM [17] and the clinical geometry at hand. The geometries used in this work were not included in the process of building the SSM. Non-rigid fitting was performed by a combination of Iterative Closest Points (ICP) and Gaussian Process (GP) regression [33]. This methodology differs from the typical rigid ICP [34], which consists of identifying the best rigid transformation between two meshes. Briefly, the main steps of the classical rigid ICP are the following:

- find candidate correspondences between the moving mesh (i.e. SSM instance) and the target (i.e. clinically derived geometry) by considering the closest point on the target mesh as a candidate;
- solve for the best rigid transform between the moving mesh and the target mesh using Procrustes analysis [32];
- transform the moving mesh using this transformation;
- repeat until convergence.

The non-rigid ICP algorithm used in this study for model fitting performs the same steps. However, instead of finding a rigid transformation, it solves for a non-rigid one using GP regression [35]. The non-rigid transformation consists of the deformation that is encoded in the SSM eigenmodes. Given a set of points (in this case belonging to an instance of the SSM), we attribute the closest point on the target as a candidate correspondence to each of the points in the set. The returned sequence of points contains the candidate correspondences to the input points. The first main idea behind ICP is to use the candidate correspondences in a GP regression to find the best model instance explaining the observed deformations even though the correspondences are not perfect. We then defined a function that, given a sequence of identifiers of model points and their candidate correspondence positions, computes a GP regression based on the resulting deformation field and returns the principal component coefficients of the model instance fitting the candidate deformations best. These coefficients were then used as input to retrieve a bi-atrial geometry that fits our target LA. The non-rigid fitting of our SSM was implemented using ScalismoLab (https://scalismo.org).

G. Co-registration of multi-modal data sets

The fitting method established correspondence between each target geometry and the SSM. Each data vector (local activation time, voltage, LGE IIR, etc.) was mapped from the original mesh to the fitted SSM using a nearest neighbour algorithm. Since the best fitted SSM instance is a deformed version of the mean shape, it always features the same number of nodes and vertex IDs. Therefore, the electrophysiological data mapped from one patient's electroanatomical map to the resulting best fit of the SSM could be easily transferred to the respective SSM instance derived from imaging data. Since we assumed that the MRI segmentation was a better representation of the patient's real atrial anatomy compared to the electroanatomical mesh, local activation time, uni- and bipolar voltage maps were registered to the SSM instance derived from the MRI fitting.

H. Resampling

Even though the SSM in general already provides a good quality mesh, electrophysiological simulations performed with finite elements methods require a fine spatial resolution [26], [36]. We therefore procedeeded with a mesh resampling step providing a final high quality mesh with an average edge length of 0.4 mm. A combined smoothing and up-sampling algorithm was performed using one iteration of Laplacian smoothing and the isotropic explicit remeshing filter of PyMeshLab [37], a Python library interfacing to MeshLab [38], an open source software to edit and process 3D triangular meshes.

I. Automated region annotation and fiber generation algorithm

Atrial fiber architecture is characterized by the presence of multiple overlapping bundles running along different directions, differently from the ventricular fibers architecture where myofibers are aligned along regular patterns. Rule-based methods are widely used strategies to generate myocardial fiber orientation in computational cardiac models [39], [40]. A particular class of algorithms is known as Laplace–Dirichlet-Rule-Based methods (LDRBM) since they rely on the solution of Laplace problems with Dirichlet boundary conditions. In this work, a fully automated method to annotate the different atrial regions and for generating fiber orientation, based on the LDRBM proposed by Piersanti et al. [41] and updated in Zheng et al. [31] was implemented.

In the pipeline, six Laplace problems for the LA and six for the RA were formulated:

$$\Delta\psi = \frac{\partial^2\psi}{\partial x^2} + \frac{\partial^2\psi}{\partial y^2} + \frac{\partial^2\psi}{\partial z^2} = 0 \tag{1}$$

with proper Dirichlet boundary conditions ψ_a and ψ_b on the respective boundaries Γ_a and Γ_b. These partial differential equations were solved using the open electrophysiology simulator openCARP [42]. The domain of the Laplace problems is the atrial mesh. The boundary condition domains were obtained using the method described in Sec. II-D. We further decreased the number of required manually selected seed points from four to two (apex of LAA and RAA), thus decreasing user interaction and effort and enhancing reproducibility. The two additional landmarks needed previously in [31] on the LAA basis were automatically identified by solving two additional Laplace equations ψ_{ab2} with $\psi_a = 0$ in the RPV and $\psi_b = 1$ at the LAA apex and ψ_{r2} with $\psi_a = 0$ at both LPV and RPV and $\psi_b = 1$ at the MV ring as Dirichlet boundary conditions. In addition, a supplementary Laplace system ψ_{v2} with $\psi_a = 1$ in the IVC and $\psi_b = 0$ at the RAA apex is solved in the RA to improve the identification of the RAA compared to Zheng et al. [31]. The complete list of boundary

conditions used can be found in Tab.1 of the Supplementary Material. The bundle selection was automatically performed and the bundles' dimension was adjusted for each patient using a region growing method. Following the bundle selection, an orthonormal local coordinate system was built at each element of the atrial domain by performing a Gram–Schmidt orthogonalization. In the case that only an endocardial surface mesh is provided as input, we computed the transversal direction as the normal vector to the atrial surface at each point and the option of generating a bilayer model [43] with different endo- and epicardial fiber arrangement was included in the pipeline.

J. Conduction velocity estimation methods

Cardiac tissue conduction velocity (CV) was estimated using four different methodologies. Regional anisotropy ratio was fixed to 3.75:1 in the LA [44]. In the first two, only non-invasive data coming from the LGE-MRI were used (i.e., IIR). The third and fourth method, estimate the CV from the clinically recorded local activation time (LAT) map.

- The first method consisted in discretely applying different CV depending on the IIR value (CV_{di}). We tuned the monodomain conductivity to reach a longitudinal CV of 1.0 m/s in the healthy tissue (IIR$<$1.2), of 0.7 m/s in the interstitial fibrosis areas (1.2$\leq$IIR$<$1.32) and of 0.6 m/s in the dense fibrosis regions (IIR$\geq$1.32) [19], [45].
- In the second method we applied a CV following a regression model (CV_{rm}) relating CV to IIR value [45]:

$$\mathrm{CV} = 1\,m/s \cdot exp(0.6731 - 0.9177 * \mathrm{IIR}). \quad (2)$$

- In the third method, we calculated the CV by fitting radial basis functions (CV_{rb}) [21], [46]. The algorithm selects stable catheter positions, finds the local activation times (LAT), considers the wall contact and calculates all CV estimates within the area covered by the catheter.
- The fourth method consisted in iteratively tuning (CV_{tu}) each element conductivity to minimize the root mean squared error (RMSE) between the simulated LAT and the recorded clinical LAT. The fiber field used is the one presented in Sec. II-I. The clinical LAT map is divided into activation bands from the earliest to the latest activation in steps of 30 ms. However, selecting the location of earliest activation as the very first activated map point or electrogram point can be error-prone. Therefore, the earliest activated point is identified as the center of mass of the region with clinical LAT within the 2.5th percentile. Firstly, the earliest 2.5th percentile LAT points are identified and then their center of mass is calculated and used as earliest activated point in the in-silico experiment. Before proceeding with the iterative fitting of the clinical LAT, we detect the nodes with an earlier activation than the neighboring vertices and mark them as wrong annotations, as illustrated in Fig. 9B. The LAT annotations in these areas are not used in the fitting process and the conductivity is chosen as the mean of the region boundary.

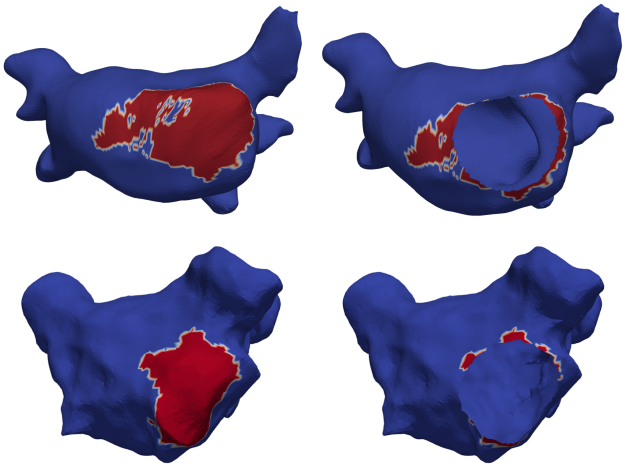

Fig. 2. Identification and generation of mitral valve opening. Elements marked as mitral valve (in red) after the co-registration procedure and the resulting mitral valve opening. The remaining high curvature region is the left atrial appendage. Top row: example based on an MRI segmentation (patient 28). Bottom row: example based on an electroanatomical map (patient 28).

K. Atrial models and computational tools

The myocyte membrane dynamics were represented with a variant of the original Courtemanche et al. model [47] reflecting AF-induced remodeling [48]. Atrial tissue regions with IIR higher than 1.2 were labelled as fibrosis. We set 30% of the elements in the fibrotic regions as almost not conductive (conductivity of 10^{-7} S/m) to account for structural remodeling and the presence of scar tissue. This approach modelled the macroscopic passive barrier behaviour caused by the electrical decoupling of the myocytes in the tissue infiltrated by fibrosis, also referred to as 'percolation' [49]. In the other 70%, several ionic conductances were rescaled to consider effects of cytokine-related remodeling [50] (-50% g_{K1}, -40% g_{Na} and -50% g_{CaL}). The spread of the electrical depolarization in the atrial myocardium was simulated by solving the monodomain equation using openCARP [42] and a time step of 0.02 ms.

III. Results

A. Removing mitral valve and pulmonary veins

The automatic annotation of the MV opening region identified the location of the MV in all 29 patients both in electroanatomical maps and MRI segmentations. Fig. 2 shows an example of both the MV labelling step and the consequent creation of the valve ring. Regions with surface curvature higher than 1.1 times the median value identified both veins and appendage in the case of MRI segmentation and the pipeline correctly proceeded with the clipping of the veins regions, though maintaining the appendage, as shown in Fig. 3. When the input geometry was derived from an electroanatomical map, the combination of high surface curvature and low bipolar voltage resulted in an accurate location of the pul-

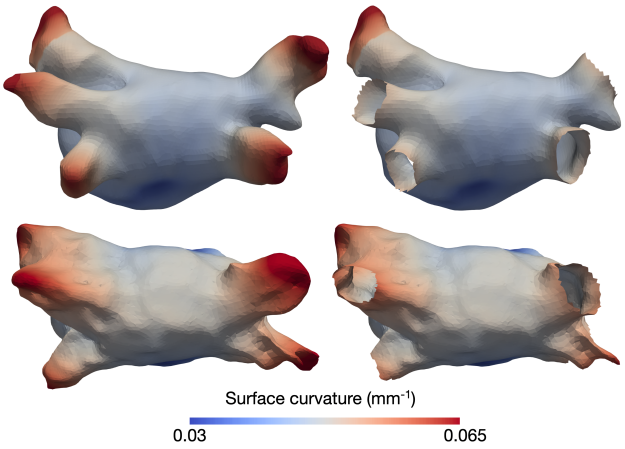

Fig. 3. Pulmonary veins clipping using the surface curvature. Regions with surface curvature higher than 1.1 the median value are shown in red and the mesh after the removal of the pulmonary veins in the right column. Top row: example based on an MRI segmentation (patient 28). Bottom row: example based on an electroanatomical map (patient 28).

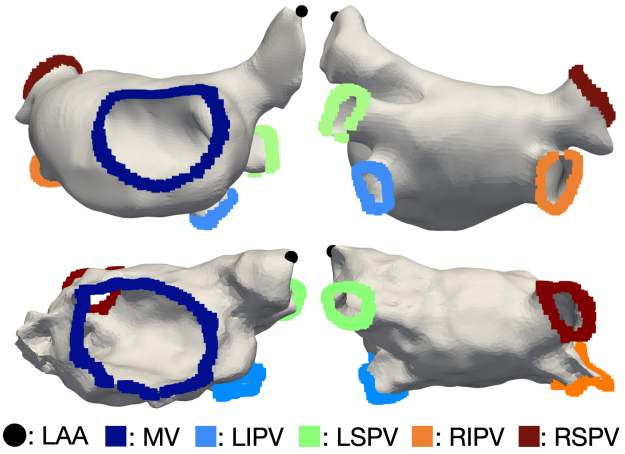

Fig. 4. Output of the atrial openings annotation step (mitral valve and roof view of the labelled atrial orifices). Top row: example based on an MRI segmentation (patient 28). Bottom row: example based on an electroanatomical map (patient 28). LAA: left atrial appendage apex, MV: mitral valve, LIPV: left inferior pulmonary vein, LSPV: left superior pulmonary vein, RIPV: right inferior pulmonary vein, RSPV: right superior pulmonary vein.

monary vein regions in the LA. The remaining high curvature area always corresponded to the LAA.

B. Atrial orifices labelling

Atrial orifices were automatically identified and correctly labelled from the pipeline in all 29 patients. The accuracy of the labelling was checked by visual inspection. An example of the resulting annotated geometry in both an MRI segmentation and an electroanatomical map is shown in Fig. 4. The decision of using only the atrial appendage apexes as reference point for the labelling method turned out to be appropriate to robustly discriminate between valves and veins in both left and right atrium.

C. Statistical shape model fitting process

All 36 landmarks were correctly and automatically identified in the whole patient cohort using the geodesic paths connecting the atrial orifices labelled in the previous step. The reference points covered most of the atrial surface and localized the most important atrial structures, as shown in Fig. 5. The non-rigid fitting procedure provided the best fitted SSM instance for each electroanatomical map and MRI segmentation, as presented in Fig. 6. Fig. 7 shows the surface-to-surface distance between the best fitted SSM and the target electroanatomical map (2.72 ± 2.17 mm). The surface-to-surface distance in the case of target atrial geometries derived from MRI segmentations was 2.13 ± 1.79 mm across all patients (Fig. 7).

D. Atrial region annotation and fiber orientation generation

Atrial structures were automatically annotated in all 29 LA SSM instances and the pipeline carefully identified each region using the previously labelled atrial orifices and the LAA apex. Finally, bilayer models including realistic fiber orientation were generated. The pipeline was therefore tested on a bi-atrial surface model coming from the mean shape of a SSM [17]. In both LA and RA, regions were correctly annotated (Fig. 8). Moreover, fiber orientation was calculated and a bi-atrial bilayer model was generated along with inter-atrial bundles, as presented in Fig. 8. We recall that in the case of a bi-atrial surface as input, the only two manual reference points needed by the full pipeline are left and right atrial appendage apexes. In Fig. 8, we show the results of region annotation and fiber orientation on a volumetric bi-atrial mesh derived from MRI segmentation [4]. The same pipeline was further applied to 100 different volumetric atrial models with homogeneous thickness coming from various instances of a SSM [17] and made publicly available [51]. In Zheng et al. [31], a volumetric bi-atrial mesh with heterogeneous myocardial thickness [52] was used as input and the pipeline proceeded with region annotation and fiber generation.

E. Conduction velocity estimation

The simulated LAT map based on an underlying CV as estimated with the fourth method from the clinical LAT for patient 1 is shown in Fig. 9. The in-silico LAT maps computed with all four CV estimation methodologies presented in Sec. II-J can be found in Fig. S1 of the Supplementary Material. The root mean square error (RMSE) between the simulated and the clinical LAT maps was calculated for each of the presented CV estimation method and presented in Tab. I.

Moreover, we computed the relative error per patient between the simulated and the clinical LAT map as:

$$\text{Relative LAT error} = \frac{\text{Simulated LAT} - \text{Clinical LAT}}{max\,(\text{Clinical LAT})} \quad (3)$$

and the distributions of the relative LAT error using the various methodologies to estimate CV are shown in Fig. 10. The relative LAT errors for each patient can be found in Fig.S2-S5 the Supplementary Material.

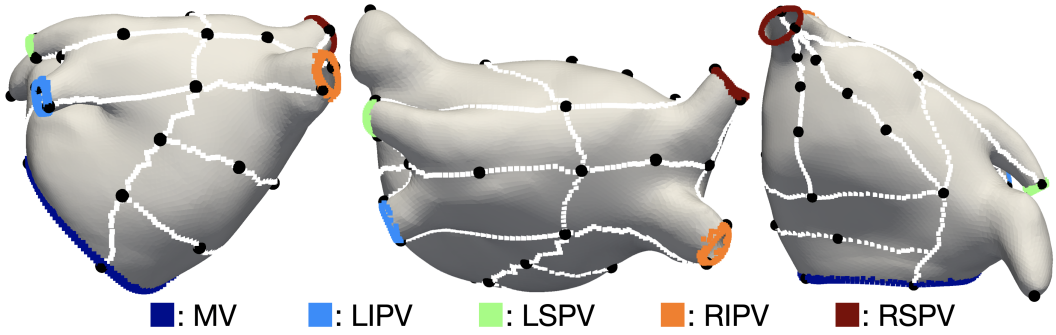

Fig. 5. Posterior, roof and anterior view of the landmarks generation procedure on the left SSM mean instance [17]. Geodesic paths used to identify the landmarks locations in white and respective 36 landmarks in black.

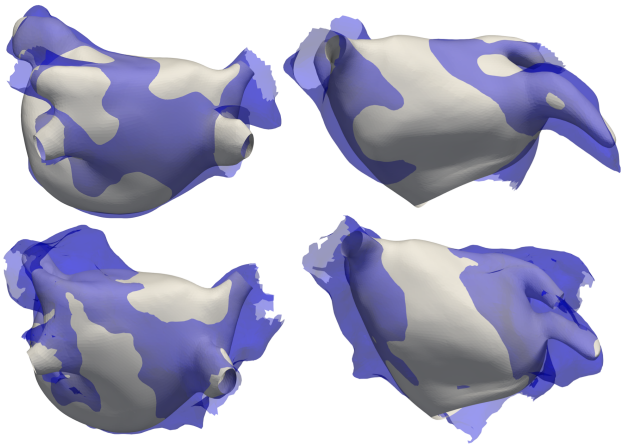

Fig. 6. Top row: Roof and anterior view of the SSM instance (grey) best fitting to the target MRI segmentation (semi-transparent blue). Bottom row: Roof and anterior view of the SSM instance (grey) best fitting to the target electroanatomical map (semi-transparent blue).

TABLE I
RMSE (MS) BETWEEN THE SIMULATED AND THE CLINICAL LAT MAPS USING THE DIFFERENT CV ESTIMATION METHODS.

CV estimation method	RMSE (ms)
CV_{di}	27.1±13.6
CV_{rm}	36.7±14.1
CV_{rb}	107.5±44.5
CV_{tu}	12.7±5.8

F. Processing time

The full pipeline took 38.4±5.7 s to complete the opening and labelling of atrial orifices, the fitting process, mesh resampling, the region annotation and fiber generation steps, demonstrating the feasibility of an in-situ application.

IV. Discussion

A. Opening and labelling atrial orifices

The pipeline automatically identified and proceeded with the opening of the atrial orifices. In comparison to CemrgApp [14], in which the user has to manually select the mitral valve and all pulmonary vein regions, the only user-interaction needed by our pipeline is the selection of the atrial appendage apex.

B. Statistical shape model fitting

The SSM fitting step allowed to establish correspondences between each geometry derived from clinical data and the SSM. Regions with higher distance were located mostly close to the appendage. However, we have to recall that the LAA volume is often only partly covered during electroanatomical mapping. The average distance of 2.13 mm between the original MRI segmentation is in the range of one to two voxels [17], [53] omitting segmentation uncertainty. Therefore, the best fitted SSM instance very well represented the original anatomy and augmented the missing anatomical structures (e.g. appendages), as shown in our previous work [33]. The SSM generalized well to unseen geometries and accurately represented relevant anatomical features. Moreover, the patient-specific generalization in regions with high inter-individual variability such as the appendages and the PVs could be improved by updating the SSM with more clinical data.

C. Region annotation and fiber generation

We have developed a highly automated pipeline that accurately generated the fiber direction of the human atria according to histological data. Additionally, we provide a pipeline that annotates the anatomical regions independently from the atrial geometrical variability due to the region growing implementation. We demonstrated how the pipeline can generate both volumetric and bilayer 3D models, perform with anatomical variations, and create accurate models of the human atrial anatomy. The pipeline well represented the complex atrial fiber architecture and captured the complex fiber bundles arrangements in both LA and RA. Different endocardial and epicardial fiber orientation were included to faithfully represent the transmural variability even in a bilayer computational model. Comparing to the existing method by Wachter et al. [40] that requires 21 manually defined seed points and a longer calculation time, our pipeline significantly reduces the calculation time and human manual interaction. The original LDRBM by Piersanti et al. [41] and updated by

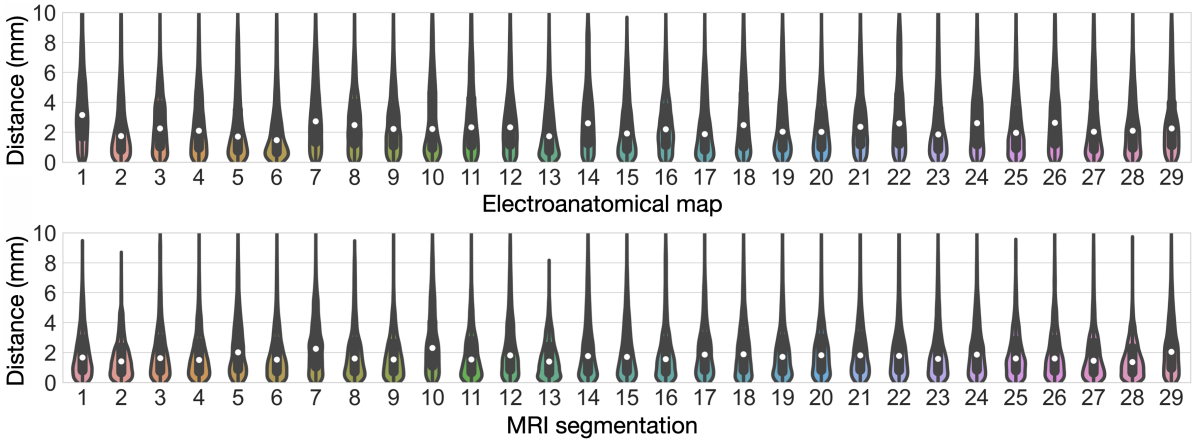

Fig. 7. Top row: surface-to-surface distance between the best fitting SSM instance and the respective electroanatomical map. Bottom row: surface-to-surface distance between the best fitting SSM instance and the respective MRI segmentation.

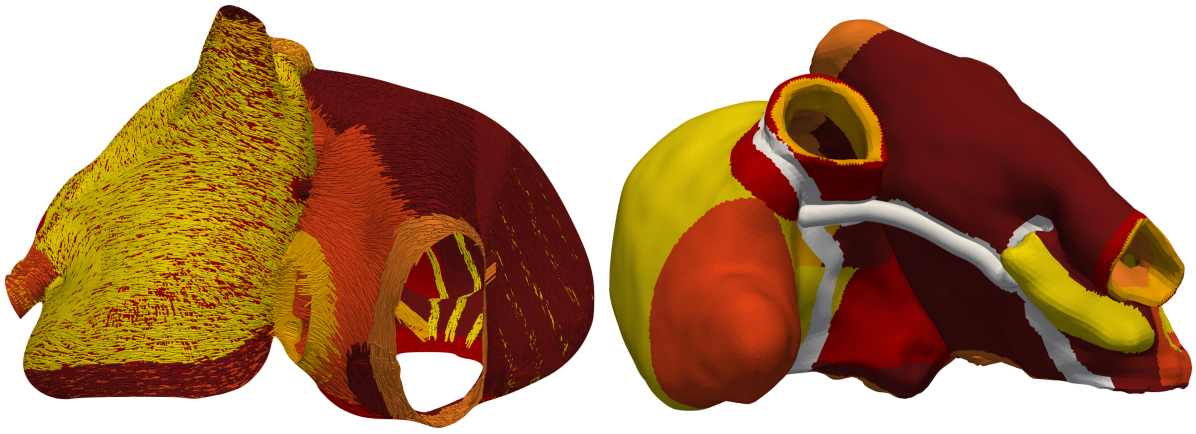

Fig. 8. Posterior view of the fiber orientation computed with AugmentA in a bi-atrial bilayer model derived from a SSM [17] and anterior view of the region annotation in a bi-atrial volumetric model [4] in which the wide Bachmann's Bundle is highlighted in white.

Zheng et al. [31] was further improved enhancing automation and reproducibility by limiting the manual user interaction to the selection of one reference point per atrium and using an extra set of Laplace solutions. Roney et al. [52] presented a methodology to assign the fiber orientation by mapping the fiber field from a human atrial fiber atlas to different patient specific atrial models. Even if the impact of the fiber field on average activation times computed in paced rhythm was relatively small, it had a larger effect on maximum LAT differences. Moreover, arrhythmia dynamics were highly dependent on the fiber field, suggesting that atrial fiber fields should be carefully assigned to patient-specific arrhythmia models. Our pipeline ensures personalization of both region annotation and specification of fiber orientation to each anatomical structure in the human atria.

D. Conduction velocity estimation

We systematically evaluated three state-of-the-art methods to estimate cardiac tissue CV from clinical data and compared them to our newly proposed iterative fitting to the clinical LAT map algorithm. Monodomain conductivity in each element was calculated directly from the CV map using a regression curve representing the relationship between CV and conductivity computed tuning the tissue conductivities to match a specific CV in a tissue slab. This approach can potentially underestimate longitudinal CV if the excitation direction is not completely parallel to the myocyte orientation. This might be part of the reason for the bias towards positive errors. The CV_{rb} method had the highest RMSE due to its sensitivity to sparse data recordings.

V. Limitations

The used SSM did not include different numbers of PVs. Therefore, the fitted SSM instance will always provide an atrial surface with four pulmonary veins. In the multi-modal data co-registration step, the data vector interpolation rather than nearest neighbor mapping might improve data fidelity.

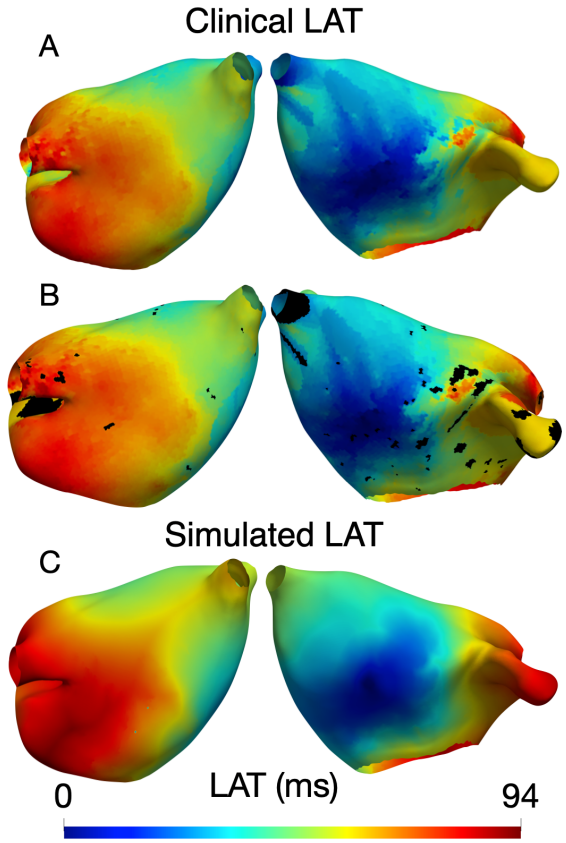

Fig. 9. A: posterior and anterior view of the clinical LAT map of patient 1. B: posterior and anterior view of the clinical LAT map of patient 1 in which we marked in black the nodes with an earlier activation with respect to the neighbours. C: posterior and anterior view of the simulated LAT map of patient 1 using the CV_{tu} estimation method.

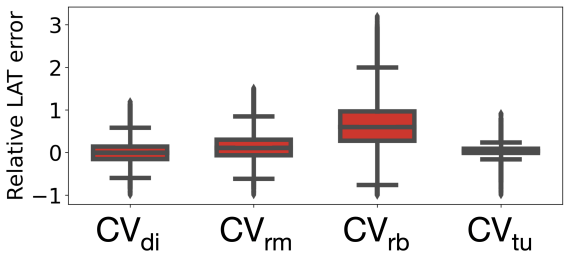

Fig. 10. Relative LAT error between simulated and clinical LAT map using the four conduction velocity estimation methods.

VI. Data availability

All personalized computational models used in this study including fiber orientation and anatomical labels are available online (https://doi.org/10.5281/zenodo.5589289).

VII. Conclusion

The pipeline presented in this work offers a highly automated, comprehensive and reproducible framework to process geometries derived from clinical data and generate atrial anatomical and functional digital twins. AugmentA was able to provide ready-to-use atrial models starting from either electroanatomical maps or imaging data. The pipeline incorporates various region labels and detailed fiber orientation reducing the user-interaction to the selection of one reference point per atrium. The pipeline was moreover tested with surface and volumetric input and it correctly proceeded with atrial structure annotation and fiber generation. AugmentA could thus become a default framework for the generation of atrial digital twin models from clinical data in future studies. This work is a step forward to improve comparability and reproducibility of atrial models derived from clinical data and to facilitate the evaluation of arrhythmia vulnerability and ablation planning automating the computational model generation steps.

References

[1] G. Hindricks *et al.*, "2020 ESC guidelines for the diagnosis and management of atrial fibrillation developed in collaboration with the european association of cardio-thoracic surgery (EACTS)," *European Heart Journal*, 8 2020.

[2] L. Azzolin, S. Schuler, O. Dössel, and A. Loewe, "A reproducible protocol to assess arrhythmia vulnerability : Pacing at the end of the effective refractory period." *Frontiers in Physiology*, vol. 12, p. 656411, 1 2021.

[3] B. Lim *et al.*, "In situ procedure for high-efficiency computational modeling of atrial fibrillation reflecting personal anatomy, fiber orientation, fibrosis, and electrophysiology," *Scientific Reports*, vol. 10, no. 1, 1 2020.

[4] M. W. Krueger, G. Seemann, K. Rhode, D. U. J. Keller, C. Schilling, A. Arujuna, J. Gill, M. D. O'Neill, R. Razavi, and O. Dössel, "Personalization of atrial anatomy and electrophysiology as a basis for clinical modeling of radio-frequency ablation of atrial fibrillation," *IEEE Trans. Med. Imaging*, vol. 32, no. 1, pp. 73–84, 2013.

[5] C. H. Roney *et al.*, "In silico comparison of left atrial ablation techniques that target the anatomical, structural, and electrical substrates of atrial fibrillation," *Frontiers in Physiology*, vol. 11, p. 1145, 2020.

[6] N. A. Trayanova, "Mathematical approaches to understanding and imaging atrial fibrillation: significance for mechanisms and management," *Circulation Research*, vol. 114, no. 9, pp. 1516–1531, 1 2014.

[7] P. M. Boyle *et al.*, "Computationally guided personalized targeted ablation of persistent atrial fibrillation." *Nature Biomedical Engineering*, 8 2019.

[8] J. Corral-Acero *et al.*, "The 'Digital Twin' to enable the vision of precision cardiology," *European Heart Journal*, vol. 41, no. 48, pp. 4556–4564, 03 2020.

[9] K. Gillette *et al.*, "A framework for the generation of digital twins of cardiac electrophysiology from clinical 12-leads ECGs," *Medical Image Analysis*, p. 102080, 1 2021.

[10] R. L. Ali, J. B. Hakim, P. M. Boyle, S. Zahid, B. Sivasambu, J. E. Marine, H. Calkins, N. A. Trayanova, and D. D. Spragg, "Arrhythmogenic propensity of the fibrotic substrate after atrial fibrillation ablation: a longitudinal study using magnetic resonance imaging-based atrial models," *Cardiovascular Research*, vol. 115, no. 12, pp. 1757–1765, 04 2019.

[11] T. E. Fastl *et al.*, "Personalized computational modeling of left atrial geometry and transmural myofiber architecture," *Medical Image Analysis*, vol. 47, pp. 180–190, 2018.

[12] S. Zahid *et al.*, "Patient-derived models link re-entrant driver localization in atrial fibrillation to fibrosis spatial pattern," *Cardiovascular Research*, vol. 110, no. 3, pp. 443–454, 04 2016.

[13] C. Corrado, S. Williams, R. Karim, G. Plank, M. O'Neill, and S. Niederer, "A work flow to build and validate patient specific left atrium electrophysiology models from catheter measurements." *Medical image analysis*, vol. 47, pp. 153–163, 7 2018.

[14] O. Razeghi, J. A. Solís-Lemus, A. W. Lee, R. Karim, C. Corrado, C. H. Roney, A. de Vecchi, and S. A. Niederer, "CemrgApp: An interactive medical imaging application with image processing, computer vision, and machine learning toolkits for cardiovascular research," *SoftwareX*, vol. 12, p. 100570, 1 2020.

[15] S. E. Williams *et al.*, "Openep: A cross-platform electroanatomic mapping data format and analysis platform for electrophysiology research," *Frontiers in Physiology*, vol. 12, p. 160, 2021.

[16] C. Corrado *et al.*, "Quantifying atrial anatomy uncertainty from clinical data and its impact on electro-physiology simulation predictions," *Medical Image Analysis*, vol. 61, p. 101626, 2020.

[17] C. Nagel, S. Schuler, O. Dössel, and A. Loewe, "A bi-atrial statistical shape model for large-scale in silico studies of human atria: model development and application to ECG simulations," *Medical Image Analysis*, p. 102210, 1 2021.

[18] C. Nagel, G. Luongo, L. Azzolin, S. Schuler, O. Dössel, and A. Loewe, "Non-invasive and quantitative estimation of left atrial fibrosis based on p waves of the 12-lead ECG-a large-scale computational study covering anatomical variability." *Journal of Clinical Medicine*, vol. 10, no. 8, 4 2021.

[19] M. Beach *et al.*, "Using the universal atrial coordinate system for MRI and electroanatomic data registration in patient-specific left atrial model construction and simulation," vol. 12738, pp. 629–638, 1 2021.

[20] S. Coveney, C. Corrado, C. H. Roney, D. O'Hare, S. E. Williams, M. D. O'Neill, S. A. Niederer, R. H. Clayton, J. E. Oakley, and R. D. Wilkinson, "Gaussian process manifold interpolation for probabilistic atrial activation maps and uncertain conduction velocity," *Philosophical Transactions of the Royal Society A: Mathematical, Physical and Engineering Sciences*, vol. 378, no. 2173, p. 20190345, 1 2020.

[21] C. Nagel, N. Pilia, L. Unger, and O. Dössel, "Performance of different atrial conduction velocity estimation algorithms improves with knowledge about the depolarization pattern," in *Current Directions in Biomedical Engineering*, vol. 5, no. 1. De Gruyter, 1 2019, pp. 101–104.

[22] C. H. Roney *et al.*, "A technique for measuring anisotropy in atrial conduction to estimate conduction velocity and atrial fibre direction," *Computers in Biology and Medicine*, vol. 104, pp. 278–290, 1 2019.

[23] N. Pilia, C. Nagel, G. Lenis, S. Becker, O. Dössel, and A. Loewe, "ECGdeli - an open source ECG delineation toolbox for MATLAB," *SoftwareX*, vol. 13, p. 100639, 2021.

[24] ——, "ECGdeli - ECG delineation algorithms," 7 2020.

[25] D. Nairn, C. Nagel, B. Müller-Edenborn, H. Lehrmann, T. Arentz, O. Dössel, A. Jadidi, and A. Loewe, "Optimal regional voltage thresholds for identifying ablation targets in patients with atrial." *Computing in Cardiology*, 2021.

[26] S. A. Niederer *et al.*, "Verification of cardiac tissue electrophysiology simulators using an n-version benchmark," *Philosophical Transactions of the Royal Society A: Mathematical, Physical and Engineering Sciences*, vol. 369, no. 1954, pp. 4331–4351, 1 2011.

[27] M. Attene, "A lightweight approach to repairing digitized polygon meshes," *The Visual Computer*, 2 2010.

[28] L. Azzolin, G. Luongo, S. Rocher, J. Saiz, O. Doessel, and A. Loewe, "Influence of gradient and smoothness of atrial wall thickness on initiation and maintenance of atrial fibrillation," in *Computing in Cardiology Conference (CinC)*, 2020.

[29] F. Ricci *et al.*, "Cardiovascular magnetic resonance reference values of mitral and tricuspid annular dimensions: the uk biobank cohort," *Journal of cardiovascular magnetic resonance*, vol. 23, no. 1, p. 5, 12 2020.

[30] C. B. Sullivan and A. A. Kaszynski, "Pyvista: 3d plotting and mesh analysis through a streamlined interface for the visualization toolkit (vtk)," *Journal of Open Source Software*, vol. 4, no. 37, p. 1450, 2019.

[31] T. Zheng, L. Azzolin, J. Sanchez, O. Dössel, and A. Loewe, "An automated pipeline for generating fiber orientation and region annotation of patient-specific atrial model," *Current Directions in Biomedical Engineering*, vol. 1, no. 1, pp. 409–412, 1 2021.

[32] W. Kabsch, "A discussion of the solution for the best rotation to relate two sets of vectors," *Acta Crystallographica Section A*, vol. 34, no. 5, pp. 827–828, Sep 1978.

[33] L. Azzolin, C. Nagel, D. Nairn, J. Sanchez, T. Zheng, M. Eichenlaub, A. Jadidi, O. Doessel, and A. Loewe, "Automated framework for the augmentation of missing anatomical structures and generation of personalized atrial models from clinical data," in *Computing in Cardiology Conference (CinC)*, 9 2021.

[34] Y. Chen and G. Medioni, "Object modelling by registration of multiple range images," *Image and Vision Computing*, vol. 10, no. 3, pp. 145–155, 1992, range Image Understanding.

[35] M. Lüthi, T. Gerig, C. Jud, and T. Vetter, "Gaussian process morphable models," *IEEE Transactions on Pattern Analysis and Machine Intelligence*, vol. 40, no. 8, pp. 1860–1873, 2018.

[36] L. A. Woodworth, B. Cansız, and M. Kaliske, "A numerical study on the effects of spatial and temporal discretization in cardiac electrophysiology." *International journal for numerical methods in biomedical engineering*, p. e3443, 1 2021.

[37] A. Muntoni and P. Cignoni, "PyMeshLab," Jan. 2021.

[38] P. Cignoni, M. Callieri, M. Corsini, M. Dellepiane, F. Ganovelli, and G. Ranzuglia, "MeshLab: an Open-Source Mesh Processing Tool," in *Eurographics Italian Chapter Conference*, V. Scarano, R. D. Chiara, and U. Erra, Eds. The Eurographics Association, 2008.

[39] J. D. Bayer, R. C. Blake, G. Plank, and N. A. Trayanova, "A novel rule-based algorithm for assigning myocardial fiber orientation to computational heart models," *Annals of Biomedical Engineering*, vol. 40, no. 10, pp. 2243–2254, 1 2012.

[40] A. Wachter, A. Loewe, M. W. Krueger, O. Dössel, and G. Seemann, "Mesh structure-independent modeling of patient-specific atrial fiber orientation," *Current Directions in Biomedical Engineering*, vol. 1, no. 1, pp. 409–412, 1 2015.

[41] R. Piersanti, P. C. Africa, M. Fedele, C. Vergara, L. Dedè, A. F. Corno, and A. Quarteroni, "Modeling cardiac muscle fibers in ventricular and atrial electrophysiology simulations," *Computer Methods in Applied Mechanics and Engineering*, vol. 373, p. 113468, 1 2021.

[42] G. Plank, A. Loewe, A. Neic, C. Augustin, Y.-L. Huang, M. A. Gsell, J. S. Elias Karabelas, Mark Nothstein, A. J. Prassl, G. Seemann, and E. J. Vigmond, "The openCARP simulation environment for cardiac electrophysiology," *Computer Methods and Programs in Biomedicine*, vol. 208, p. 106223, 2021.

[43] S. Labarthe, J. Bayer, Y. Coudiere, J. Henry, H. Cochet, P. Jais, and E. Vigmond, "A bilayer model of human atria: mathematical background, construction, and assessment," *EP Europace*, vol. 16 Suppl 4, pp. iv21–iv29, 1 2014.

[44] A. Loewe, M. W. Krueger, P. G. Platonov, F. Holmqvist, O. Dössel, and G. Seemann, "Left and right atrial contribution to the P-wave in realistic computational models," *Lect. Notes Comput. Sci.*, vol. 9126, pp. 439–447, 2015.

[45] G. Caixal *et al.*, "Accuracy of left atrial fibrosis detection with cardiac magnetic resonance: correlation of late gadolinium enhancement with endocardial voltage and conduction velocity." *EP Europace*, 11 2020.

[46] M. Mase and F. Ravelli, "Automatic reconstruction of activation and velocity maps from electro-anatomic data by radial basis functions," *Conf Proc IEEE Eng Med Biol Soc*, vol. 2010, pp. 2608–2611, 1 2010.

[47] M. Courtemanche, R. J. Ramirez, and S. Nattel, "Ionic mechanisms underlying human atrial action potential properties: insights from a mathematical model," *The American Journal of Physiology*, vol. 225, pp. 301–321, 1998.

[48] A. Loewe, M. Wilhelms, O. Dössel, and G. Seemann, "Influence of chronic atrial fibrillation induced remodeling in a computational electrophysiological model," *Biomed. Eng.*, vol. 59, no. S1, pp. S929–S932, 2014.

[49] E. Vigmond, A. Pashaei, S. Amraoui, H. Cochet, and M. Hassaguerre, "Percolation as a mechanism to explain atrial fractionated electrograms and reentry in a fibrosis model based on imaging data," *Heart Rhythm*, vol. 13, no. 7, pp. 1536–1543, 1 2016.

[50] C. H. Roney, J. D. Bayer, S. Zahid, M. Meo, P. M. J. Boyle, N. A. Trayanova, M. Haïssaguerre, R. Dubois, H. Cochet, and E. J. Vigmond, "Modelling methodology of atrial fibrosis affects rotor dynamics and electrograms," *Europace*, vol. 18, no. suppl 4, pp. iv146–iv155, 12 2016.

[51] C. Nagel, J. Sanchez, L. Azzolin, T. Zheng, S. Schuler, O. Dössel, and A. Loewe, "A Bi-atrial Statistical Shape Model and 100 Volumetric Anatomical Models of the Atria," Jun. 2021.

[52] C. H. Roney, R. Bendikas, F. Pashakhanloo, C. Corrado, E. J. Vigmond, E. R. McVeigh, N. A. Trayanova, and S. A. Niederer, "Constructing a human atrial fibre atlas." *Annals of biomedical engineering*, 5 2020.

[53] R. Karim *et al.*, "Algorithms for left atrial wall segmentation and thickness - evaluation on an open-source CT and MRI image database." *Medical image analysis*, vol. 50, pp. 36–53, 12 2018.

Personalized ablation vs. conventional ablation strategies to terminate atrial fibrillation and prevent recurrence: a systematic in silico study

Luca Azzolin*, Martin Eichenlaub*, Claudia Nagel, Deborah Nairn, Jorge Sanchez, Laura Unger, Olaf Dössel, Amir Jadidi*, Axel Loewe*

*These authors contributed equally

Abstract

Aims

The long-term success rate of ablation therapy is still sub-optimal in patients with persistent atrial fibrillation (AF), mostly due to arrhythmia recurrence originating from arrhythmogenic atrial sites outside the pulmonary veins. Computational modeling provides a framework to integrate and augment clinical data, potentially enabling the patient-specific identification of AF mechanisms and the identification of optimal ablation sites. We developed a technology to tailor ablations in anatomical and functional digital atrial twins of patients with persistent AF aiming to identify the most successful ablation strategy.

Methods and Results

Twenty-nine patient-specific computational models integrating clinical information from tomographic imaging and electro-anatomical activation time and voltage maps were generated. Areas sustaining AF were identified by a personalized induction protocol at 20-30 evenly distributed left atrial locations. State-of-the-art anatomical and substrate ablation strategies were compared to our proposed Personalized Ablation Lines (PersonAL) plan, which consists of iteratively targeting emergent high dominant frequency (HDF) regions, to identify the optimal ablation strategy. Localized ablations were connected to the closest non-conductive barrier to prevent recurrence of AF or atrial tachycardia. The first application of the HDF strategy had a success of >98% and isolated only 5-6% of the left atrial myocardium. In contrast, conventional ablation strategies targeting anatomical or structural substrate resulted in isolation of up to 20% of left atrial myocardium. After a second iteration of the HDF strategy, no further arrhythmia episode could be induced in any of the patient-specific models.

Conclusion

The novel PersonAL technology allows to unveil all AF-perpetuating areas and personalize ablation by leveraging atrial digital twins. Feasibility was demonstrated in a cohort of 29 patients and integration of computer simulations in clinical workflows could guide patient-specific catheter ablation therapy for atrial fibrillation.

Translational Perspective

This study highlights that ablation of the fibrotic substrate leads to high success (>90%) but crucially depends on accurately localization of these areas. A reliable way of identifying the arrhythmogenic substrate was dominant frequency in computational digital twin models. Iteratively ablation high dominant frequency regions resulted in termination of atrial fibrillation and prevented recurrence in the entire patient cohort in silico. Connecting localized ablation points to the nearest non-conductive barrier prevented recurrence and increased ablation success. Atrial digital twins in combination with personalized induction protocols from multiple sites pre- and post-ablation enabled unveiling all emergent atrial fibrillation drivers.

Introduction

Atrial fibrillation (AF) is the most common supraventricular arrhythmia in humans with both increasing prevalence and incidence globally[1]. More than 46.3 million individuals were diagnosed with AF worldwide in 2016[2]. The pulmonary veins are the main arrhythmia sources in paroxysmal AF[3] and pulmonary vein isolation (PVI) is associated with high (80-85%) 12-month arrhythmia freedom rates in patients with paroxysmal AF[4]. In contrast, one-year success rates after AF ablation in patients with persistent AF are reduced with 50% of patients experiencing AF or atrial tachycardia recurrences[5,6]. This unsatisfactory success rate is associated with the higher incidence of fibrosis-related atrial conduction slowing in these patients, which constitutes the arrhythmogenic substrate for AF[7].
Currently, two diagnostic methods are used to identify atrial fibrotic substrate. During electrophysiological mapping studies, atrial fibrotic areas can be detected as areas displaying low voltage and fractionated late potentials during sinus rhythm[8]. An alternative magnetic resonance imaging (MRI)-based method to diagnose atrial fibrosis is the use of late gadolinium-enhancement (LGE). Recent studies revealed that presence of atrial fibrosis as assessed during electrophysiological mapping or MRI is associated with onset of AF, AF persistency and increased arrhythmia recurrences after PVI underlining the clinical relevance of atrial fibrotic remodeling[9–14].

Over the last years, catheter-based ablation of atrial fibrillation (AF) has become the first-line therapeutic option in case of symptomatic episodes[2]. Catheter ablation (CA) of AF relies on PVI as the cornerstone of any ablation procedure[15]. However, extra-PV regions become more relevant in AF initiation and maintenance as atrial remodeling evolves and the underlying substrate gains complexity in persistent and long-standing persistent types of AF[6]. A common strategy to treat symptomatic AF episodes after permanent PVI is to ablate other atrial anatomical structures (e.g., mitral isthmus, roof, vein of Marshall) potentially associated with AF onset and perpetuation. However, many of these atrial regions are empirically targeted for ablation without robust underlying supportive mechanistic insights.

Recent advances in mapping technologies have enabled the development of more patient-specific ablation strategies that complement standard approaches in persistent AF. These can directly target either AF sources (ectopic triggers or rotational drivers (RDs)) identified invasively using basket catheters[16] or non-invasively using body surface electrodes[17], or regions where the atrial substrate is expected to be arrhythmogenic, such as low-voltage areas (LVA)[13] or high LGE areas[18]. The role of RDs as drivers for AF has been long recognized[19,20]. However, RD-guided ablation is limited by the challenges of mapping and visualizing electrical activity on the endocardial surface with sufficiently high resolution. This can explain contradictory outcomes of multi-center trials, some of which have shown favorable outcomes of RD-guided ablation[21], while others have failed to demonstrate advantages of this approach compared to PVI[22]. Recent studies demonstrated that low-voltage guided ablation was associated with a significantly higher arrhythmia-free survival compared with a conventional CA approach[9,13,14]. However, a large-scale multicenter study is lacking. A recent study by Bisbal et al.[23] and the lately presented DECAAF-II trial by Marrouche et al.[24] reported no additional benefit of MRI-guided ablation compared to a conventional PVI-only ablation approach.

We sought to develop a technology for tailored ablations in atrial digital twins of patients with persistent AF. We aimed at unveiling all areas vulnerable to sustain AF applying personalized

inducing protocols at multiple sites on anatomical and functional atrial digital twins. We designed a platform to comprehensively compare state-of-the-art ablation strategies targeting anatomical structures and substrate with our proposed Personalized Ablation Lines (PersonAL) approach. The PersonAL plan consists of an iterative process to identify and terminate all possible latent AF drivers that could manifest post-ablation. We pursued a unique personalization of anatomy, fibrosis and electrophysiology of the digital twin models, which enables to uncover potential arrhythmogenic substrates and predict the optimal minimal set of ablation targets to eliminate AF and prevent recurrence. We eventually sought to demonstrate the clinical feasibility in guiding ablation integrating the final PersonAL plan into the original clinical map.

Materials and Methods

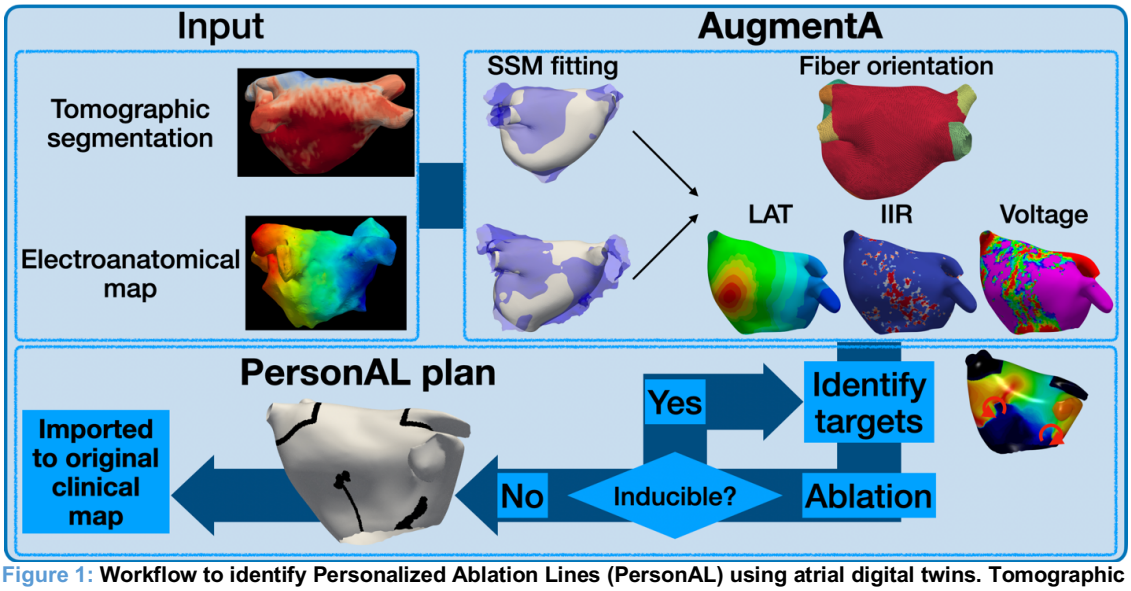

Figure 1: Workflow to identify Personalized Ablation Lines (PersonAL) using atrial digital twins. Tomographic segmentations (CT or LGE-MRI) and/or electro-anatomical maps (EAM) are processed by a highly automated pipeline to generate a patient-specific Augmented Atria (AugmentA)[25] computational model. In case both LGE-MRI and EAM are given, an augmented anatomical and functional digital twin integrating both non-invasive and invasive electrophysiological data is provided. Tailored simulations are performed to assess atrial fibrillation (AF) inducibility using the Pacing at the End of the Effective Refractory Period (PEERP) protocol[26] and regions vulnerable to sustain AF are identified. Then, AF drivers are targeted for ablation and connecting lines to the closest non-conductive barrier (anatomical orifice or previous ablation) are included. The PEERP protocol is then repeated to localize post-ablation emergent AF episodes. If new drivers are identified, they are targeted for ablation. The latter two processes are repeated until no AF episode can be induced in the patient's model. The PersonAL plan is finally exported to the clinical mapping system data format. SSM: statistical shape model; LAT: local activation time; IIR: image-intensity-ratio.

An overview of the automatic pipeline to assess AF vulnerability in personalized atrial computational models and provide PersonAL is illustrated in Figure 1 and briefly described here before providing details for each step in the following sections. The only user interaction needed for the whole pipeline is the choice of one reference point per atrium[25]. The input can be atrial surfaces obtained from an electro-anatomical mapping system or derived from tomographic segmentation (e.g. MRI or CT). In this study, both input modalities were available. Input geometries are pre-processed and patient-specific Augmented Atria (AugmentA)[25] models are generated by fitting a statistical shape model[27] and adding anatomical structures annotation and fiber orientation along with the electrophysiological information present in the original clinical data. Fibrotic distribution can be retrieved from substrate data, e.g. either using image-intensity-ratio

(IIR) of LGE-MRI or low-voltage-areas (LVA) derived from electro-anatomical maps. Conduction velocity is locally adapted to reproduce the clinical local activation time (LAT) from the patient's electrophysiological mapping data[25]. Patient-specific inducibility is assessed by applying Pacing at the End of the Effective Refractory Period (PEERP)[26] at variable pacing locations placed at 2 cm inter-point distance. Then, the optimal ablation targets are determined based on the left atrial geometry from non-invasive MRI, intra-cardiac electrophysiological voltage maps and activation maps to identify sites of slow conduction. Inducible models are iteratively treated with PersonAL until free from current and emergent AF episodes. Re-inducibility is tested by re-applying the PEERP protocol. Finally, the PersonAL plan is provided to the cardiologist.

Dataset

	All patients (n=29)
Age (years)	65±9
Male sex, n (%)	25 (86)
BMI (kg/m^2)	28±3
Hypertension, n (%)	20 (69)
Diabetes mellitus, n (%)	3 (10)
Heart failure, n (%)	8 (28)
Prior stroke or TIA, n (%)	0 (0)
Structural cardiomyopathy, n (%)	5 (17)
Coronary artery disease, n (%)	4 (14)
CHA_2DS_2-VASc-score	2 (1-3)
Patients with antiarrhythmic therapy, n (%)	15 (52)
LA diameter (mm)	47±7
LVEF (%)	55±8
LA-LVS at 0.5 mV (% of LA surface)	6.3 (0.1-13.5)
LA-LVS at 1.0 mV (% of LA surface)	16.8 (1.8-30.1)
LGE at IIR 1.20 (% of LA surface)	15.0 (4.4-27.9)
LGE at IIR 1.32 (% of LA surface)	8.3 (0.3-14.0)

Table 1: Patients' characteristics. BMI: body mass index, IIR: image intensity ration, LA: left atrial, LVEF: left ventricular ejection fraction, LVS: low-voltage, TIA: transient ischemic attack.

A cohort of 29 patients with persistent AF (65±9 years, 86% male) including both electro-anatomical maps and MRI segmentations of the LA were included in this study. A high-density electro-anatomical bi-atrial map (2129±484 sites) was acquired in sinus rhythm prior to PVI using a 20-pole mapping catheter and the CARTO 3 system (Biosense Webster Inc., Diamond Bar, CA, USA). The post-processing of the LA LGE-MRI (Siemens 3 T) was performed by a blinded expert laboratory (Adas3D Medical SL, Barcelona, Spain). Patients' characteristics are available in Table 1. The study was approved by the institutional review board, registered in the German WHO primary registry DRKS (unique identifier: DRKS00014687), and all patients provided written informed consent prior to enrollment.

Personalized atrial model generation

For each patient, our recently proposed AugmentA generation pipeline[25] was applied to each electro-anatomical map and LGE-MRI segmentation. An automated algorithm manually selecting only one reference point (left atrial appendage apex) was applied to open atrial orifices. The mitral valve and the pulmonary veins were automatically identified and labelled. Each target geometry was at first rigidly aligned with the mean shape of a previously built bi-atrial statistical shape model[27]. Subsequently, 36 landmarks were automatically computed and a fitting procedure was

applied. In this regard, non-rigid shape model fitting using Iterative Closest Points and Gaussian Process regression[28] was performed to establish dense point-by-point correspondence between the bi-atrial statistical shape model and each target geometry. The fitted instances were resampled to obtain a higher mesh resolution (406±14 μm). Then, each data vector (e.g., LAT, voltage) was mapped from the original mesh to the fitted SSM using a nearest neighbor approach. Since the resulting instance is a deformed version of the mean shape, all models had the same number of nodes and vertices and the nodes always represented the same anatomical structures. Therefore, the electrophysiological data mapped from one patient's electro-anatomical map to the resulting SSM instance could be easily transferred to the SSM instance derived from the respective MRI segmentation. Since we assumed that the MRI segmentation was a better representation of the patient's real atrial anatomy compared to the electro-anatomical map, we decided to register local activation time as well as uni- and bipolar voltage maps to the SSM instance derived from the MRI data. Finally, AugmentA automatically annotated the various anatomical structures and computed the fiber orientation using a Laplace-Dirichlet-Rule-based-Method[29,30]. The resulting bilayer atrial model[31] was ready-to-use for electrophysiological simulations.

Modelling atrial electrophysiology in fibrotic and non-fibrotic tissue

We used established methods to represent electrophysiology of persistent AF patients including substrate remodeling[26,32]. Briefly, a human action potential model reflecting persistent AF-induced remodeling[32] represented the cellular scale kinetics. A fixed conductivity anisotropy ratio of 3.75 was applied to the myocardium[26,33]. Conduction velocity was personalized by tuning each element's conductivity to minimize the root mean square error between the simulated LAT map and the recorded clinical LAT map of the individual patient[25]. Two series of experiments in which fibrotic tissue was modeled informed by different clinical measurements were performed: atrial tissue regions with IIR higher than 1.2 or bipolar voltage less than 0.5 mV were labelled as fibrosis. In these fibrotic regions, 30% of the elements were modeled as non-conductive (10^{-7} S/m) to account for structural remodeling. This approach modelled the macroscopic passive barrier behavior caused by the electrical decoupling of the myocytes in the tissue infiltrated by fibrosis, also referred to as 'percolation'[8,34]. In the other 70%, several ionic conductances were rescaled to consider effects of cytokine-related and elevated TGF-β1 remodeling[35,36] (-50% g_{K1}, -40% g_{Na} and -50% g_{CaL}).

Induction protocol and arrhythmia analysis

Arrhythmia initiation vulnerability was assessed by applying the Pacing at the End of the Effective Refractory Period (PEERP) protocol[26]. We tested inducibility of arrhythmic episodes by pacing from stimulus locations placed on the endocardial surface with inter-point distance of 2 cm. This pacing site distribution allowed capturing all possible arrhythmias that could arise in the given patient-specific model as shown in Azzolin et al[26]. At each stimulus location, a transmembrane current of 30 μA/cm^2 was injected in an area of 2 mm x 2 mm.

We considered a point to be 'inducing' if the application of the PEERP protocol at that location induced an arrhythmia that was sustained for at least 5 s. Dominant frequency (DF) maps were computed based on the last 1.5 s of each reentrant episode's transmembrane potential. All pacing-induced arrhythmias were analyzed to determine an initial set of ablation lesions.

The frequency spectrum was estimated using fast Fourier transform and DF was identified as the highest peak in the power spectrum. To identify regions of high DF (HDF), a threshold was applied at 1 standard deviation above the mean and HDF points were clustered into connected regions[37].

Modelling ablation scars

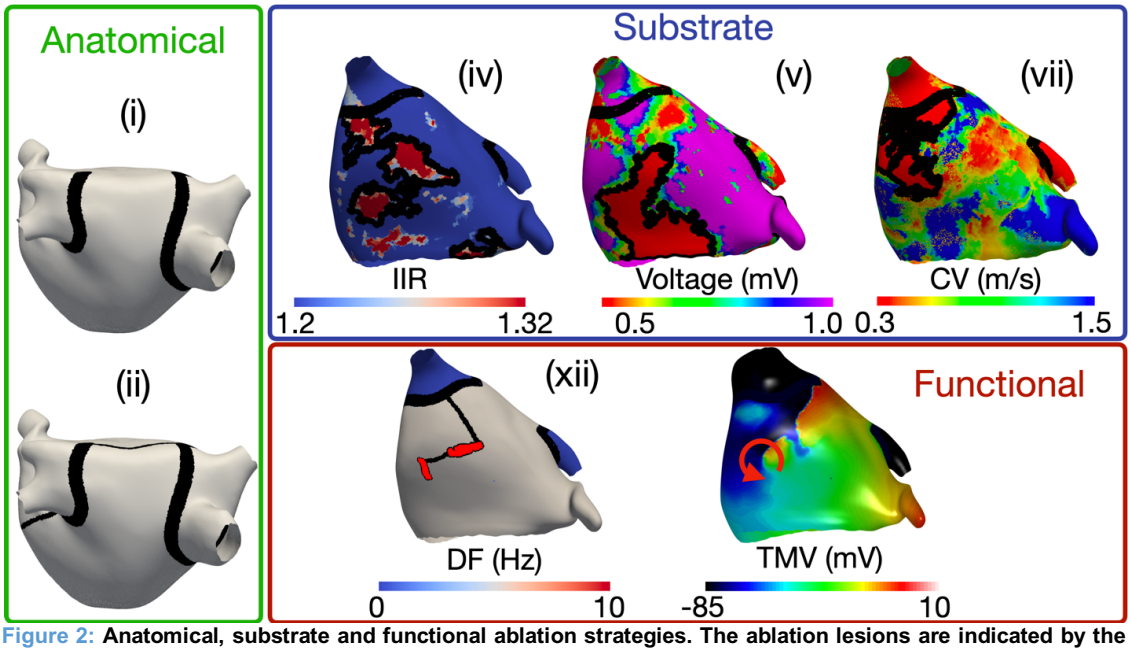

Figure 2: Anatomical, substrate and functional ablation strategies. The ablation lesions are indicated by the black ablation lines. Ablation approaches targeting anatomical structures, shown in the green box, consist in PVI (i) and PVI+RL+ML (ii). Substrate ablations, shown in the blue box, include, e.g., approaches targeting regions with IIR>1.2 (iv), LVAs (v), and regions with CV<0.3 m/s (vii). Functional ablation strategies, shown in the red box, targeted HDF areas (xii).

We tested twelve different ablation approaches: (i) PVI alone, modeled as circumferential isolation of the ipsilateral pulmonary veins; PVI together with: (ii) roof and mitral isthmus lines; (iii) isolating all regions with IIR>1.32; (iv) isolating all regions with IIR>1.2; (v) isolating all LVAs (bipolar voltage <0.5 mV); (vi) isolating all low conduction velocity regions (CV<0.4 m/s); (vii) isolating all low conduction velocity regions (CV<0.3 m/s); and (viii) isolating all HDF regions. All previously described ablation strategies included connecting lines to the closest non-conductive barrier. Finally, we also assessed how omitting these connecting lines isolating affects (ix) ablation targeting regions with IIR>1.32, (x) ablation targeting regions with IIR>1.2, (xi) LVAs ablation and (xii) HDF ablation. Figure 2 shows exemplary anatomical, substrate and functional ablation strategies for patient #18.

The ablation lesions were automatically applied and produced consistent lesions across patients. The technical details regarding the ablation strategies are described in the Supplementary Material. Virtual ablation lesions consisted of the myocardial tissue within 2 mm of the direct line (ablation lesion radius for standard irrigated-tip catheters)[38] and were modeled as non-conductive. Ablation targeting substrate regions were limited to the boundary of the regions instead of the whole region to minimize procedural time.

Ablation success was automatically classified as either ongoing AF, termination or atrial tachycardia (AT). AT was defined as cases with DF<4.7 Hz or with more than 50% of the atrial surface having a DF≥ the 95th DF percentile[37,39,40].

Reinducibility assessment after ablation

CA therapies for atrial arrhythmias often take the suppression of inducibility as treatment endpoint. Therefore, in the atrial models in which a specific ablation strategy was able to terminate all AF episodes, we assessed reinducibility by applying the PEERP protocol again from all initial stimulation points located in non-isolated tissue.

Importing personalized targets into the clinical electro-anatomic navigation system

To facilitate clinical translation, optimal ablation targets identified by PersonAL were transferred to the electro-anatomical map. The point correspondence between the SSM instances derived from the MRI and electro-anatomical map allowed for a trivial mapping of the ablation locations from the MRI-fitted digital twin to the respective electro-anatomical map. Merging patient-specific imaging with electro-anatomic mapping data to display ablation targets in the mapping system together with the current position of the catheter increases usability[41,42].

Results

Inducibility and identification of AF drivers

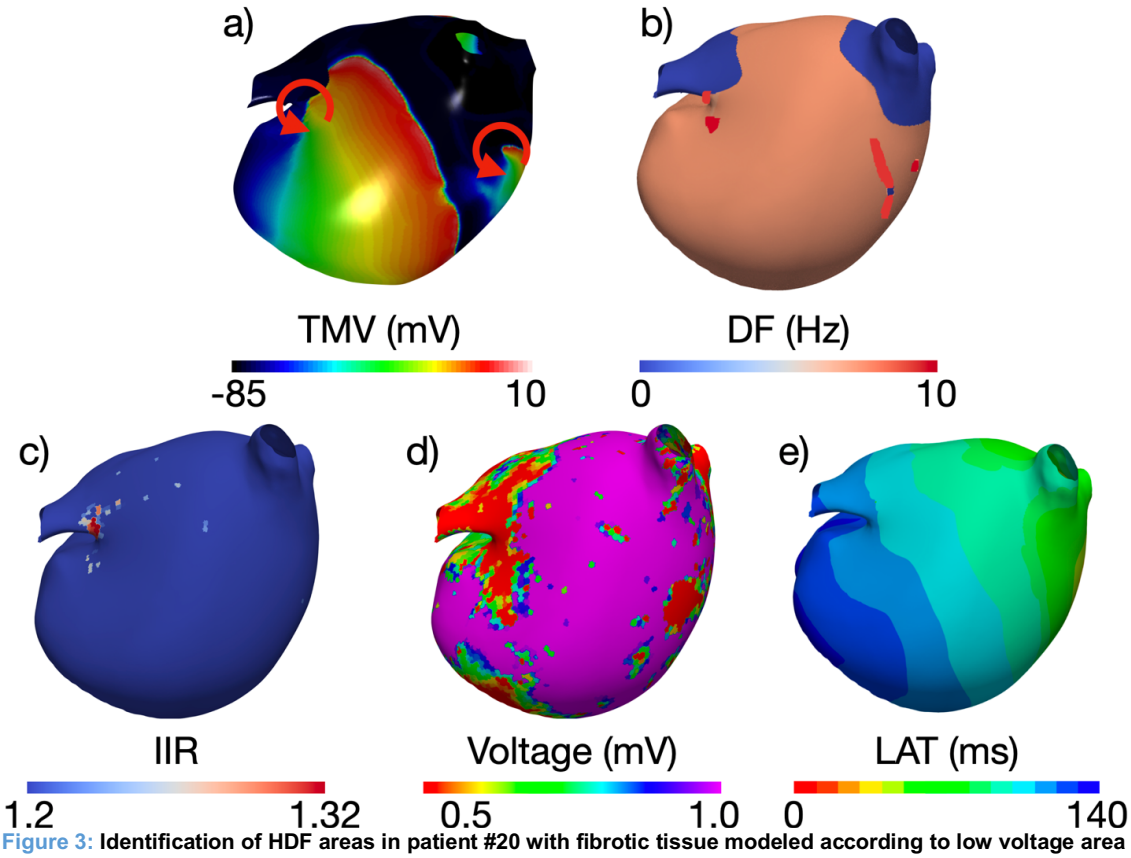

Figure 3: Identification of HDF areas in patient #20 with fibrotic tissue modeled according to low voltage area <0.5mV (LVA) in the clinical voltage map. a) AF episode perpetuated in LVAs close to the inferior left pulmonary vein and at the posterior septum; b) DF map; c) IIR map; d) bipolar voltage map; e) simulated activation (LAT) map.

The PEERP induction protocol in led to AF episodes in 17/29 and 20/29 patient digital twins when fibrotic tissue was modeled where the voltage was <0.5 mV or IIR >1.2 in the clinical maps, respectively. These episodes were induced from 99 and 88, respectively. AF drivers were correctly identified by HDF regions as shown for patient #20 with fibrosis distributed according to LVA in Figure 3.

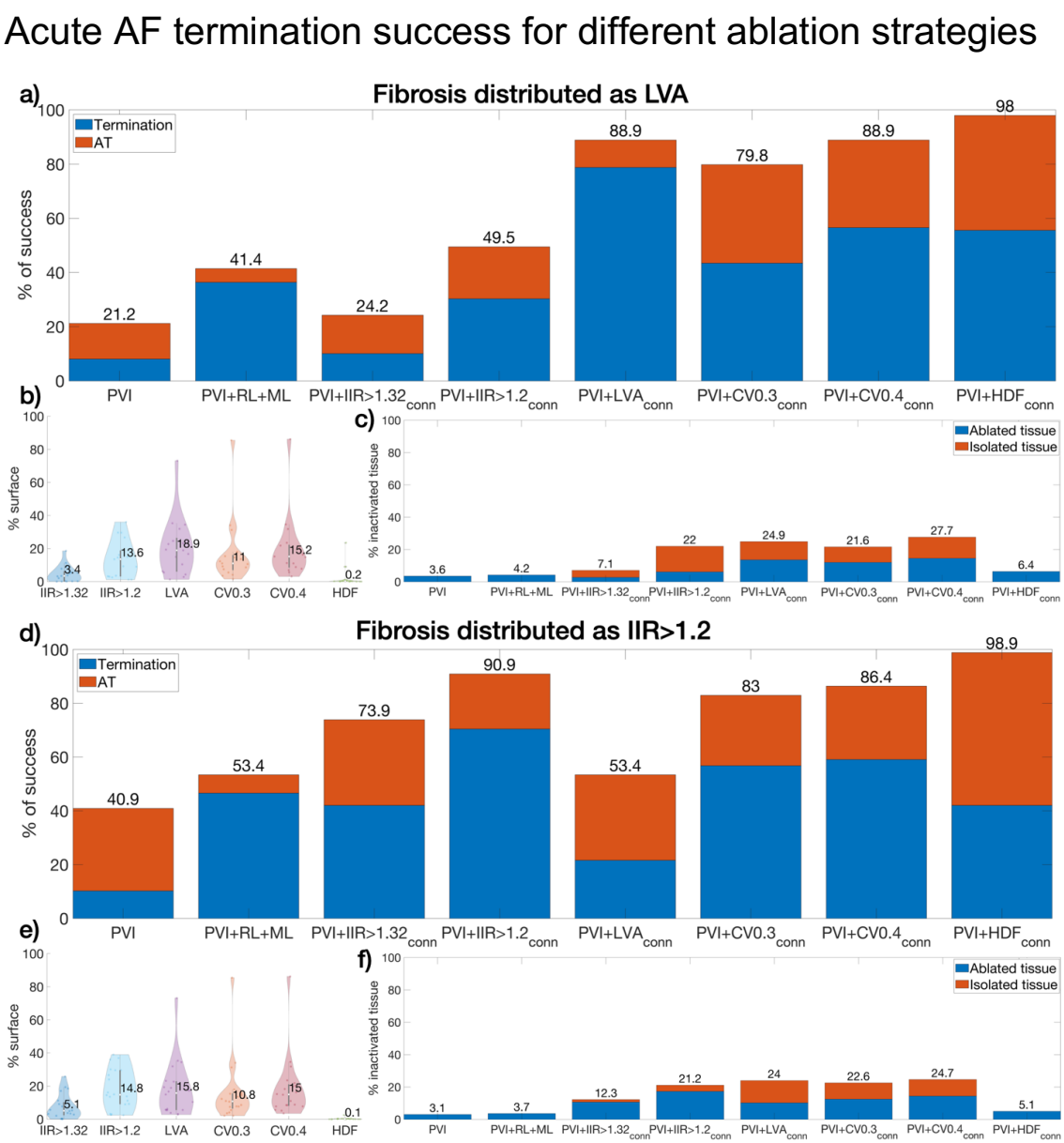

Figure 4: Success rate of each ablation strategy applied to the patient models cohort in which distribution of fibrotic tissue was modeled according to either voltage <0.5mV (LVA) in clinical electrophysiological voltage maps a) or LGE-MRI areas as identified by image intensity ratio (IIR) >1.2 d). Ablation strategies that resulted in AF termination are shown in blue and conversion to atrial tachycardia (AT) in red. Percentage of atrial surface identified as substrate by the different substrate mapping methods prior to ablation in inducible patients with fibrosis adapted according to either LVA b) or IIR >1.2 e). Percentage of inactivated myocardium following each ablation strategy categorized in ablated tissue and isolated tissue in atrial models with fibrosis applied according to either LVA c) or IIR >1.2 f). IIR>1.32: atrial regions with image intensity ratio (IIR) >1.32. IIR>1.2: atrial regions with image intensity ratio (IIR) >1.2. LVA: low voltage areas (bipolar voltage <0.5 mV). CV0.3: atrial regions with conduction velocity (CV) <0.3 m/s. CV0.4: atrial regions with CV <0.4 m/s. HDF: high dominant frequency (HDF) areas. PVI: pulmonary vein isolation. PVI+( )$_{conn}$: PVI plus ablation targeting anatomical/structural/functional substrates and connecting localized ablation lesions to the closest non-conductive barrier (anatomical orifice or previous ablation). PVI+RL+ML: PVI plus roof line (RL) plus mitral isthmus line (ML).

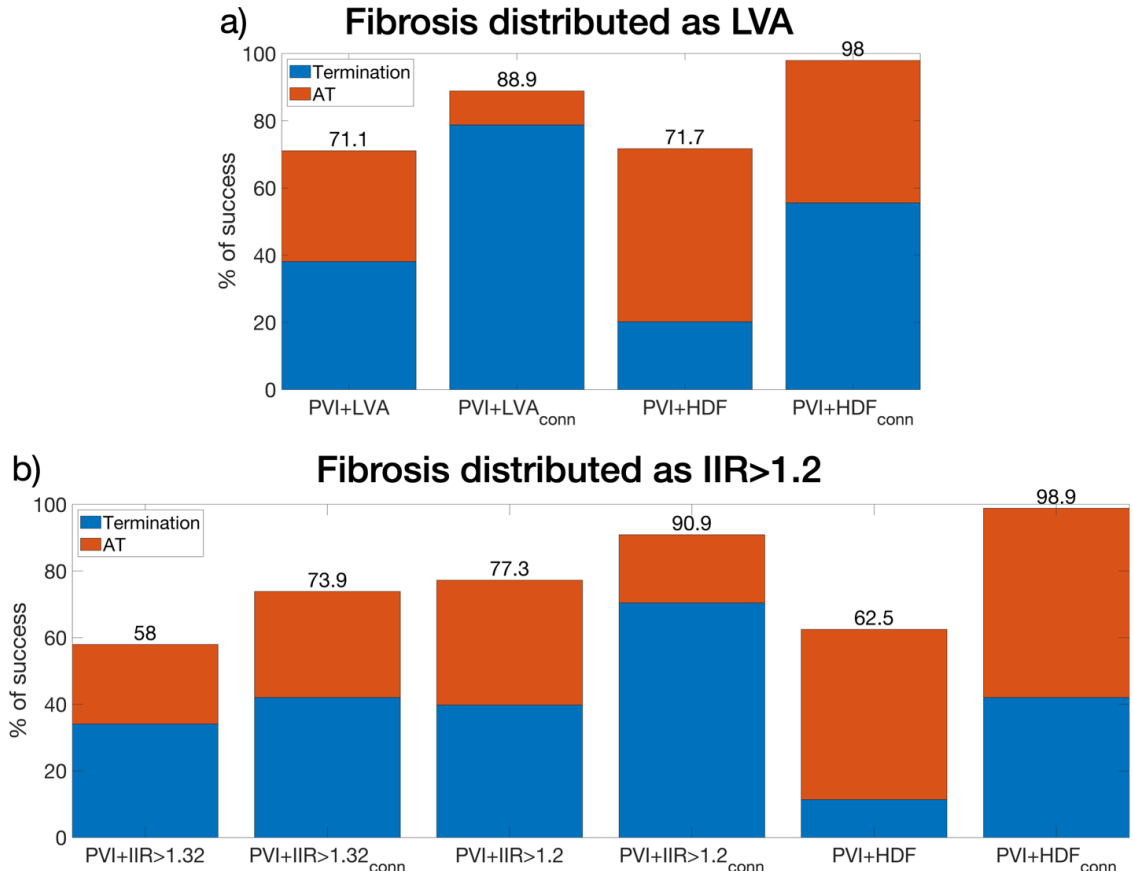

Figure 5: Success rate of each ablation strategy applied to the patient models cohort in which distribution of fibrotic tissue was modeled according to either voltage <0.5mV (LVA) in clinical electrophysiological voltage maps a) or LGE-MRI areas as identified by image intensity ratio (IIR) >1.2 b). Ablation strategies that resulted in AF termination are shown in blue and conversion to atrial tachycardia (AT) in red. IIR>1.32: atrial regions with image intensity ratio (IIR) >1.32. IIR>1.2: atrial regions with image intensity ratio (IIR) >1.2. LVA: low voltage areas (bipolar voltage <0.5 mV). HDF: high dominant frequency (HDF) areas. PVI: pulmonary vein isolation. PVI+( ): PVI plus ablation targeting anatomical/structural/functional substrates. PVI+( )$_{conn}$: PVI plus ablation targeting anatomical/structural/functional substrates and connecting localized ablation lesions to the closest non-conductive barrier (anatomical orifice or previous ablation).

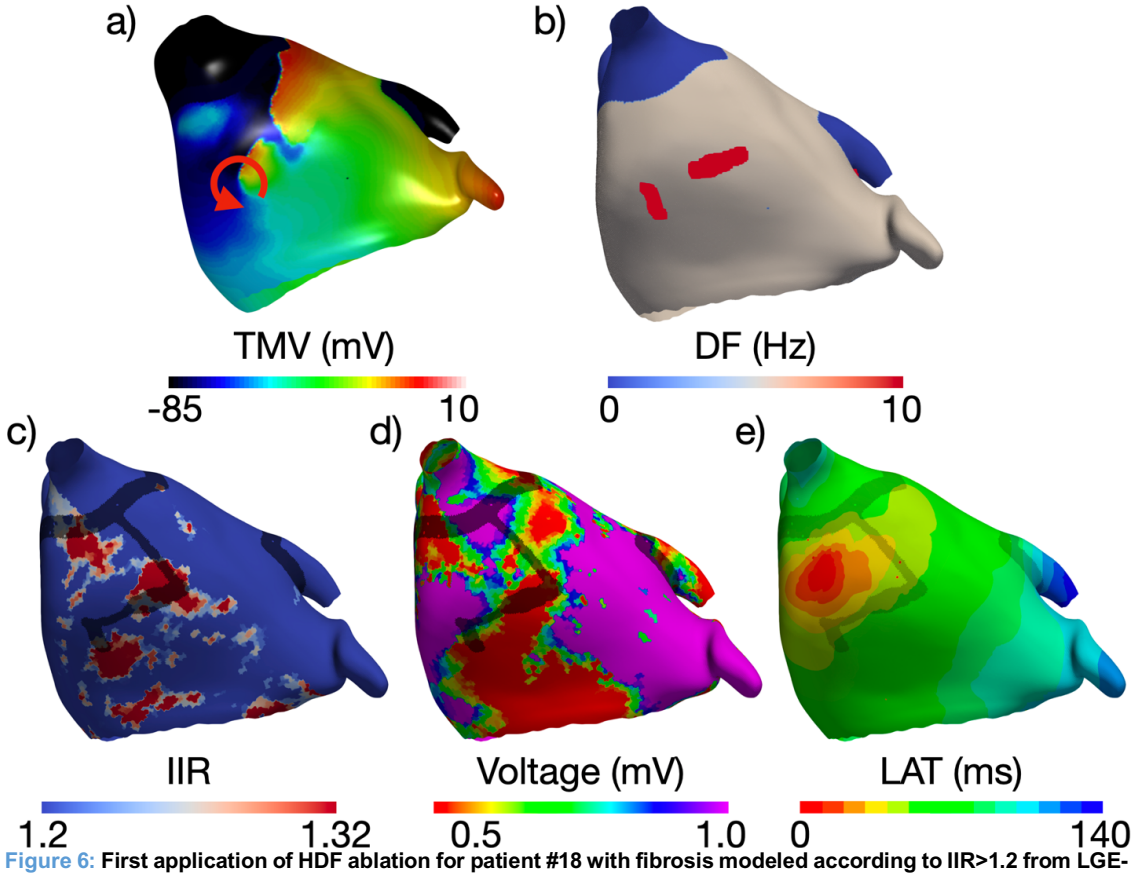

Figure 6: First application of HDF ablation for patient #18 with fibrosis modeled according to IIR>1.2 from LGE-MRI. a) sustained AF episode in slow conduction area located on the anterior wall in proximity to the border zone of a low voltage/IIR>1.2 area; b) DF map; c) IIR map; d) bipolar voltage map; e) adapted electrophysiological LAT map.

Ablation outcomes, classified as AT or termination, varied considerably across the cohorts of patients with fibrosis modeled according to either voltage <0.5 mV or IIR >1.2 depending on the ablation strategy, as shown in Figure 4. 18.9% of the LA surface area was identified as low-voltage (<0.5mV) in this cohort of inducible ablation-naive persistent AF patients (Figure 4b) and 14.8% were identified as IIR>1.2 in LGE-MRI (Figure 4e). PVI-only was the ablation strategy with lowest acute success rate in our persistent AF patient cohort with the comprehensive PEERP protocol. Anatomical ablation approaches led to the smallest share of atrial tissue being ablated (3.1-4.2%). Targeting the regions modelled as fibrotic tissue successfully terminated or converted AF to AT in 88.9% and 90.9% of the AF episodes when fibrosis distribution patterns were modeled according to voltage <0.5 mV and IIR >1.2, respectively. When the fibrosis could not be exactly localized (i.e., when it was modeled where IIR>1.2 but ablated according to LVA or vice versa), the success rates dropped to 49.5% and 53.4%, respectively. Inactive tissue after ablation strategies targeting atrial substrate varied between 21% and 28% of the atrial myocardium. The first application of the ablation strategy aiming at HDF areas led in both cases to termination or conversion to AT of more than 98% of all AF episodes. However, following the same ablation strategies without connecting the targeted areas to the closest non-conductive barriers resulted in a decrease of the success rate by 15-35%, as shown in Figure 5. An example of the ablation plan targeting HDF areas applied to patient #18 is presented in Figure 6. The amount of inactive tissue post-ablation isolating the HDF areas including connection lines was of 5-6% of the atrial tissue.

Ablation of emergent AF drivers and re-inducibility

The PersonAL plan consists of iteratively identifying and targeting AF-perpetuating areas, defined as HDF regions, until a patient-specific digital twin model is rendered completely non-inducible. Therefore, in the models in which the first application of HDF areas ablation did not terminate all AF episodes or converted into AT (2 and 1 episodes in atrial models with fibrosis modeled according to voltage <0.5 mV or IIR >1.2, respectively), the emergent AF drivers were detected and new ablations were added. A second application resulted in 100% success rate and no further AF episode could be induced in any of the models.

Discussion

Ablation of fibrotic substrate is linked to high acute success

Our study showed that a clear identification of the arrhythmogenic substrate (fibrotic or slow conducting areas) is needed to obtain high ablation success. When there was mismatch between where fibrosis was modeled in the digital twin and where it was assumed to be for identifying ablation sites, the success rate dropped by around 40% (columns 4 and 5 in Figure 3a and 4a). The limited accuracy of current technology in detection of the fibrotic substrate can therefore explain the sub-optimal results of previous clinical trials targeting substrate[6,23].

Clinical studies ablating fibrotic tissue distribution determined using LGE-MRI had no evident improvement in respect to the standard-in-practice PVI. This may be explained by the lack of reproducible and standardized characterization of the substrate by atrial LGE-MRI[23,43]. Moreover, current LGE-MRI technology does not have the required resolution to well distinguish fibrosis within the thin atrial myocardial wall. Accuracy is essential in this case, as inclusion of external structures in the segmented myocardium can lead to a consideration of fat or outer tissue as scar or fibrosis, and omitting parts of the myocardium in the segmentation may hinder detection of fibrotic areas[44]. The presence of multiple devices and algorithms from different manufacturers makes reproducibility of results difficult. Moreover, evidence of the relationship between MRI-characterized scar and histological fibrosis has not been proven on atrial myocardium but for the thick-walled ventricular myocardium in ischemic and dilatative cardiomyopathy. Clinical trials based on LGE-MRI-guided ablation[10,23,24] failure in showing higher success compared to conventional catheter ablation might be also due to the lack of connecting lines to prevent emergent AF drivers. Our in silico experiments clearly showed that the ablation outcome of IIR-based strategies dropped when these connecting lines were not included (Figure 4b).

LVA ablation presented promising results in various clinical trials in persistent AF patients[9,13,14,45,46]. However, ablation strategies guided by LVA also have their limitations, due to the challenges in classifying AF-perpetuating atrial tissue. Bipolar voltage is affected by the bipole orientation with respect to the direction of the electrical propagation wavefront. Approaches using high density mapping or omnipolar electrograms hold promise to overcome the dependence on directionality[47]. Nevertheless, no clear voltage threshold has been determined to clearly identify arrhythmogenic substrate. Recently, a region-specific bipolar voltage thresholding method was proposed as a possible solution[48].

Our current work also reveals that reentrant AF driver sites localize to slow conduction areas in electro-anatomical LAT maps. However, methodologies to accurately and robustly elucidate slow conduction regions from clinical data are needed[49].

Connecting ablated areas to non-conductive barriers increase success

Our work highlights the beneficial effect of including ablation lines connecting the targeted area to the closest anatomical orifice or previous ablation. The ablation success of the same ablation strategy decreased by 15-35% when no connecting lines were added. The idea behind this approach is to prevent the formation of macroreentries around the isolated tissue, to prevent anchoring of reentrant drivers and to prevent AT. This could explain the not consistent success rate of focal impulse and rotor modulation clinical trials[38,50–52].

Highest success applying the PersonAL strategy

The identification and consequent ablation of fibrotic tissue had in general high success (≈80-90%) but still lower than a first application of the strategy targeting AF-perpetuating areas (≈98-99%), characterized as HDF areas. This means that even if a clear determination of fibrotic tissue and/or slow conduction regions will be possible with high resolution mapping technologies and imaging data in combination with advanced analysis algorithms, we would nevertheless miss possible AF-perpetuation areas. Moreover, substrate driven ablation strategies led to >20% of inactive/dead tissue, compared to only ≈5-6% of electrically isolated tissue with tailored ablation lines targeting AF drivers. Fewer lesions have the advantage of shorter ablation procedures, more remaining viable cardiac tissue which is beneficial for hemodynamic performance and fewer possible complications for the patient. The PersonAL strategy consists of iterative personalized simulations and AF assessment, locating resulting HDF areas and targeting them with ablation connected to existing non-conducting structures. Previous studies showed that HDF regions are prone to develop at slow conduction sites identified during sinus rhythm mapping[8]. However, clinical studies failed to show an increased success[53]. The advantages of our approach are that we integrated connecting lines and that we leveraged digital twins to integrate and augment clinical data. Our patient-specific models were exposed to aggressive and comprehensive inducibility tests pre- and post-ablation from various locations unveiling all areas vulnerable to sustain AF, which is not feasible in vivo. Moreover, the in silico DF maps were computed considering multiple episodes and finally merged to determine all HDF regions. Conversely, clinical DF mapping is able to identify only ongoing AF episodes. For PersonAL, DF was computed based on the localized transmembrane voltage information and not on extracellular potentials as measured by clinical electrograms, which are impaired by different kinds of artifacts including far field and noise. Lately, promising studies proposed methodologies to identify AF drivers location during AF mapping in clinics using DF or AF cycle length statistics[54,55]. However, a more accurate identification required longer recordings. Our strategy could be further extended to address also AT episodes and prevent AT recurrence by integrating computational methods to reveal latent macro-reentrant pathways in the workflow[56]. Tailored ablation lines targeting these pathways could finally prevent recurrence of both AF and AT.

Assessing inducibility pre- and post-ablation from multiple sites to unveil all AF episodes

All current AF mapping techniques are only able to identify drivers that manifest in a patient in that specific moment or induced AF episodes. New possible AF drivers, which could spontaneously arise before or after an initial set of ablation lesions modifies the atrial substrate and can lead to AF recurrence are not considered. Moreover, assessing inducibility pre- and post-ablation from multiple locations in clinical practice will considerably prolong the procedure.

However, in our computer models, AF inducibility was assessed by applying the exhaustive and aggressive PEERP protocol from multiple locations in the same patient. In this way, all possible arrhythmic episodes which could sustain in that specific atrial digital twin could be unveiled. After testing AF reinducibility in all patients treated with the PersonAL plan, only AT episodes could be initiated. Therefore, the proposed PeronAL strategy was not only able to terminate all AF episodes or convert them to AT, but the treated models were unsusceptible to future AF.

Proof-of-concept clinical feasibility study

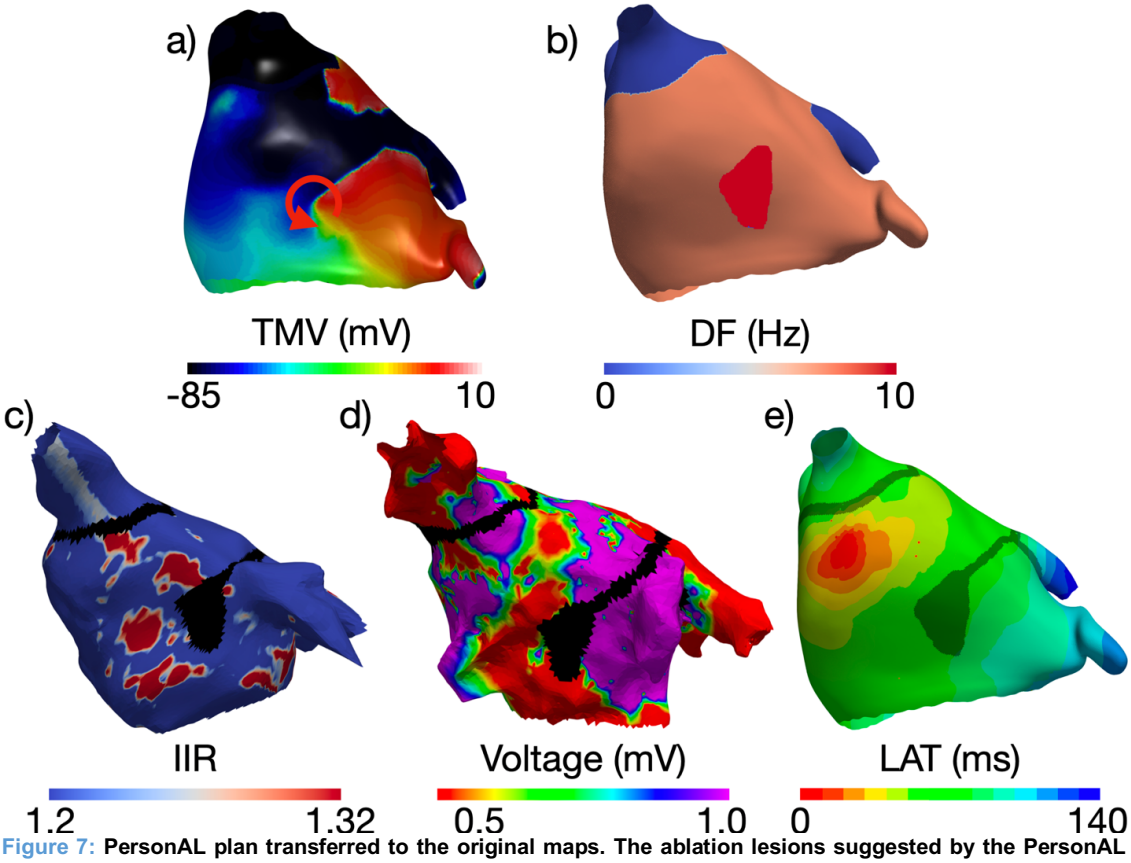

Figure 7: PersonAL plan transferred to the original maps. The ablation lesions suggested by the PersonAL strategy are shown as black lines. a) sustained AF episode after PVI in patient #18 color coded by transmembrane voltage (TMV) with fibrosis distributed according to voltage <0.5mV; b) DF map; c) original LGE-MRI segmentation color coded by IIR; d) original electro-anatomical map color coded by clinical bipolar voltage; e) atrial model color coded by the in silico LAT map.

The final step of our pipeline consists in importing the PersonAL plan into the original clinical maps. The integration of computer model predicted ablation targets and consequent proposed ablation lines into the clinical procedure as shown in Figure 7 for patient #18 facilitates future clinical translation. Importing the PersonAL strategy into the clinical mapping system could provide not only a reliable and accurate prediction of AF ablation targets but could also avoid time-consuming and difficult mapping of AF drivers.

Comparison to previous studies providing computer guided ablation strategies

Previous works attempted to use personalized computational simulations to guide clinical ablation of AF in patients[57–59].

In Shim et al.[58], atrial models consisted of endocardial CT-based LA shells only and AF was induced using a non-personalized pacing protocol (rapid pacing) applied only at the Bachmann's bundle location. Fiber orientation was not considered in the atrial models. A fixed isotropic conduction velocity of 0.4 m/s and no regional differences in myocyte action potentials were considered to represent patient electrophysiology. Four different anatomical ablation strategies (PVI only, PVI+lines), manually applied point-by-point on a user interface, and a CFAE guided ablation were tested and the best-performing in the simulations was empirically selected as the one to be executed clinically. No AF reinducibility was assessed post-ablation.

The OPTIMA approach presented by Boyle et al.[57] targeted, in personalized bi-atrial models, the RD-perpetuating areas within the fibrotic substrate derived from LGE-MRI, including those that appeared after a first application of virtual ablation. AF was induced using the same train of pulses for each patient. Conduction velocity in non-fibrotic tissue was set to 0.43 m/s. The final plan was imported, via co-registration, on the electro-anatomical mapping system. Nonetheless, the lack of full patient-specific electrophysiological properties could bring a level of uncertainty in identifying the OPTIMA targets. While RD dynamics are influenced by fibrosis distribution, other factors play important roles as well [60,61]. In Deng et al.[60] and Hakim et al.[61], fibrotic tissue was included in the models based on the IIR and the conduction velocity was modified within the fibrotic regions. Therefore, slow conduction areas were set to be the same as fibrotic tissue. Even in that case, changes in APD/CV enhanced or decreased the probability that an RD anchored to a specific location[60]. Even if using non-invasive clinical data only can be seen as an advantage due to the extended time frame to generate computational models, the level of uncertainty present in patient-specific atrial models reconstructed without any invasive measurements (i.e., incorporating each individual's unique distribution of fibrotic tissue from medical imaging alongside an average representation of AF-remodeled electrophysiology) is sufficiently high that a personalized ablation strategy based on targeting simulation-predicted RD trajectories alone may not be related to the real arrhythmogenic substrate in the patient[60]. Therefore, having insights on electrophysiological properties is important since they could result in RDs sometimes relocating to or appearing in other portions of the atria.

In Lim et al.[59], the generation of atrial models requires multiple manual steps, from the pre-processing of the clinical geometries to the registration of the electro-anatomical map onto the imaging segmentation. Even if the registration between the electro-anatomical map and the CT model was performed by an experienced technician, any registration error due to the manual procedure during the clinical mapping process that may have had an impact on the accuracy of the model cannot be excluded. Computer simulations are performed on a monolayer surface mesh, neglecting the myocardial thickness and the different fiber arrangement between endocardium and epicardium. Inducibility was assessed stimulating from one point close to the Bachmann bundle only. Reducing drastically the chances of unveiling all possible regions vulnerable to sustain arrhythmia. No virtual ablation is performed and, therefore, no ablation success rate is delivered.

In Roney et al.[62], atrial geometries derived from tomographic segmentations were manually processed and labeled. The endocardial and epicardial fibers were not calculated on the respective anatomical mesh but were mapped from an atlas and integrated in the model using the universal atrial coordinates. Fixed conductivity values were initially globally assigned to the

models and then regionally scaled according to the normalized LGE-MRI intensity values. However, electrophysiological remodeling was modified regionally according to the IIR values. A single and equivalent phase distribution map consisting of four phase singularities was used as initial state to induce AF in all atrial models. The substrate ablation strategies were limited to target fibrotic tissue identified using LGE-MRI maps. No re-inducibility was tested.

We proposed a highly automated framework to generate atrial digital twins with the selection of only one reference point per atrium[25]. In the case both non-invasive imaging data and intra-cardiac maps are available, all electrophysiological information were automatically integrated in the resulting bi-layer atrial models augmented by using a statistical shape model and rule-based fiber orientation. Fibrotic tissue can be modeled according to any clinical modality (e.g., IIR or LVA) and conduction velocity is locally tuned to match the clinical LAT map. AF vulnerability is assessed on the patient-specific atrial models using our personalized inducing protocol[26] in multiple pacing locations, unveiling all possible AF-sustaining regions. Drivers are automatically identified and targeted for ablation. The process is repeated until no AF episode can be initiated. Finally, the final PersonAL plan is transferred to the original clinical system (tomographic imaging or electro-anatomical mapping system). Moreover, numerous different ablation strategies were exhaustively compared in a rather large patient cohort and the ablation success was evaluated in almost 200 induced AF episodes.

Limitations

Heterogeneous anatomical thickness was shown to have an influence on RD dynamics[63]. However, this was mostly presented in the right atrium, in the proximity of the pectinate muscles and crista terminalis[63,64]. Even if no volumetric meshes were used in the current atrial models, the bilayer models demonstrated to be able to simulate endo-epicardial wave propagation delay and integrated different fiber arrangements in the endocardium and epicardium[31].

Although right atrial driver sites in patients with AF are less frequent than triggers in the LA, the current LA-only models would not be able to detect RA trigger sites. However, the pipeline was shown to be able to generate bi-atrial personalized models when both LA and RA were provided[25]. AF vulnerability assessment and ablation of AF drivers could be conducted following the same methodology in a bi-atrial model.

Conclusion

Our pipeline offers a reproducible and comprehensive platform to assess AF vulnerability and provide patient-specific treatments using highly detailed anatomical and functional atrial digital twins. We have presented a new technology for tailored ablation guided by computer simulations which outperformed conventional approaches and demonstrated its feasibility in an in silico study in a cohort of 29 patients. Our study highlighted that a clear characterization and ablation of the fibrotic substrate leads to high success (>90%). Iteratively identifying and targeting for ablation high dominant frequency regions with our PersonAL plan resulted in AF termination and prevented recurrence in the whole patients' cohort. Connecting lines to the nearest non-conductive barrier prevented recurrence and increased ablation success. This work is a step forward in the direction of personalized medicine using digital twins to guide patient-specific catheter ablation therapy for the most common human arrhythmias as atrial fibrillation and atrial tachycardia.

Author Contributions

L.A., M.E., A.J and A.L. conceived and designed the study. O.D. and A.L. supervised the project. M.E and A.J recorded the clinical data. L.A., D.N. and L.U. processed the clinical data. L.A and J.S outlined the ablation strategies. C.N. built the SSM. L.A. constructed the atrial models, implemented all methods and protocols and the final pipeline, ran the simulations, analyzed the data, and drafted the manuscript. All authors edited and approved the manuscript.

Acknowledgements

This work was performed on the supercomputer bwUniCluster 2.0 funded by the Ministry of Science, Research and Arts of Baden-Württemberg and by the German Federal Ministry of Education and Research.

Funding

This work was supported by European Union's Horizon 2020 research and innovation programme under the Marie Skłodowska-Curie grant agreement No.766082 (MY-ATRIA project), the EMPIR programme co-financed by the participating states and from the European Union's Horizon 2020 research and innovation programme under grant MedalCare 18HLT07, and by Deutsche Forschungsgemeinschaft (DFG) (project ID 391128822, LO 2093/1-1).

Data availability

The data anatomical models underlying this article are publicly available on Zenodo: https://doi.org/10.5281/zenodo.5589289. Simulations were performed using the open electrophysiology simulator openCARP[65].

References

1. Kornej J, Börschel CS, Benjamin EJ, Schnabel RB. Epidemiology of Atrial Fibrillation in the 21st Century: Novel Methods and New Insights. *Circ Res* 2020;**127**:4–20.

2. Hindricks G, Potpara T, Dagres N, Arbelo E, Bax JJ, Blomström-Lundqvist C, Boriani G, Castella M, Dan G-A, Dilaveris PE, Fauchier L, Filippatos G, Kalman JM, La Meir M, Lane DA, Lebeau J-P, Lettino M, Lip GYH, Pinto FJ, Thomas GN, Valgimigli M, Van Gelder IC, Van Putte BP, Watkins CL. 2020 ESC Guidelines for the diagnosis and management of atrial fibrillation developed in collaboration with the European Association of Cardio-Thoracic Surgery (EACTS). *European Heart Journal* 2020;

3. Haïssaguerre M, Jaïs P, Shah DC, Takahashi A, Hocini M, Quiniou G, Garrigue S, Le Mouroux A, Le Métayer P, Clémenty J. Spontaneous Initiation of Atrial Fibrillation by Ectopic Beats Originating in the Pulmonary Veins. *New England Journal of Medicine* 1998;**339**:659–666.

4. Duytschaever M, Vijgen J, De Potter T, Scherr D, Van Herendael H, Knecht S, Kobza R, Berte B, Sandgaard N, Albenque J-P, Szeplaki G, Stevenhagen YJ, Taghji P, Wright M, Macours N, Gupta D. Standardized pulmonary vein isolation workflow to enclose veins with contiguous lesions: the multicentre VISTAX trial. *EP Europace* 2020;**22**:1645–1652.

5. Tilz RR, Rillig A, Thum A-M, Arya A, Wohlmuth P, Metzner A, Mathew S, Yoshiga Y, Wissner E, Kuck K-H, Ouyang F. Catheter Ablation of Long-Standing Persistent Atrial Fibrillation. *Journal of the American College of Cardiology* 2012;**60**:1921–1929.

6. Verma A, Jiang C, Betts TR, Chen J, Deisenhofer I, Mantovan R, Macle L, Morillo CA, Haverkamp W, Weerasooriya R, Albenque J-P, Nardi S, Menardi E, Novak P, Sanders P. Approaches to catheter ablation for persistent atrial fibrillation. *The New England Journal of Medicine* 2015;**372**:1812–22.

7. Platonov PG, Mitrofanova LB, Orshanskaya V, Ho SY. Structural Abnormalities in Atrial Walls Are Associated With Presence and Persistency of Atrial Fibrillation But Not With Age. *Journal of the American College of Cardiology* 2011;**58**:2225–2232.

8. Jadidi A, Nothstein M, Chen J, Lehrmann H, Dössel O, Allgeier J, Trenk D, Neumann F-J, Loewe A, Müller-Edenborn B, Arentz T. Specific Electrogram Characteristics Identify the Extra-Pulmonary Vein Arrhythmogenic Sources of Persistent Atrial Fibrillation – Characterization of the Arrhythmogenic Electrogram Patterns During Atrial Fibrillation and Sinus Rhythm. *Sci Rep* 2020;**10**:9147.

9. Rolf S, Kircher S, Arya A, Eitel C, Sommer P, Richter S, Gaspar T, Bollmann A, Altmann D, Piedra C, Hindricks G, Piorkowski C. Tailored Atrial Substrate Modification Based on Low-Voltage Areas in Catheter Ablation of Atrial Fibrillation. *Circ: Arrhythmia and Electrophysiology* 2014;**7**:825–833.

10. Marrouche NF, Wilber D, Hindricks G, Jais P, Akoum N, Marchlinski F, Kholmovski E, Burgon N, Hu N, Mont L, Deneke T, Duytschaever M, Neumann T, Mansour M, Mahnkopf C, Herweg B, Daoud E, Wissner E, Bansmann P, Brachmann J. Association of Atrial Tissue Fibrosis Identified by Delayed Enhancement MRI and Atrial Fibrillation Catheter Ablation: The DECAAF Study. *JAMA* 2014;**311**:498.

11. McGann C, Akoum N, Patel A, Kholmovski E, Revelo P, Damal K, Wilson B, Cates J, Harrison A, Ranjan R, others. Atrial fibrillation ablation outcome is predicted by left atrial remodeling on MRI. *Circulation: Arrhythmia and Electrophysiology* Am Heart Assoc; 2014;**7**:23–30.

12. Mahnkopf C, Badger TJ, Burgon NS, Daccarett M, Haslam TS, Badger CT, McGann CJ, Akoum N, Kholmovski E, Macleod RS, others. Evaluation of the left atrial substrate in patients with lone atrial fibrillation using delayed-enhanced MRI: implications for disease progression and response to catheter ablation. *Heart Rhythm* Elsevier; 2010;**7**:1475–1481.

13. Jadidi AS, Lehrmann H, Keyl C, Sorrel J, Markstein V, Minners J, Park C-I, Denis A, Jaïs P, Hocini M, Potocnik C, Allgeier J, Hochholzer W, Herrera-Siklody C, Kim S, Omri YE, Neumann F-J, Weber R, Haïssaguerre M, Arentz T. Ablation of Persistent Atrial Fibrillation Targeting Low-Voltage Areas With Selective Activation Characteristics. *Circ Arrhythm Electrophysiol* 2016;**9**.

14. Kircher S, Arya A, Altmann D, Rolf S, Bollmann A, Sommer P, Dagres N, Richter S, Breithardt O-A, Dinov B, Husser D, Eitel C, Gaspar T, Piorkowski C, Hindricks G. Individually tailored vs. standardized substrate modification during radiofrequency catheter ablation for atrial fibrillation: a randomized study. *EP Europace* 2018;**20**:1766–1775.

15. Park C-I, Lehrmann H, Keyl C, Weber R, Schiebeling J, Allgeier J, Schurr P, Shah A, Neumann F-J, Arentz T, Jadidi AS. Mechanisms of Pulmonary Vein Reconnection After Radiofrequency Ablation of Atrial Fibrillation: The Deterministic Role of Contact Force and Interlesion Distance: Mechanisms of Pulmonary Vein Reconnection After Radiofrequency Ablation of Atrial Fibrillation. *Journal of Cardiovascular Electrophysiology* 2014;**25**:701–708.

16. Narayan SM, Baykaner T, Clopton P, Schricker A, Lalani GG, Krummen DE, Shivkumar K, Miller JM. Ablation of Rotor and Focal Sources Reduces Late Recurrence of Atrial Fibrillation Compared With Trigger Ablation Alone. *Journal of the American College of Cardiology* 2014;**63**:1761–1768.

17. Haissaguerre M, Hocini M, Denis A, Shah AJ, Komatsu Y, Yamashita S, Daly M, Amraoui S, Zellerhoff S, Picat M-Q, Quotb A, Jesel L, Lim H, Ploux S, Bordachar P, Attuel G, Meillet V, Ritter P, Derval N, Sacher F, Bernus O, Cochet H, Jais P, Dubois R. Driver domains in persistent atrial fibrillation. *Circulation* 2014;**130**:530–538.

18. Kottkamp H, Berg J, Bender R, Rieger A, Schreiber D. Box Isolation of Fibrotic Areas (BIFA): A Patient-Tailored Substrate Modification Approach for Ablation of Atrial Fibrillation: Substrate Modification BIFA in AF Ablation. *J Cardiovasc Electrophysiol* 2016;**27**:22–30.

19. Gray RA, Pertsov AM, Jalife J. Spatial and temporal organization during cardiac fibrillation. *Nature* 1998;**392**:75–78.

20. Sahadevan J, Ryu K, Peltz L, Khrestian CM, Stewart RW, Markowitz AH, Waldo AL. Epicardial mapping of chronic atrial fibrillation in patients: preliminary observations. *Circulation* 2004;**110**:3293–3299.

21. Miller JM, Kalra V, Das MK, Jain R, Garlie JB, Brewster JA, Dandamudi G. Clinical benefit of ablating localized sources for human atrial fibrillation: the Indiana University FIRM Registry. *Journal of the American College of Cardiology* 2017;**69**:1247–1256.

22. Mohanty S, Mohanty P, Trivedi C, Gianni C, Della Rocca DG, Di Biase L, Natale A. Long-term outcome of pulmonary vein isolation with and without focal impulse and rotor modulation mapping: insights from a meta-analysis. *Circulation: Arrhythmia and Electrophysiology* 2018;**11**:e005789.

23. Bisbal F, Benito E, Teis A, Alarcón F, Sarrias A, Caixal G, Villuendas R, Garre P, Soto N, Cozzari J, Guasch E, Juncà G, Prat-Gonzalez S, Perea RJ, Bazán V, Tolosana JM, Arbelo E, Bayés-Genís A, Mont L. Magnetic Resonance Imaging-Guided Fibrosis Ablation for the Treatment of Atrial Fibrillation. *Circulation: Arrhythmia and Electrophysiology* 2020;**13**:e008707.

24. Marrouche NF, Greene T, Dean JM, Kholmovski EG, Boer LM, Mansour M, Calkins H, Marchlinski F, Wilber D, Hindricks G, Mahnkopf C, Jais P, Sanders P, Brachmann J, Bax J, Dagher L, Wazni O, Akoum N, The DECAAF II Investigators. Efficacy of LGE-MRI-guided fibrosis ablation versus conventional catheter ablation of atrial fibrillation: The DECAAF II trial: Study design. *J Cardiovasc Electrophysiol* 2021;**32**:916–924.

25. Azzolin L, Eichenlaub M, Nagel C, Nairn D, Sanchez J, Unger LA, Doessel O, Jadidi A, Loewe A. AugmentA: patient-specific Augmented Atria Generation Tool. *Submitted* 2021;

26. Azzolin L, Schuler S, Dössel O, Loewe A. A Reproducible Protocol to Assess Arrhythmia Vulnerability : Pacing at the End of the Effective Refractory Period. *Frontiers in Physiology* 2021;**12**:656411.

27. Nagel C, Schuler S, Dössel O, Loewe A. A bi-atrial statistical shape model for large-scale in silico studies of human atria: Model development and application to ECG simulations. *Medical Image Analysis* 2021;**74**:102210.

28. Azzolin L, Nagel C, Nairn D, Sanchez J, Zheng T, Eichenlaub M, Jadidi A, Doessel O, Loewe A. Automated Framework for the Augmentation of Missing Anatomical Structures and Generation of Personalized Atrial Models from Clinical Data. *Computing in Cardiology Conference (CinC)* 2021.

29. Piersanti R, Africa PC, Fedele M, Vergara C, Dedè L, Corno AF, Quarteroni A. Modeling cardiac muscle fibers in ventricular and atrial electrophysiology simulations. *Computer Methods in Applied Mechanics and Engineering* 2021;**373**:113468.

30. Zheng T, Azzolin L, Sanchez J, Dössel O, Loewe A. An automated pipeline for generating fiber orientation and region annotation of patient-specific atrial model. *Current Directions in Biomedical Engineering* De Gruyter; 2021;**1**:409–412.

31. Labarthe S, Bayer J, Coudiere Y, Henry J, Cochet H, Jais P, Vigmond E. A bilayer model of human atria: mathematical background, construction, and assessment. *Europace : European Pacing, Arrhythmias, and Cardiac Electrophysiology : Journal of the Working Groups on Cardiac Pacing, Arrhythmias, and Cardiac Cellular Electrophysiology of the European Society of Cardiology* 2014;**16 Suppl 4**:iv21–iv29.

32. Loewe A, Wilhelms M, Dössel O, Seemann G. Influence of chronic atrial fibrillation induced remodeling in a computational electrophysiological model. *Biomed Eng* 2014;**59**:S929–S932.

33. Loewe A, Krueger MW, Platonov PG, Holmqvist F, Dössel O, Seemann G. Left and Right Atrial Contribution to the P-wave in Realistic Computational Models. *Lect Notes Comput Sci* 2015;**9126**:439–447.

34. Vigmond E, Pashaei A, Amraoui S, Cochet H, Hassaguerre M. Percolation as a mechanism to explain atrial fractionated electrograms and reentry in a fibrosis model based on imaging data. *Heart Rhythm : the Official Journal of the Heart Rhythm Society* 2016;**13**:1536–1543.

35. Ramos-Mondragón R, Vega AV, Avila G. Long-term modulation of Na+ and K+ channels by TGF-β1 in neonatal rat cardiac myocytes. *Pflugers Arch - Eur J Physiol* 2011;**461**:235–247.

36. Roney CH, Bayer JD, Zahid S, Meo M, Boyle PMJ, Trayanova NA, Haïssaguerre M, Dubois R, Cochet H, Vigmond EJ. Modelling methodology of atrial fibrosis affects rotor dynamics and electrograms. *Europace* 2016;**18**:iv146–iv155.

37. Roney CH, Beach ML, Mehta AM, Sim I, Corrado C, Bendikas R, Solis-Lemus JA, Razeghi O, Whitaker J, O'Neill L, Plank G, Vigmond E, Williams SE, O'Neill MD, Niederer SA. In silico Comparison of Left Atrial Ablation Techniques That Target the Anatomical, Structural, and Electrical Substrates of Atrial Fibrillation. *Frontiers in Physiology* 2020;**11**:1–162.

38. Narayan SM, Krummen DE, Shivkumar K, Clopton P, Rappel W-J, Miller JM. Treatment of Atrial Fibrillation by the Ablation of Localized Sources: CONFIRM (Conventional Ablation for Atrial Fibrillation With or Without Focal Impulse and Rotor Modulation) Trial. *Journal of the American College of Cardiology* 2012;**60**:628–636.

39. Jarman JW, Wong T, Kojodjojo P, Spohr H, Davies JE, Roughton M, Francis DP, Kanagaratnam P, Markides V, Davies DW, others. Spatiotemporal behavior of high dominant frequency during paroxysmal and persistent atrial fibrillation in the human left atrium. *Circulation: Arrhythmia and Electrophysiology* Am Heart Assoc; 2012;**5**:650–658.

40. Ng J, Kadish AH, Goldberger JJ. Effect of electrogram characteristics on the relationship of dominant frequency to atrial activation rate in atrial fibrillation. *Heart Rhythm* Elsevier; 2006;**3**:1295–1305.

41. Bertaglia E, Bella PD, Tondo C, Proclemer A, Bottoni N, De Ponti R, Landolina M, Bongiorni MG, Coro L, Stabile G, others. Image integration increases efficacy of paroxysmal atrial fibrillation catheter ablation: results from the CartoMerge™ Italian Registry. *Europace* Oxford University Press; 2009;**11**:1004–1010.

42. Martinek M, NESSER H-J, Aichinger J, Boehm G, Purerfellner H. Impact of integration of multislice computed tomography imaging into three-dimensional electroanatomic mapping on clinical outcomes, safety, and efficacy using radiofrequency ablation for atrial fibrillation. *Pacing and Clinical Electrophysiology* Wiley Online Library; 2007;**30**:1215–1223.

43. Chen J, Arentz T, Cochet H, Müller-Edenborn B, Kim S, Moreno-Weidmann Z, Minners J, Kohl P, Lehrmann H, Allgeier J, Trenk D, Hocini M, Jais P, Haissaguerre M, Jadidi A. Extent and spatial distribution of left atrial arrhythmogenic sites, late gadolinium enhancement at magnetic resonance imaging, and low-voltage areas in patients with persistent atrial fibrillation: comparison of imaging vs. electrical parameters of fibrosis and arrhythmogenesis. *EP Europace* 2019;**21**:1484–1493.

44. Pontecorboli G, Figueras i Ventura RM, Carlosena A, Benito E, Prat-Gonzales S, Padeletti L, Mont L. Use of delayed-enhancement magnetic resonance imaging for fibrosis detection in the atria: a review. *EP Europace* 2017;**19**:180–189.

45. Masuda M, Asai M, Iida O, Okamoto S, Ishihara T, Nanto K, Kanda T, Tsujimura T, Matsuda Y, Okuno S, Hata Y, Mano T. Additional Low-Voltage-Area Ablation in Patients With Paroxysmal Atrial Fibrillation: Results of the Randomized Controlled VOLCANO Trial. *Journal of the American Heart Association* 2020;**9**:e015927.

46. Nery PB, Alqarawi W, Nair GM, Sadek MM, Redpath CJ, Golian M, Al Dawood W, Chen L, Hansom SP, Klein A, Wells GA, Birnie DH. Catheter Ablation of Low-Voltage Areas for Persistent Atrial Fibrillation: Procedural Outcomes Using High-Density Voltage Mapping. *Canadian Journal of Cardiology* 2020;**36**:1956–1964.

47. Nairn D, Lehrmann H, Müller-Edenborn B, Schuler S, Arentz T, Dössel O, Jadidi A, Loewe A. Comparison of Unipolar and Bipolar Voltage Mapping for Localization of Left Atrial Arrhythmogenic Substrate in Patients With Atrial Fibrillation. *Front Physiol* 2020;**11**:575846.

48. Nairn D, Nagel C, Müller-Edenborn B, Lehrmann H, Arentz T, Doessel O, Jadidi A, Loewe A. Optimal Regional Voltage Thresholds for Identifying Ablation Targets in Patients with Atrial Fibrillation. *Computing in Cardiology Conference (CinC)* 2021.

49. Acosta J, Andreu D, Penela D, Cabrera M, Carlosena A, Korshunov V, Vassanelli F, Borras R, Martínez M, Fernández-Armenta J, Linhart M, Tolosana JM, Mont L, Berruezo A. Elucidation of hidden slow conduction by double ventricular extrastimuli: a method for further arrhythmic substrate identification in ventricular tachycardia ablation procedures. *EP Europace* 2018;**20**:337–346.

50. Henley P, Foreman JR, Padanilam BJ, Nair GV, Olson JA, Joshi S, Aziz Z, Foster T, Prystowsky EN. Single-center experience of the FIRM technique to ablate paroxysmal and persistent atrial fibrillation. *J Cardiovasc Electrophysiol* 2019;**30**:493–502.

51. Tilz RR, Lenz C, Sommer P, Roza M-S, Sarver AE, Williams CG, Heeger C, Hindricks G, Vogler J, Eitel C. Focal Impulse and Rotor Modulation Ablation vs. Pulmonary Vein isolation for the treatment of paroxysmal Atrial Fibrillation: results from the FIRMAP AF study. *EP Europace* 2021;**23**:722–730.

52. Steinberg JS, Shah Y, Bhatt A, Sichrovsky T, Arshad A, Hansinger E, Musat D. Focal impulse and rotor modulation: Acute procedural observations and extended clinical follow-up. *Heart Rhythm* 2017;**14**:192–197.

53. Sanders P, Berenfeld O, Hocini M, Jaïs P, Vaidyanathan R, Hsu L-F, Garrigue S, Takahashi Y, Rotter M, Sacher F, Scavée C, Ploutz-Snyder R, Jalife J, Haïssaguerre M. Spectral Analysis Identifies Sites of High-Frequency Activity Maintaining Atrial Fibrillation in Humans. *Circulation* 2005;**112**:789–797.

54. Li X, Chu GS, Almeida TP, Vanheusden FJ, Salinet J, Dastagir N, Mistry AR, Vali Z, Sidhu B, Stafford PJ, Schlindwein FS, Ng GA. Automatic Extraction of Recurrent Patterns of High Dominant Frequency Mapping During Human Persistent Atrial Fibrillation. *Front Physiol* 2021;**12**:649486.

55. Unger LA, Azzolin L, Nothstein M, Sánchez J, Luik A, Seemann G, Yeshwant S, Oesterlein T, Dössel O, Schmitt C, Spector P, Loewe A. Cycle length statistics during human atrial fibrillation reveal refractory properties of the underlying substrate: a combined in silico and clinical test of concept study. *EP Europace* 2021;**23**:i133–i142.

56. Loewe A, Poremba E, Oesterlein T, Luik A, Schmitt C, Seemann G, Dössel O. Patient-Specific Identification of Atrial Flutter Vulnerability–A Computational Approach to Reveal Latent Reentry Pathways. *Front Physiol* 2019;**9**:1910.

57. Boyle PM, Zghaib T, Zahid S, Ali RL, Deng D, Franceschi WH, Hakim JB, Murphy MJ, Prakosa A, Zimmerman SL, Ashikaga H, Marine JE, Kolandaivelu A, Nazarian S, Spragg DD, Calkins H, Trayanova NA. Computationally guided personalized targeted ablation of persistent atrial fibrillation. *Nat Biomed Eng* 2019;**3**:870–879.

58. Shim J, Hwang M, Song J-S, Lim B, Kim T-H, Joung B, Kim S-H, Oh Y-S, Nam G-B, On YK, Oh S, Kim Y-H, Pak H-N. Virtual In-Silico Modeling Guided Catheter Ablation Predicts Effective Linear Ablation Lesion Set for Longstanding Persistent Atrial Fibrillation: Multicenter Prospective Randomized Study. *Front Physiol* 2017;**8**:792.

59. Lim B, Kim J, Hwang M, Song J-S, Lee JK, Yu H-T, Kim T-H, Uhm J-S, Joung B, Lee M-H, Pak H-N. In situ procedure for high-efficiency computational modeling of atrial fibrillation reflecting personal anatomy, fiber orientation, fibrosis, and electrophysiology. *Sci Rep* 2020;**10**:2417.

60. Deng D, Murphy MJ, Hakim JB, Franceschi WH, Zahid S, Pashakhanloo F, Trayanova NA, Boyle PM. Sensitivity of reentrant driver localization to electrophysiological parameter variability in image-based computational models of persistent atrial fibrillation sustained by a fibrotic substrate. *Chaos* 2017;**27**:093932.

61. Hakim JB, Murphy MJ, Trayanova NA, Boyle PM. Arrhythmia dynamics in computational models of the atria following virtual ablation of re-entrant drivers. *EP Europace* 2018;**20**:iii45–iii54.

62. Roney CH, Beach ML, Mehta AM, Sim I, Corrado C, Bendikas R, Solis-Lemus JA, Razeghi O, Whitaker J, O'Neill L, Plank G, Vigmond E, Williams SE, O'Neill MD, Niederer SA. In silico Comparison of Left Atrial Ablation Techniques That Target the Anatomical, Structural, and Electrical Substrates of Atrial Fibrillation. *Frontiers in Physiology* 2020;**11**:1–162.

63. Azzolin L, Luongo G, Rocher S, Saiz J, Doessel O, Loewe A. Influence of Gradient and Smoothness of Atrial Wall Thickness on Initiation and Maintenance of Atrial Fibrillation. *Computing in Cardiology Conference (CinC)* 2020.

64. Hansen BJ, Zhao J, Csepe TA, Moore BT, Li N, Jayne LA, Kalyanasundaram A, Lim P, Bratasz A, Powell KA, Simonetti OP, Higgins RSD, Kilic A, Mohler PJ, Janssen PML, Weiss R, Hummel JD, Fedorov VV. Atrial fibrillation driven by micro-anatomic intramural re-entry revealed by simultaneous sub-epicardial and sub-endocardial optical mapping in explanted human hearts. *European Heart Journal* 2015;**36**:2390–401.

65. Plank G, Loewe A, Neic A, Augustin C, Huang Y-L, Gsell MAF, Elias Karabelas JS Mark Nothstein, Prassl AJ, Seemann G, Vigmond EJ. The openCARP Simulation Environment for Cardiac Electrophysiology. *Computer Methods and Programs in Biomedicine* 2021;**208**:106223.

Chapter 6

Summary, outlook, and conclusion

In this thesis, two major studies were presented. At first, cardiac computational modeling was leveraged to better understand the mechanisms behind atrial fibrillation (AF) onset and perpetuation. Finally, a comprehensive platform was developed and provided to automatically generate personalized atrial models of patients with AF integrating multiple clinical datasets, assess AF vulnerability, identify ablation targets and perform virtual ablation. The underlying algorithms and the respective results achieved using them, were systematically evaluated and compared to state-of-the-art methods. In the first presented study, we quantitatively evaluated different methods to induce arrhythmia in-silico, evaluated their influence of both, initiation and perpetuation of AF episodes and finally provided a fast and easily reproducible method to standardize AF vulnerability assessment of atrial models [15]. All protocols used in this study are open source to enhance comparability, reproducibility and foster the adoption of our novel proposed method as a community standard. The results obtained from the comparison with the other methods showed that our parameter-free method induced different degrees of arrhythmic complexity, unveiled more areas vulnerable to maintain AF with a lower number of stimuli, while being therefore computationally inexpensive. Therefore, our study highlighted and confirmed the impact of the choice of the inducing protocol on AF onset and perpetuation. Considering the findings of the previous study [15], the influence of heterogeneity in atrial anatomical thickness on initiation and maintenance of AF was investigated [16]. Arrhythmic episodes were initiated on atrial models with different degrees of augmented heterogeneous anatomical thickness. Long-living re-entrant drivers (RDs) were detected and tracked over time to analyze AF dynamics. Our work showed that RDs steer towards borders between regions with various thicknesses and are maintained in the proximity of steep rims. In addition, higher thickness heterogeneity increased arrhythmia complexity and unveiled new vulnerable areas prone to AF initiation and perpetuation. Therefore, we concluded that gradient and smoothing of anatomical thickness had an influence on both AF inducibility and maintenance, mostly in the right atrium (RA). Finally, we proposed wall thickness gradient and curvature as

complementary a priori measures to investigate substrate arrhythmogenicity and suggest target areas for ablation. Considering the insights acquired in the previous studies, the final work leveraging atrial digital twins for AF vulnerability assessment and personalized ablation was conducted. An automated algorithm fitting a bi-atrial statistical shape model (SSM) [115] to atrial geometries derived from clinical data augmenting missing anatomical structures was implemented [17]. Fiber arrangement and anatomical region annotations were automatically integrated within the models. The framework was tested on both, a geometry coming from an electroanatomical map and a magnetic resonance imaging segmentation. The resulting SSM instances accurately represented the original atrial anatomies and were able to infer the shape of the RA when only geometrical information of the left atrium (LA) was available. Finally, a unique pipeline to generate anatomical and functional digital twins from either tomographic imaging or electroanatomical maps was developed and tested on a cohort of 29 patients [18]. The platform pre-processes geometries derived from clinical data, providing a surface with closed boundaries. It proceeds with the identification and opening of the atrial orifices, and eventually, a resampling step is performed. If the user chooses to fit an SSM to the original surface, a non-rigid fitting algorithm is applied after the mesh shape and the input geometry were rigidly pre-aligned. An anatomically personalized atrial model including region annotation and fiber orientation is delivered. Then, atrial tissue's electrical properties are locally tuned to proceed with the functional twinning. Therefore, our conduction velocity estimation method consists of minimizing the difference between the simulated and the clinical local activation time map. A comprehensive comparison with state-of-the-art methods is presented. Our pipeline provided ready-to-use personalized computer models derived from clinical data outperforming other methods in representing the depolarization wave propagation in the myocardium. The presented platform is currently under review to be patented. The unique level of personalization achieved in this work gave us the chance of addressing the urgent need for a tool to help clinicians to tailor ablation strategies in patients with persistent AF [116]. Therefore, a technology to assess AF vulnerability and propose personalized ablation lines (PersonAL) on patient-specific atrial models was developed. The PersonAL strategy consists in iteratively identify and target for ablation emerging AF drivers (e.g. high dominant frequency areas) until no further AF episode can be initiated. Along with our tailored ablation plan, different standard-in-practice ablation strategies were tested and the ablation success, defined as AF termination or conversion to atrial tachycardia (AT), was evaluated. The pipeline was applied to 29 LA anatomical and functional digital twins generated with the methods in our previous work [18]. The optimal ablation targets are defined using information from both, non-invasive and intracardiac mapping systems to discriminate arrhythmogenic sites. AF episodes are initiated with our novel proposed inducing protocol [15], and RDs are automatically identified and targeted for ablation connecting the isolated sites with the closest non-conductive barrier to prevent emerging AF or AT cases. The process of arrhythmia vulnerability assessment and identification and ablation of emerging RDs is iterated until AF becomes non-inducible in the models. The first application of the high dominant frequency (HDF) regions ablation had a success of over 98%, better than all other tested anatomical and substrate approaches.

However, a clear characterization of the arrhythmogenic substrate and techniques aiming at isolating these AF-perpetuating areas also led to a high success (89-90%). Although, using these conventional techniques the amount of inactive tissue after ablation strategies targeting arrhythmogenic substrate was more than 20%, compared to only 5-6% using the HDF ablation. In addition, no further AF episode could be induced after a second iteration of the HDF ablation strategy. The possibility of integrating the final PersonAL plan into the original clinical mapping system suggesting ablation lines predicted by a computer model proved the clinical feasibility of our technology.

This thesis and its limitations could foster future projects. Exploiting the potential of computational modeling to build a bridge between medicine and engineering is the essential theme presented in this work. We hope that our work will promote the use of comprehensive virtual tools in health care which integrate coherently clinical data for each individual using deterministic and statistical models, the so called 'digital twin' [110]. Our knowledge of physiology and the fundamental laws of physics and chemistry is encapsulated in the mechanistic models. They provide the perfect framework for a deeper understanding of mechanisms and to predict outcomes, integrating and augmenting experimental and clinical data. Examples of such mechanistic models are the bidomain equations for cardiac electrophysiology presented in 3.2.1. Statistical models complement the knowledge and relations inferred from data. They allow the generation of population-based patterns and the identification and optimal combinations of individualized biomarkers with mathematical rules. Examples of statistical models applied to computational cardiology are decision tree classifiers for non-invasive assessment of AF driver locations [19] or Gaussian processes to build statistical shape models [115]. There are surely clinical questions that can be answered with a single modeling approach. However, the combination of both mechanistic and statistical models can overcome each one's limitations. Mechanistic models are constricted by their premises (assumptions and principles), while statistical models are constrained by the amount of available observations. Therefore, a mechanistic model may be preferred when the mechanisms of a system are well understood. On the contrary, a statistical model can find predictive relations based on limited knowledge of the underlying mechanisms. Our final studies are good examples of synergy between mechanistic and statistical models [17, 18, 116].

The pipeline developed in this thesis to generate atrial digital twins from clinical data left room for improvement. Due to the extensive computational cost of simulating wave propagation on highly detailed volumetric bi-atrial models, we move towards bi-layer modeling [117]. This modeling technique approximates myocardial thickness coupling endocardial and epicardial surfaces with linear resistors. In the presented studies [17, 18, 116], a fixed conductivity value was applied to model homogeneous thickness. However, a better representation of reality could be obtained by varying the conductivities regionally in case individualized anatomical thickness is known. Lately, mathematical formulations combining microscale reaction-diffusion systems with macroscale Eikonal models were generalized to handle re-entrant activation patterns and wavefront collisions typically seen during ar-

rhythmia. These reaction-diffusion Eikonal models are an approximation of the bidomain equations aspiring to consistently reduce the computation time, while keeping at the same time a high level of representation of the reality. The employment of such models solved with GPUs in the current pipeline could provide personalized ablation plans in procedural time. In addition, simulation time could be further decreased using dynamic and adaptive remeshing to concentrate the elements to areas with large gradients (depolarization front). Heart functioning is intrinsically a multi-physical ensemble of mechanisms. Therefore, atrial models integrating electro-fluid-mechanic coupling could be relevant when investigating the impact of AF or ablation lines on clinical measures such as the ejection fraction. Moreover, a quantitative evaluation of the risk of thrombosis in the left atrial appendage could be performed. Moreover, incorporating realistic catheters models to validate simulations and in-silico electrograms might provide deeper insights into arrhythmogenic substrate detection. Finally, statistical shape models (SSM) offer a valuable approach to build a cohort of AF patients, assess AF vulnerability and evaluate the optimal ablation for each cohort. Using SSMs a large virtual patient cohort can be compiled as a basis of generating synthetic datasets large enough for machine learning applications. Therefore, a machine learning algorithm could be implemented to propose the best personalized ablation strategy and predict the ablation outcome for each new patient.

The general aim of this thesis was to standardize AF assessment, guide therapy and help clinicians leveraging computer simulations for an improved patient outcome. In this thesis, novel mathematical tools were implemented and the predictive power of computational models were exploited to better understand AF onset and perpetuation mechanisms, leading to relevant insights in the human atrial patho-physiology. The studies presented in this thesis promote the state-of-the-art digital twins for healthcare and in personalized medicine. Novel technologies to process and augment clinical data and eventually merge multi-modal datasets were implemented. An efficient pipeline to reproducibly compute and automatically integrate fiber orientation on patient-specific virtual hearts to evaluate AF vulnerability, identify the main drivers, and propose the optimal ablation strategy were developed. It was successfully tested on a patient cohort and the final ablation plan was imported in the original mapping system to provide clinicians a tailored ablation strategy. To summarise, our studies lay the foundations for a better cardiac arrhythmia management and treatment guided by personalized computational models. Thus, the individual patient's discomfort, the ablation procedural time, the recurrence rate of AF, and finally, the social-economical burden of AF might be alleviated.

Appendix A

Appendix

A.1 Supplementary Materials

frontiers

Supplementary Material for *A Reproducible Protocol to Assess Arrhythmia Vulnerability in silico: Pacing at the End of the Effective Refractory Period*

Luca Azzolin*, Steffen Schuler, Olaf Dössel, Axel Loewe

Institute of Biomedical Engineering, Karlsruhe Institute of Technology (KIT)

Correspondence: publications@ibt.kit.edu

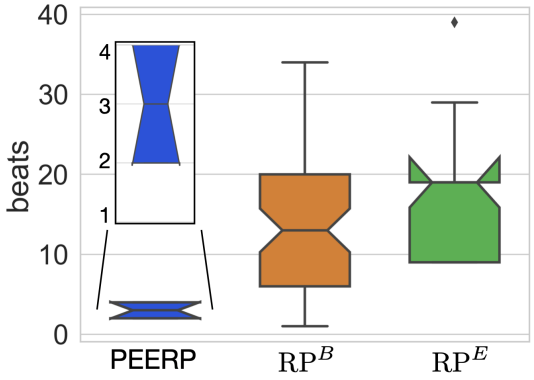

Figure S1. Total number of beats applied in the protocols PEERP, RP^B and RP^E inducing arrhythmic episodes in the model H4B.

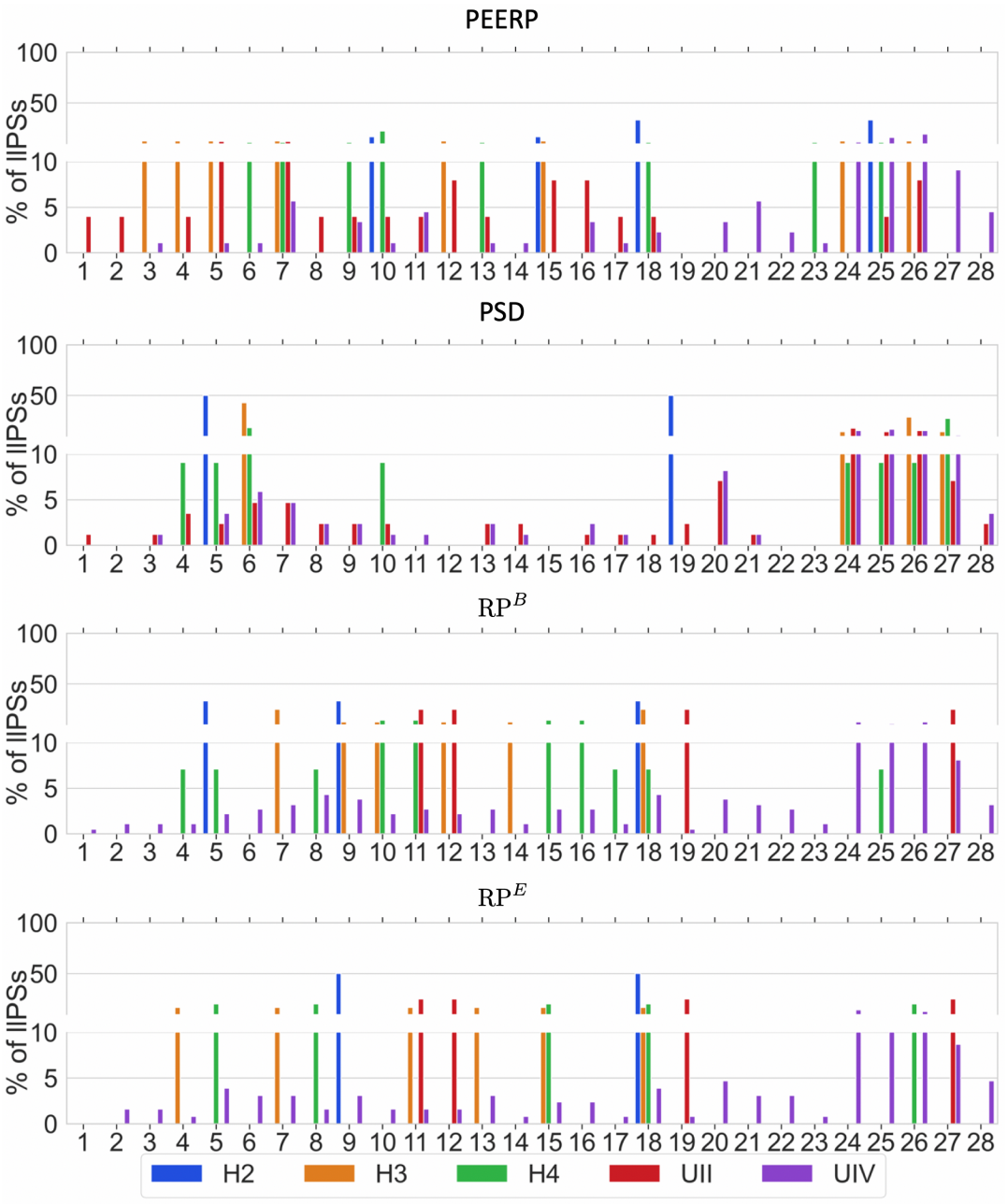

Figure S2. Atrial segments in which inducing points were identified applying the various protocols in the different models.

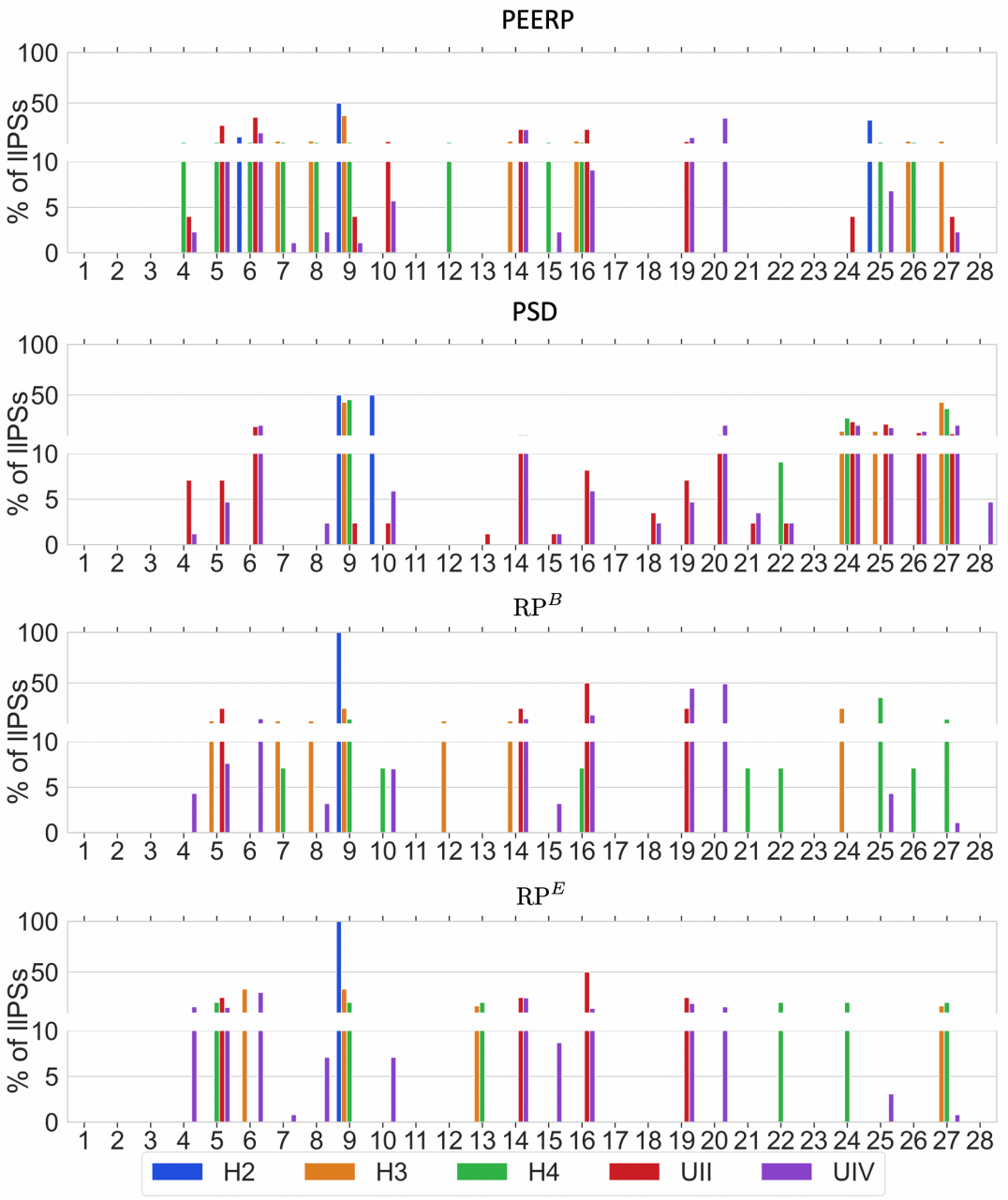

Figure S3. Atrial segments in which stable llPSs were maintained in the different models applying each protocol.

Supplementary Material: AugmentA: Patient-specific Augmented Atrial model Generation Tool

Luca Azzolin, Martin Eichenlaub, Claudia Nagel, Deborah Nairn, Jorge Sánchez, Laura Unger, Olaf Dössel, Amir Jadidi, and Axel Loewe

TABLE I
DIRICHLET BOUNDARY CONDITIONS OF THE TWELVE LAPLACE PROBLEMS.

Atrium	ψ	ψ_a	Γ_a	ψ_b	Γ_b
LA	ψ_{tran}	1	Γ_{epi}	0	Γ_{endo}
	ψ_{ab}	2	Γ_{rpv}	1	Γ_{mv}
		0	Γ_{lpv}	-1	Γ_{ap}
	ψ_{ab2}	1	Γ_{ap}	0	Γ_{rpv}
	ψ_v	1	Γ_{rpv}	0	Γ_{lpv}
	ψ_r	1	Γ_{mv}	0	$\Gamma_{lpv} \cup \Gamma_{rpv} \cup \Gamma_{mv}$
	ψ_{r2}	1	Γ_{mv}	0	$\Gamma_{rpv} \cup \Gamma_{lpv}$
RA	ψ_{tran}	1	Γ_{epi}	0	Γ_{endo}
	ψ_{ab}	2	Γ_{ivc}	1	Γ_{tv}
		0	Γ_{svc}	-1	Γ_{ap}
	ψ_v	1	Γ_{ivc}	0	$\Gamma_{svc} \cup \Gamma_{ap}$
	ψ_{v2}	1	Γ_{ivc}	0	Γ_{ap}
	ψ_r	1	Γ_{tv}	0	Γ_{top}
	ψ_w	1	Γ_{tv_s}	0	Γ_{tv_l}

S.I. Fiber generation

The Dirichlet boundary for the twelve Laplace problem are presented in Tab. I, in which the values ψ_a and ψ_b are applied on the boundary regions Γ_a and Γ_b.

S.II. Landmarks

1) ls_o: point on left superior PV farthest away from left inferior PV;
2) ls_i: point on left superior PV closest to left inferior PV;
3) li_i: point on left superior PV closest to left inferior PV;
4) li_o point on left inferior PV farthest away from left superior PV;
5) rs_o: point on right superior PV farthest away from right inferior PV;
6) rs_i: point on right superior PV closest to right inferior PV;
7) ri_i: point on right superior PV closest to right inferior PV;
8) ri_o: point on right inferior PV farthest away from right superior PV;
9) mv_l: point on the left lateral side of the mitral valve ring;
10) mv_r: point on the septal side of the mitral valve ring;
11) mv_an_middle: point on the anterior wall of the mitral valve ring;
12) mv_po_middle: point on the septal side of the mitral valve ring;
13) lpv_base: point at the left pulmonary veins base;
14) roof_25: point at 25% of the path on the roof connecting lpv_base to rpv_base;
15) roof_50: point at 50% of the path on the roof connecting lpv_base to rpv_base;
16) roof_75: point at 75% of the path on the roof connecting lpv_base to rpv_base;
17) rpv_base: point at the left pulmonary veins base;
18) lat_50: point at 50% of the path on the left lateral wall connecting lpv_base to mv_l;
19) laa: left atrial appendage apex;
20) sep_50: point at 50% of the path on the septal wall connecting rpv_base to mv_r;
21) sep_25: point at 25% of the path on the septal wall connecting rpv_base to mv_r;
22) p1: point at 50% of the path on the roof connecting ls_o to rs_o;
23) p1_mv_50: point at 50% of the path connecting p1 to mv_an_middle;
24) p1_mv_sep_50: point at 50% of the path connecting p1_mv_50 to sep_50;
25) p1_mv_sep_75: point at 50% of the path connecting p1_mv_75(point at 75% of the path connecting p1 to mv_an_middle) to sep_25;
26) p2: point at 50% of the path on the roof connecting li_o to ri_o;
27) p2_mv_33: point at 33% of the path connecting p2 to mv_po_middle;
28) p2_mv_66: point at 66% of the path connecting p2 to mv_po_middle;
29) p2_mv_sep_50: point at 50% of the path connecting p2_mv_33 to sep_50;
30) p2_mv_sep_75: point at 75% of the path connecting p2_mv_66 to sep_25;
31) rspvo_p1_mv_30: point at 30% of the path connecting rs_o to p1_mv_50;
32) rspvo_p1_mv_50: point at 50% of the path connecting rs_o to p1_mv_50;
33) rspvo_p1_mv_70: point at 70% of the path connecting rs_o to p1_mv_50;
34) rspvo_p1_mv_sep_30: point at 30% of the path connect-

ing rs_o to p1_mv_sep_50;
35) rspvo_p1_mv_sep_50: point at 50% of the path connecting rs_o to p1_mv_sep_50;
36) rspvo_p1_mv_sep_70: point at 70% of the path connecting rs_o to p1_mv_sep_50.

S.III. Conduction velocity estimation

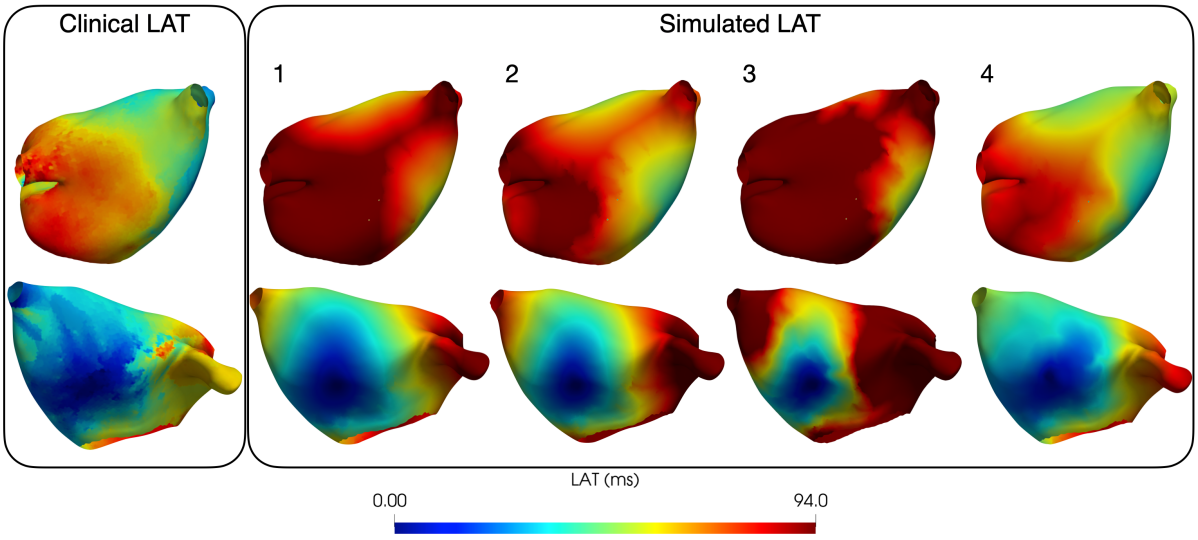

S1. First column: posterior and anterior view of the clinical LAT map of patient 1. Second column: posterior and anterior view of the patient 1 simulated LAT map using the CV_{di} estimation method. Third column: posterior and anterior view of the patient 1 simulated LAT map using the CV_{rm} estimation method. Fourth column: posterior and anterior view of the patient 1 simulated LAT map using the CV_{rb} estimation method. Fifth column: posterior and anterior view of the patient 1 simulated LAT map using the CV_{tu} estimation method.

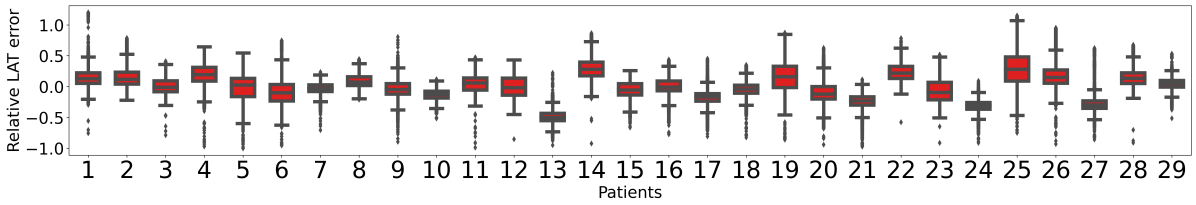

S2. Relative LAT errors per patient using the CV_{di} estimation method.

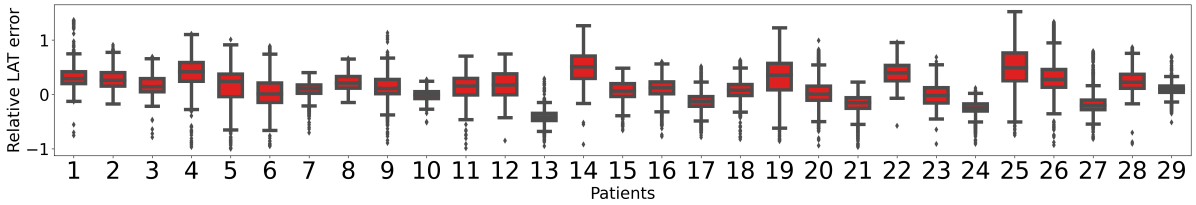

S3. Relative LAT errors per patient using the CV_{rm} estimation method.

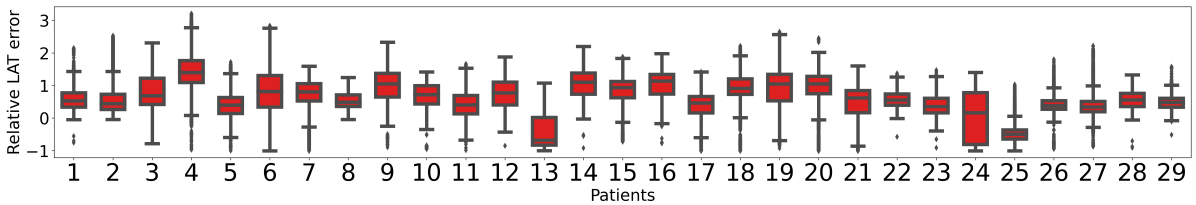

S4. Relative LAT errors per patient using the CV_{rb} estimation method.

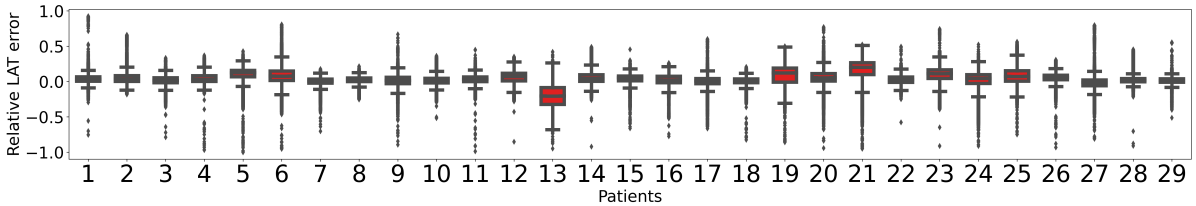

S5. Relative LAT errors per patient using the CV_{tu} estimation method.

Supplementary material of Personalized ablation vs. conventional ablation strategies to terminate atrial fibrillation and prevent recurrence: a systematic in silico study

Modelling ablation scars

The twelve different ablation approaches were defined as follows: pulmonary veins isolation (PVI) was applied at a fixed distance from the pulmonary veins (PVs) with the junction of the LA body. The roof line was applied by calculating the shortest path between the points in the left and right superior PVs furthest away point from the inferior PVs and the mitral isthmus line computing the shortest path between the PVI and the MV annulus. To identify regions to target for ablation using image-intensity-ratio (IIR), LGE-MRI maps were first identified respectively as IIR>1.32 (dense fibrosis) and IIR>1.2 (interstitial fibrosis)[1]. Low voltage areas were identified as the bipolar voltage values derived directly from the electro-anatomical map <0.5 mV[2,3]. A threshold at, respectively, 0.4 and 0.3 m/s[4,5], in the conduction velocity (CV) maps computed minimizing the error between the simulated and the clinical local activation time map[6] was chosen to identify low CV regions. Driver region ablation was performed in the same way as fibrosis region ablation but determined according to dominant frequency maps at 1 standard deviation above the mean. Identified tissue was then separated into connected component regions, and the area of each region was calculated. Connected regions with a surface area < 1 cm^2 were neglected. For approaches including connecting lines to the nearest non-conductive barrier, the regions selected for ablation were connected to the closest anatomical obstacle or ablation lesion via a shortest-distance linear lesion to prevent the formation of AT[7].

References

1. Caixal G, Alarcón F, Althoff TF, Nuñez-Garcia M, Benito EM, Borràs R, Perea RJ, Prat-González S, Garre P, Soto-Iglesias D, Gunturitz C, Cozzari J, Linhart M, Tolosana JM, Arbelo E, Roca-Luque I, Sitges M, Guasch E, Mont L. Accuracy of left atrial fibrosis detection with cardiac magnetic resonance: correlation of late gadolinium enhancement with endocardial voltage and conduction velocity. *Europace : European pacing, arrhythmias, and cardiac electrophysiology : journal of the working groups on cardiac pacing, arrhythmias, and cardiac cellular electrophysiology of the European Society of Cardiology* 2020;

2. Kircher S, Arya A, Altmann D, Rolf S, Bollmann A, Sommer P, Dagres N, Richter S, Breithardt O-A, Dinov B, Husser D, Eitel C, Gaspar T, Piorkowski C, Hindricks G. Individually tailored vs. standardized substrate modification during radiofrequency catheter ablation for atrial fibrillation: a randomized study. *EP Europace* 2018;**20**:1766–1775.

3. Rolf S, Kircher S, Arya A, Eitel C, Sommer P, Richter S, Gaspar T, Bollmann A, Altmann D, Piedra C, Hindricks G, Piorkowski C. Tailored Atrial Substrate

Modification Based on Low-Voltage Areas in Catheter Ablation of Atrial Fibrillation. *Circ: Arrhythmia and Electrophysiology* 2014;**7**:825–833.

4. Balaban G, Halliday BP, Mendonca Costa C, Bai W, Porter B, Rinaldi CA, Plank G, Rueckert D, Prasad SK, Bishop MJ. Fibrosis Microstructure Modulates Reentry in Non-ischemic Dilated Cardiomyopathy: Insights From Imaged Guided 2D Computational Modeling. *Front Physiol* 2018;**9**:1832.

5. Verma B, Oesterlein T, Loewe A, Luik A, Schmitt C, Dössel O. Regional conduction velocity calculation from clinical multichannel electrograms in human atria. *Computers in Biology and Medicine* Elsevier; 2018;**92**:188–196.

6. Azzolin L, Eichenlaub M, Nagel C, Nairn D, Sanchez J, Unger LA, Doessel O, Jadidi A, Loewe A. AugmentA: patient-specific Augmented Atria Generation Tool. *Submitted* 2021;

7. Rappel W-J, Zaman JAB, Narayan SM. Mechanisms for the Termination of Atrial Fibrillation by Localized Ablation: Computational and Clinical Studies. *Circ: Arrhythmia and Electrophysiology* 2015;**8**:1325–1333.

References

[1] G. W. H. Organization, "World health statistics 2021: monitoring health for the sdgs, sustainable development goals," in *World health statistics 2021: monitoring health for the SDGs, sustainable development goals*. World Health Organization, 2021.

[2] V. L. Feigin, G. A. Roth, M. Naghavi, et al., "Global burden of stroke and risk factors in 188 countries, during 1990–2013: a systematic analysis for the global burden of disease study 2013," *The Lancet Neurology*, vol. 15, pp. 913–924, 2016.

[3] K. S. Coyne, C. Paramore, S. Grandy, M. Mercader, M. Reynolds, and P. Zimetbaum, "Assessing the direct costs of treating nonvalvular atrial fibrillation in the united states," *Value in Health*, vol. 9, pp. 348–356, 2006.

[4] V. Fuster, L. E. Rydén, D. S. Cannom, et al., "Acc/aha/esc 2006 guidelines for the management of patients with atrial fibrillation: A report of the american college of cardiology/american heart association task force on practice guidelines and the european society of cardiology committee for practice guidelines (writing committee to revise the 2001 guidelines for the management of patients with atrial fibrillation): Developed in collaboration with the european heart rhythm association and the heart rhythm society," *Circulation*, vol. 114, pp. e257–e354, 2006.

[5] J.-Y. Le Heuzey, O. Paziaud, O. Piot, et al., "Cost of care distribution in atrial fibrillation patients: the cocaf study," *American heart journal*, vol. 147, pp. 121–126, 2004.

[6] Y. Miyasaka, M. E. Barnes, K. R. Bailey, et al., "Mortality trends in patients diagnosed with first atrial fibrillation: a 21-year community-based study," *Journal of the American College of Cardiology*, vol. 49, pp. 986–992, 2007.

[7] S. M. Narayan and D. E. Krummen, "Targeting stable rotors to treat atrial fibrillation," *Arrhythmia & Electrophysiology Review*, vol. 1, pp. 34–38, 2012.

[8] S. Magnani, D. Muser, W. Chik, and P. Santangeli, "Adjunct ablation strategies for persistent atrial fibrillation-beyond pulmonary vein isolation," *Journal of Thoracic Disease*, vol. 7, pp. 178–184, 2015. doi:10.3978/j.issn.2072-1439.2015.01.25

[9] S. M. Narayan, K. Shivkumar, D. E. Krummen, J. M. Miller, and W.-J. Rappel, "Panoramic electrophysiological mapping but not electrogram morphology identifies stable sources for human atrial fibrillation: stable atrial fibrillation rotors and focal sources relate poorly to fractionated electrograms," *Circulation. Arrhythmia and Electrophysiology*, vol. 6, pp. 58–67, 2013. doi:10.1161/CIRCEP.111.977264

[10] M. Haissaguerre, M. Hocini, A. Denis, et al., "Driver domains in persistent atrial fibrillation," *Circulation*, vol. 130, pp. 530–538, 2014. doi:10.1161/CIRCULATIONAHA.113.005421

[11] A. S. Jadidi, H. Lehrmann, C. Keyl, et al., "Ablation of persistent atrial fibrillation targeting low-voltage areas with selective activation characteristics," *Circulation: Arrhythmia and Electrophysiology*, vol. 9, pp. 480–491, 2016. doi:10.1161/CIRCEP.115.002962

[12] R. L. Winslow, N. Trayanova, D. Geman, and M. I. Miller, "Computational medicine: translating models to clinical care," *Science translational medicine*, vol. 4, pp. 158rv11–158rv11, 2012.

[13] P. M. Boyle, T. Zghaib, S. Zahid, et al., "Computationally guided personalized targeted ablation of persistent atrial fibrillation." *Nature Biomedical Engineering*, 2019. doi:10.1038/s41551-019-0437-9

[14] T. W. Lim, I. S. Jassal, D. L. Ross, and S. P. Thomas, "Medium-term efficacy of segmental ostial pulmonary vein isolation for the treatment of permanent and persistent atrial fibrillation," *Pacing and Clinical Electrophysiology*, vol. 29, pp. 374–379, 2006. doi:https://doi.org/10.1111/j.1540-8159.2006.00356.x

[15] L. Azzolin, S. Schuler, O. Dössel, and A. Loewe, "A reproducible protocol to assess arrhythmia vulnerability in silico: Pacing at the end of the effective refractory period," *Frontiers in Physiology*, vol. 12, p. 420, 2021. doi:10.3389/fphys.2021.656411

[16] L. Azzolin, G. Luongo, S. Rocher, J. Saiz, O. Doessel, and A. Loewe, "Influence of gradient and smoothness of atrial wall thickness on initiation and maintenance of atrial fibrillation," in *Computing in Cardiology Conference (CinC)*, 2020. doi:10.22489/CinC.2020.261

[17] L. Azzolin, C. Nagel, D. Nairn, et al., "Automated framework for the augmentation of missing anatomical structures and generation of personalized atrial models from clinical data," in *Computing in Cardiology Conference (CinC)*, 9 2021.

[18] L. Azzolin, M. Eichenlaub, C. Nagel, et al., "Augmenta: Patient-specific augmented atrial model generation tool," *under review*, 2021.

[19] G. Luongo, L. Azzolin, S. Schuler, et al., "Machine learning enables noninvasive prediction of atrial fibrillation driver location and acute pulmonary vein ablation success using the 12-lead ECG," *Cardiovascular Digital Health Journal*, vol. 2, pp. 126–136, 2021. doi:10.1016/j.cvdhj.2021.03.002

[20] ZooFarie. Heart diagram. https://commons.wikimedia.org/wiki/File:Heart_diagram-en.svg

[21] R. W. Pearl, "Hurst's the heart, 12th edition, 12th edition," *Journal of the American College of Surgeons*, vol. 207, p. e4, 2008. doi:https://doi.org/10.1016/j.jamcollsurg.2008.03.018

[22] P. A. Iaizzo, *Handbook of cardiac anatomy, physiology, and devices*, pp. 61–88. Cham : Springer, 1 2015.

[23] R. M. Anderson, *The gross physiology of the cardiovascular system*. Tucson: Racquet Press, 2012.

[24] O. College. Dual system of human circulation. https://commons.wikimedia.org/wiki/File:2003_Dual_System_of_Human_Circulation.jpg

[25] S. Pollnow, "Characterizing cardiac electrophysiology during radiofrequency ablation: An integrative ex vivo, in silico, and in vivo approach," PhD thesis, Karlsruhe Institute of Technology (KIT), Karlsruhe, 2019. doi:10.5445/KSP/1000089807

[26] M. W. Krüger, *Personalized multi-scale modeling of the atria: Heterogeneities, fiber architecture, hemodialysis and ablation therapy*, vol. 19. KIT Scientific Publishing, 2013. doi:10.5445/KSP/1000031226

[27] F. Bukauskas, *Molecular organization, gating, and function of gap junction channels*, pp. 85–94. Elsevier Inc., 12 2014. doi:10.1016/B978-1-4557-2856-5.00008-X

[28] S. Y. Ho and D. Sanchez-Quintana, "The importance of atrial structure and fibers," *Clinical Anatomy*, vol. 22, pp. 52–63, 2009. doi:10.1002/ca.20634

[29] D. Sánchez-Quintana, R. Anderson, J. Cabrera, et al., "The terminal crest: Morphological features relevant to electrophysiology," *Heart (British Cardiac Society)*, vol. 88, pp. 406–11, 2002.

[30] A. Siddiqui, R. Daimi, K. Gandhi, et al., "Crista terminalis, musculi pectinati, and taenia sagittalis: Anatomical observations and applied significance," *ISRN Anatomy*, vol. 2013, 2013. doi:10.5402/2013/803853

[31] K. Wang, S. Y. Ho, D. G. Gibson, and R. H. Anderson, "Architecture of atrial musculature in humans," *British Heart Journal*, vol. 73, pp. 559–565, 1995.

[32] D. Sanchez-Quintana, J. A. Cabrera, V. Climent, J. Farre, M. C. d. Mendonca, and S. Y. Ho, "Anatomic relations between the esophagus and left atrium and relevance for ablation of atrial fibrillation," *Circulation*, vol. 112, pp. 1400–1405, 2005. doi:10.1161/CIRCULATIONAHA.105.551291

[33] C. Stöllberger, G. Ernst, E. Bonner, J. Finsterer, and J. Slany, *Left atrial appendage morphology: Comparison of transesophageal images and postmortem casts*, vol. 92, no. 4, pp. 303–308. Springer Berlin / Heidelberg Zeitschrift für Kardiologie, 1 2003.

[34] R. Lemery, L. Soucie, B. Martin, A. S. L. Tang, M. Green, and J. Healey, "Human study of biatrial electrical coupling: determinants of endocardial septal activation and conduction over interatrial connections," *Circulation*, vol. 110, pp. 2083–2089, 2004.

[35] S. Y. Ho, D. Sanchez-Quintana, J. A. Cabrera, and R. H. Anderson, "Anatomy of the left atrium: implications for radiofrequency ablation of atrial fibrillation," *J Cardiovasc Electrophysiol*, vol. 10, pp. 1525–1533, 1999.

[36] S.-I. Sakamoto, T. Nitta, Y. Ishii, Y. Miyagi, H. Ohmori, and K. Shimizu, "Interatrial electrical connections: the precise location and preferential conduction," *Journal of Cardiovascular Electrophysiology*, vol. 16, pp. 1077–1086, 2005. doi:10.1111/j.1540-8167.2005.40659.x

[37] M. Varela, R. Morgan, A. Theron, et al., "Novel mri technique enables non-invasive measurement of atrial wall thickness," *IEEE Transactions on Medical Imaging*, vol. 36, pp. 1607–1614, 2017. doi:10.1109/TMI.2017.2671839

[38] P. G. Platonov, V. Ivanov, S. Y. Ho, and L. Mitrofanova, "Left atrial posterior wall thickness in patients with and without atrial fibrillation: data from 298 consecutive autopsies," *Journal of Cardiovascular Electrophysiology*, vol. 19, pp. 689–692, 2008. doi:10.1111/j.1540-8167.2008.01102.x

[39] M. P. Review. Action potential. http://www.pathophys.org/physiology-of-cardiac-conduction-and-contractility/

[40] L. Schmidt, F. Lang, and M. Heckmann, *Physiologie des menschen*, vol. 31, pp. 518–20. überarb. und aktualisierte Aufl. Heidelberg: Springer, 2011.

[41] O. College. Conduction system of heart. https://commons.wikimedia.org/wiki/File:2018_Conduction_System_of_Heart.jpg

[42] A. J. Camm, G. Y. H. Lip, R. De Caterina, et al., "2012 focused update of the ESC guidelines for the management of atrial fibrillation: an update of the 2010 ESC guidelines for the management of atrial fibrillation. developed with the special contribution of the european heart rhythm association." *European Heart Journal*, vol. 33, pp. 2719–47, 2012. doi:10.1093/eurheartj/ehs253

[43] G. Hindricks, T. Potpara, N. Dagres, et al., "2020 ESC guidelines for the diagnosis and management of atrial fibrillation developed in collaboration with the european association of cardio-thoracic surgery (EACTS)," *European Heart Journal*, 2020. doi:10.1093/eurheartj/ehaa612

[44] F. D. R. Hobbs, D. A. Fitzmaurice, J. Mant, et al., "A randomised controlled trial and cost-effectiveness study of systematic screening (targeted and total population screening) versus routine practice for the detection of atrial fibrillation in people aged 65 and over. the SAFE study," *Health Technol Assess.*, 2005.

[45] H. Calkins, K. H. Kuck, R. Cappato, et al., "2012 HRS/EHRA/ECAS expert consensus statement on catheter and surgical ablation of atrial fibrillation: recommendations for patient selection, procedural techniques, patient management and follow-up, definitions, endpoints, and research trial design," *J Interv Card Electrophysiol*, vol. 33, pp. 171–257, 2012. doi: 10.1007/s10840-012-9672-7

[46] A. J. Camm, P. Kirchhof, G. Y. H. Lip, et al., "Guidelines for the management of atrial fibrillation: the task force for the management of atrial fibrillation of the european society of cardiology (ESC)," *European Heart Journal*, vol. 31, pp. 2369–2429, 2010. doi:10.1093/eurheartj/ehq278

[47] N. M. de Groot, R. P. Houben, J. L. Smeets, et al., "Electropathological substrate of longstanding persistent atrial fibrillation in patients with structural heart disease," *Circulation*, vol. 122, pp. 1674–1682, 2010. doi:10.1161/CIRCULATIONAHA.109.910901

[48] C. Mahnkopf, T. J. Badger, N. S. Burgon, et al., "Evaluation of the left atrial substrate in patients with lone atrial fibrillation using delayed-enhanced mri: implications for disease progression and response to catheter ablation," *Heart Rhythm*, vol. 7, pp. 1475–1481, 2010.

[49] S. Nattel, B. Burstein, and D. Dobrev, "Atrial remodeling and atrial fibrillation: Mechanisms and implications," *Circ Arrhythmia Electrophysiol*, vol. 1, pp. 62–73, 2008.

[50] J. Andrade, P. Khairy, D. Dobrev, and S. Nattel, "The clinical profile and pathophysiology of atrial fibrillation: relationships among clinical features, epidemiology, and mechanisms," *Circulation Research*, vol. 114, pp. 1453–1468, 2014. doi:10.1161/CIRCRESAHA.114.303211

[51] U. Schotten, D. Dobrev, P. G. Platonov, H. Kottkamp, and G. Hindricks, "Current controversies in determining the main mechanisms of atrial fibrillation." *Journal of Internal Medicine*, vol. 279, pp. 428–38, 2016. doi:10.1111/joim.12492

[52] Y. Guo, G. Y. Lip, and S. Apostolakis, "Inflammation in atrial fibrillation," *Journal of the American College of Cardiology*, vol. 60, pp. 2263–2270, 2012. doi:https://doi.org/10.1016/j.jacc.2012.04.063

[53] R. A. Nishimura, C. M. Otto, R. O. Bonow, et al., "2014 AHA/ACC guideline for the management of patients with valvular heart disease: a report of the american college of cardiology/american heart association task force on practice guidelines." *The Journal of Thoracic and Cardiovascular Surgery*, vol. 148, pp. e1–e132, 2014. doi:10.1016/j.jtcvs.2014.05.014

[54] D. Scherf, "Studies on auricular tachycardia caused by aconitine administration," *Proceedings of the Society for Experimental Biology and Medicine*, vol. 64, pp. 233–239, 1947. doi: 10.3181/00379727-64-15754

[55] J. Waks and M. Josephson, "Mechanisms of atrial fibrillation - reentry, rotors and reality." *Arrhythmia & Electrophysiology Review*, vol. 3 2, pp. 90–100, 2014.

[56] M. Haissaguerre, P. Jaïs, D. C. Shah, et al., "Spontaneous initiation of atrial fibrillation by ectopic beats originating in the pulmonary veins," *New England Journal of Medicine*, vol. 339, pp. 659–666, 1998.

[57] U. Schotten, S. Verheule, P. Kirchhof, and A. Goette, "Pathophysiological mechanisms of atrial fibrillation: A translational appraisal," *Physiological Reviews*, vol. 91, pp. 265–325, 2011, pMID: 21248168. doi:10.1152/physrev.00031.2009

[58] L. Roten, N. Derval, and P. Jaïs, "Catheter ablation for persistent atrial fibrillation," *Circulation: Arrhythmia and Electrophysiology*, vol. 5, pp. 1224–1232, 2012. doi:10.1161/CIRCEP.112.974873

[59] A. Loewe, "Modeling human atrial patho-electrophysiology from ion channels to ECG: substrates, pharmacology, vulnerability, and p-waves," PhD thesis, Karlsruhe Institute of Technology (KIT), Karlsruhe, 2016. doi:10.5445/KSP/1000054615

[60] V. Markides and R. J. Schilling, "Atrial fibrillation: classification, pathophysiology, mechanisms and drug treatment," *Heart*, vol. 89, pp. 939–943, 2003. doi:10.1136/heart.89.8.939

[61] H. Oral, B. P. Knight, H. Tada, et al., "Pulmonary vein isolation for paroxysmal and persistent atrial fibrillation," *Circulation*, vol. 105, pp. 1077–1081, 2002.

[62] Y.-k. Iwasaki, K. Nishida, T. Kato, and S. Nattel, "Atrial fibrillation pathophysiology: implications for management," *Circulation*, vol. 124, pp. 2264–2274, 2011. doi:10.1161/CIRCULATIONAHA.111.019893

[63] Z. Lu, B. J. Scherlag, J. Lin, et al., "Atrial fibrillation begets atrial fibrillation," *Circulation: Arrhythmia and Electrophysiology*, vol. 1, pp. 184–192, 2008. doi:10.1161/CIRCEP.108.784272

[64] M. C. Wijffels, C. J. Kirchhof, R. Dorland, and M. A. Allessie, "Atrial fibrillation begets atrial fibrillation. a study in awake chronically instrumented goats," *Circulation*, vol. 92, pp. 1954–1968, 1995.

[65] R. Beinart and S. Nazarian, "Role of magnetic resonance imaging in atrial fibrillation ablation," *Current Treatment Options in Cardiovascular Medicine*, vol. 16, 2014. doi:10.1007/s11936-014-0316-3

[66] G. T. Herman, *Fundamentals of computerized tomography: image reconstruction from projections*. Springer Science & Business Media, 2009.

[67] Y. Zhao, L. Dagher, C. Huang, P. Miller, and N. F. Marrouche, "Cardiac MRI to manage atrial fibrillation," *Arrhythmia & Electrophysiology Review*, vol. 9, pp. 189–194, 2020. doi:10.15420/aer.2020.21

[68] P. Della Bella, G. Fassini, M. Cireddu, et al., "Image integration-guided catheter ablation of atrial fibrillation: A prospective randomized study," *Journal of Cardiovascular Electrophysiology*, vol. 20, pp. 258–265, 2009. doi:10.1111/j.1540-8167.2008.01311.x

[69] M. Njeim, B. Desjardins, and F. Bogun, "Multimodality imaging for guiding ep ablation procedures," *JACC: Cardiovascular Imaging*, vol. 9, pp. 873–886, 2016. doi:https://doi.org/10.1016/j.jcmg.2016.03.009

[70] L. Gepstein, G. Hayam, and S. A. Ben-Haim, "A novel method for nonfluoroscopic catheter-based electroanatomical mapping of the heart. in vitro and in vivo accuracy results," *Circulation*, vol. 95, pp. 1611–1622, 1997.

[71] M. Scaglione, L. Biasco, D. Caponi, et al., "Visualization of multiple catheters with electroanatomical mapping reduces x-ray exposure during atrial fibrillation ablation," *EP Europace*, vol. 13, pp. 955–962, 2011. doi:10.1093/europace/eur062

[72] A. Luik, A. Radzewitz, M. Kieser, et al., "Cryoballoon versus open irrigated radiofrequency ablation in patients with paroxysmal atrial fibrillation: The prospective, randomized, controlled, noninferiority freezeAF study," *Circulation*, vol. 132, pp. 1311–1319, 2015. doi:10.1161/CIRCULATIONAHA.115.016871

[73] A. Verma, C.-y. Jiang, T. R. Betts, et al., "Approaches to catheter ablation for persistent atrial fibrillation." *The New England Journal of Medicine*, vol. 372, pp. 1812–22, 2015. doi:10.1056/NEJMoa1408288

[74] K. C. Wong, J. R. Paisey, M. Sopher, et al., "No benefit of complex fractionated atrial electrogram ablation in addition to circumferential pulmonary vein ablation and linear ablation: benefit of complex ablation study," *Circulation: Arrhythmia and Electrophysiology*, vol. 8, pp. 1316–1324, 2015.

[75] J. Brachmann, J. D. Hummel, D. J. Wilber, et al., "Prospective randomized comparison of rotor ablation vs conventional ablation for treatment of persistent atrial fibrillation—the reaffirm trial," *Heart Rhythm*, vol. 16, pp. 963–965, 2019.

[76] M. Masuda, M. Asai, O. Iida, et al., "Additional low‐voltage‐area ablation in patients with paroxysmal atrial fibrillation: Results of the randomized controlled volcano trial," *Journal of the American Heart Association*, vol. 9, p. e015927, 2020. doi:10.1161/JAHA.120.015927

[77] I.-S. Kim, B. Lim, J. Shim, et al., "Clinical usefulness of computational modeling-guided persistent atrial fibrillation ablation: Updated outcome of multicenter randomized study," *Frontiers in Physiology*, vol. 10, 2019. doi:10.3389/fphys.2019.01512

[78] A. Prakosa, H. J. Arevalo, D. Deng, et al., "Personalized virtual-heart technology for guiding the ablation of infarct-related ventricular tachycardia," *Nature Biomedical Engineering*, 2018. doi:10.1038/s41551-018-0282-2

[79] physiomeproject. Courtemanche ionic model. https://models.physiomeproject.org/workspace/courtemanche_ramirez_nattel_1998/@@rawfile/c26e4d53792b0e3161b2f8638afa2819fc999610/courtemanche_1998.png

[80] T. Yu, C. M. Lloyd, D. P. Nickerson, et al., "The physiome model repository 2," *Bioinformatics*, vol. 27, pp. 743–744, 2011. doi:10.1093/bioinformatics/btq723

[81] A. L. Hodgkin and A. F. Huxley, "A quantitative description of membrane current and its application to conduction and excitation in nerve," *Journal of Physiology*, vol. 117, pp. 500–544, 1952.

[82] M. Courtemanche, R. J. Ramirez, and S. Nattel, "Ionic mechanisms underlying human atrial action potential properties: insights from a mathematical model." *The American Journal of Physiology*, vol. 275, pp. H301–21, 1998.

[83] J. P. Sánchez Arciniegas, "A multiscale in silico study to characterize the atrial electrical activity of patients with atrial fibrillation : A translational study to guide ablation therapy," PhD thesis, Institute of Biomedical Engineering, Karlsruhe Institute of Technology (KIT), 2021. doi:10.5445/IR/1000134665

[84] W. T. r. Miller and D. B. Geselowitz, "Simulation studies of the electrocardiogram. II. ischemia and infarction," *Circulation Research*, vol. 43, pp. 315–323, 1978.

[85] O. H. Schmitt, "Biological information processing using the concept of interpenetrating domains," in *Information processing in the nervous system*. Springer, 1969, pp. 325–331.

[86] L. Tung, "A bidomain model for describing ischemic myocardial d-c potentials," PhD thesis, Massachusetts Institute of Technology. Dept. of Electrical Engineering and Computer Science, 1978.

[87] S. M. Kandel, "The electrical bidomain model: a review," *Sch. Acad. J. Biosci*, vol. 3, pp. 633–639, 2015.

[88] J. P. Keener and J. Sneyd, *Mathematical physiology*, vol. 1. Springer, 1998.

[89] P. Kirchhof, S. Benussi, D. Kotecha, et al., "The task force for the management of atrial fibrillation of the european society of cardiology (esc). 2016 esc guidelines for the management of atrial fibrillation developed in collaboration with eacts," *Eur Heart J*, vol. 37, pp. 2893–2962, 2016.

[90] E. J. Benjamin, P. Muntner, A. Alonso, et al., "Heart disease and stroke statistics—2019 update: a report from the american heart association," *Circulation*, vol. 139, pp. e56–e528, 2019.

[91] S. S. Chugh, R. Havmoeller, K. Narayanan, et al., "Worldwide epidemiology of atrial fibrillation: a global burden of disease 2010 study," *Circulation*, vol. 129, pp. 837–847, 2014.

[92] S. Colilla, A. Crow, W. Petkun, D. E. Singer, T. Simon, and X. Liu, "Estimates of current and future incidence and prevalence of atrial fibrillation in the us adult population," *The American journal of cardiology*, vol. 112, pp. 1142–1147, 2013.

[93] B. P. Krijthe, A. Kunst, E. J. Benjamin, et al., "Projections on the number of individuals with atrial fibrillation in the european union, from 2000 to 2060," *European Heart Journal*, vol. 34, pp. 2746–2751, 2013.

[94] J. Heijman, D. Linz, and U. Schotten, "Dynamics of atrial fibrillation mechanisms and comorbidities," *Annual Review of Physiology*, vol. 83, pp. 83–106, 2021.

[95] A. Roy, M. Varela, and O. Aslanidi, "Image-based computational evaluation of the effects of atrial wall thickness and fibrosis on re-entrant drivers for atrial fibrillation," *Frontiers in Physiology*, vol. 9, p. 1352, 2018.

[96] M. Varela, M. A. Colman, J. C. Hancox, and O. V. Aslanidi, "Atrial heterogeneity generates re-entrant substrate during atrial fibrillation and anti-arrhythmic drug action: mechanistic insights from canine atrial models," *PLoS Computational Biology*, vol. 12, p. e1005245, 2016.

[97] H. Dierckx, E. Brisard, H. Verschelde, and A. V. Panfilov, "Drift laws for spiral waves on curved anisotropic surfaces," *Phys. Rev. E.*, vol. 88, p. 012908, 2013.

[98] I. V. Biktasheva, H. Dierckx, and V. N. Biktashev, "Drift of scroll waves in thin layers caused by thickness features: Asymptotic theory and numerical simulations," *Phys. Rev. Lett.*, vol. 114, p. 068302, 2015.

[99] M. Yamazaki, S. Mironov, C. Taravant, et al., "Heterogeneous atrial wall thickness and stretch promote scroll waves anchoring during atrial fibrillation," *Cardiovascular Research*, vol. 94, pp. 48–57, 2012.

[100] J. Park, C. H. Park, H.-J. Lee, et al., "Left atrial wall thickness rather than epicardial fat thickness is related to complex fractionated atrial electrogram," *International Journal of Cardiology*, vol. 172, pp. e411–e413, 2014.

[101] S. Nattel, "New ideas about atrial fibrillation 50 years on," *Nature*, vol. 415, pp. 219–226, 2002.

[102] R. A. Gray, A. M. Pertsov, and J. Jalife, "Spatial and temporal organization during cardiac fibrillation," *Nature*, vol. 392, pp. 75–78, 1998.

[103] J. Sahadevan, K. Ryu, L. Peltz, et al., "Epicardial mapping of chronic atrial fibrillation in patients: preliminary observations," *Circulation*, vol. 110, pp. 3293–3299, 2004.

[104] A. N. Ganesan, N. J. Shipp, A. G. Brooks, et al., "Long-term outcomes of catheter ablation of atrial fibrillation: a systematic review and meta-analysis," *Journal of the American Heart Association*, vol. 2, p. e004549, 2013.

[105] C. McGann, N. Akoum, A. Patel, et al., "Atrial fibrillation ablation outcome is predicted by left atrial remodeling on mri," *Circulation: Arrhythmia and Electrophysiology*, vol. 7, pp. 23–30, 2014.

[106] A. Blandino, F. Bianchi, S. Grossi, et al., "Left atrial substrate modification targeting low-voltage areas for catheter ablation of atrial fibrillation: a systematic review and meta-analysis," *Pacing and Clinical Electrophysiology*, vol. 40, pp. 199–212, 2017.

[107] H. Kottkamp, J. Berg, R. Bender, A. Rieger, and D. Schreiber, "Box isolation of fibrotic areas (bifa): a patient-tailored substrate modification approach for ablation of atrial fibrillation," *Journal of Cardiovascular Electrophysiology*, vol. 27, pp. 22–30, 2016.

[108] J. M. Miller, V. Kalra, M. K. Das, et al., "Clinical benefit of ablating localized sources for human atrial fibrillation: the indiana university firm registry," *Journal of the American College of Cardiology*, vol. 69, pp. 1247–1256, 2017.

[109] S. Mohanty, P. Mohanty, C. Trivedi, et al., "Long-term outcome of pulmonary vein isolation with and without focal impulse and rotor modulation mapping: insights from a meta-analysis," *Circulation: Arrhythmia and Electrophysiology*, vol. 11, p. e005789, 2018.

[110] J. Corral-Acero, F. Margara, M. Marciniak, et al., "The 'digital twin' to enable the vision of precision cardiology," *European Heart Journal*, vol. 41, pp. 4556–4564, 2020. doi:10.1093/eurheartj/ehaa159

[111] M. J. Cartoski, P. P. Nikolov, A. Prakosa, P. M. Boyle, P. J. Spevak, and N. A. Trayanova, "Computational identification of ventricular arrhythmia risk in pediatric myocarditis," *Pediatric Cardiology*, vol. 40, pp. 857–864, 2019.

[112] H. J. Arevalo, F. Vadakkumpadan, E. Guallar, et al., "Arrhythmia risk stratification of patients after myocardial infarction using personalized heart models," *Nature communications*, vol. 7, pp. 1–8, 2016.

[113] K. Gillette, M. A. Gsell, A. J. Prassl, et al., "A framework for the generation of digital twins of cardiac electrophysiology from clinical 12-leads ECGs," *Medical Image Analysis*, p. 102080, 2021. doi:10.1016/j.media.2021.102080

[114] S. Niederer, Y. Aboelkassem, C. D. Cantwell, et al., "Creation and application of virtual patient cohorts of heart models," *Philosophical Transactions of the Royal Society A*, vol. 378, p. 20190558, 2020.

[115] C. Nagel, S. Schuler, O. Dössel, and A. Loewe, "A bi-atrial statistical shape model for large-scale in silico studies of human atria: model development and application to ECG simulations," *Medical Image Analysis*, p. 102210, 2021. doi:10.1016/j.media.2021.102210

[116] L. Azzolin, M. Eichenlaub, C. Nagel, et al., "Personalized ablation vs. conventional ablation strategies to terminate atrial fibrillation and prevent recurrence: a systematic in silico study," *under review*, 2021.

[117] S. Labarthe, J. Bayer, Y. Coudiere, et al., "A bilayer model of human atria: mathematical background, construction, and assessment," *EP Europace*, vol. 16 Suppl 4, pp. iv21–iv29, 2014. doi:10.1093/europace/euu256

List of Publications and Supervised Theses

Journal Articles

- **L. Azzolin**, M. Eichenlaub, C. Nagel, D. Nairn, J. Sánchez, L. Unger, O. Dössel, A. Jadidi, and A. Loewe *Personalized ablation vs. conventional ablation strategies to terminate atrial fibrillation and prevent recurrence: a systematic in silico study*, under review 2021;-(-):
- **L. Azzolin**, M. Eichenlaub, C. Nagel, D. Nairn, J. Sánchez, L. Unger, O. Dössel, A. Jadidi, and A. Loewe *AugmentA: Patient-specific Augmented Atrial model Generation Tool*, under review 2021;-(-):
- **L. Azzolin**, S. Steffen, O. Dössel, and A. Loewe *A Reproducible Protocol to Assess Arrhythmia Vulnerability in silico: Pacing at the End of the Effective Refractory Period*, Frontiers in Physiology 2021,-:-
- G. Luongo, **L. Azzolin**, S. Schuler, M.W. Rivolta, T.P. Almeida, J.P. Martínez, D.C. Soriano, L. Armin, B. Müller-Edenborn, A. Jadidi, O. Dössel, , R. Sassi, P. Laguna, and A. Loewe *Machine learning enables noninvasive prediction of atrial fibrillation driver location and acute pulmonary vein ablation success using the 12-lead ECG*, Cardiovascular Digital Health Journal 2021;2(2):126-136
- L. Unger, **L. Azzolin**, M. Nothstein, J. Sánchez, A. Luik, G. Seemann, S. Yeshwant, T. Oesterlein, O. Dössel, C. Schmitt, P. Spector and A. Loewe *Cycle length statistics during human atrial fibrillation reveal refractory properties of the underlying substrate: a combined in silico and clinical test of concept study*, EP Europace 2021, 23(1):i133–i142
- C. Nagel, G. Luongo, **L. Azzolin**, S. Schuler, O. Dössel, A. Loewe *Non-Invasive and Quantitative Estimation of Left Atrial Fibrosis Based on P Waves of the 12-Lead ECG—A Large-Scale Computational Study Covering Anatomical Variability*, Journal of Clinical Medicine 2021, 10(8):1797
- **L. Azzolin**, L. Dedè, A. Gerbi and A. Quarteroni *Effect of fibre orientation and bulk modulus on the electromechanical modelling of human ventricles*, Mathematics in Engineering 2020, 2(4):614–638

Refereed Conference Articles

- T. Zheng, **L. Azzolin**, J. Sánchez, O. Dössel, and A. Loewe *An automated pipeline for generating fiber orientation and region annotation of patient-specific atrial model*, Current Directions in Biomedical Engineering, Hannover, Germany, 2021
- **L. Azzolin**, C. Nagel, D. Nairn, J. Sánchez, T. Zheng, M. Eichenlaub, A. Jadidi, O. Dössel and A. Loewe *Automated Framework for the Augmentation of Missing Anatomical Structures and Generation of Personalized Atrial Models from Clinical Data*, 2021 Computing in Cardiology, Brno, Czech Republic, 2021
- G. Luongo, **L. Azzolin**, M. W. Rivolta, T. P. Almeida, J. P. Martínez, D.C. Soriano, O. Dössel, R. Sassi, P. Laguna, and A. Loewe *Machine Learning to Find Areas of Rotors Sustaining Atrial Fibrillation from the ECG*, 2020 Computing in Cardiology, vol. 47, Rimini, Italy, 2020
- **L. Azzolin**, G. Luongo, S.R. Ventura, J. Saiz, O. Dössel, and A. Loewe *Influence of Gradient and Smoothness of Atrial Wall Thickness on Initiation and Maintenance of Atrial Fibrillation*, 2020 Computing in Cardiology, vol. 47, Rimini, Italy, 2020
- T. Walz, **L. Azzolin**, E. Chleilat and A. Hermenegild *Potential Roles of Purkinje Fibers in Ischemia-Induced Arrhythmias*, 2020 Computing in Cardiology, vol. 47, Rimini, Italy, 2020

Refereed Conference Abstracts

- **L. Azzolin**, O. Dössel, and A. Loewe. *Influence of the protocol used to induce arrhythmia on atrial fibrillation vulnerability*, Atrial Signals Conference, Bordeaux, France, 2020
- **L. Azzolin**, O. Dössel, and A. Loewe. *Influence of the protocol used to induce arrhythmia on atrial fibrillation vulnerability*, 41 Annual International Conference of the IEEE Engineering in Medicine and Biology Society (EMBC), Berlin, Germany, 2019
- **L. Azzolin**, J. Sánchez, S. Schuler, O. Dössel, and A. Loewe. *Initiation and maintenance of re-entrant cardiac propagation: a computational vulnerability study*, Gordon Research Conference - Cardiac Arrhythmia Mechanisms, Lucca, Italy, 2019

Invited Talks

- Computer assisted assessment of atrial vulnerability, Atrial Signals 2021, Karlsruhe, Germany, 2021

Supervised Student Theses

- Tianbao Zheng, *Automatic patient-specific atrial model fiber generation and region annotation to study arrhythmia vulnerability*, Master's Thesis, Institute of Biomedical Engineering, Karlsruhe Institute of Technology (KIT), 2021
- Angelo Aracri, *Innovative ablation strategies to terminate reentrant activity on simplified left atrium geometry*, Student's Project, Institute of Biomedical Engineering, Karlsruhe Institute of Technology (KIT), 2021
- Erik Oberschulte, *Low-energy pacing to control cardiac arrhythmia*, Bachelor's Thesis, Institute of Biomedical Engineering, Karlsruhe Institute of Technology (KIT), 2021
- Jose Maria Esnaola Capa, *Co-Registration of Multimodal Datasets in Patient-Specific Computational Models to Correlate Fibrotic Area and Electrograms' Signals*, Master's Thesis, Institute of Biomedical Engineering, Karlsruhe Institute of Technology (KIT), 2020
- Vincent Nitzke, *Non-invasive atrial rotors and focal sources characterization using ECG*, Bachelor's Thesis, Institute of Biomedical Engineering, Karlsruhe Institute of Technology (KIT), 2020
- Angelo Aracri, *OpenCARP-XL*, Student's Project, Institute of Biomedical Engineering, Karlsruhe Institute of Technology (KIT), 2020
- Christoph Seemann, *Quantitative analysis of filaments and phase singularities to assess atrial vulnerability to arrhythmia*, Bachelor's Thesis, Institute of Biomedical Engineering, Karlsruhe Institute of Technology (KIT), 2019

Invention Disclosures

- **L.Azzolin**, A. Loewe, O. Dössel, D. Nairn, C. Nagel, J. Sánchez, L. Unger and T. Zheng "Automated pipeline to generate augmented anatomical and functional atrial digital twins", 2021
- **L.Azzolin**, A. Loewe, O. Dössel, A. Jadidi, and M. Eichenlaub "Personalized computed models to assess arrhythmia vulnerability and guide targeted catheter ablation for atrial fibrillation", 2021

Awards

- Preis für Patientensicherheit in der Medizintechnik, 2nd prize, *Machine learning enables noninvasive prediction of atrial fibrillation driver location and acute pulmonary vein*

ablation success using the 12-lead ECG, by the Deutsche Gesellschaft für Biomedizinische Technik (DGBMT), 2021

- Simula Summer School in Computational Physiology travel grant, by the Simula Research Laboratory, UC San Diego, University of Oslo, 2019
- Gordon Research Conference travel grant, by the Deutsche Herzstiftung, 2019